

1 Genome sequences of four *Ixodes* species expands 2 understanding of tick evolution 3

4 Alexandra Cerqueira de Araujo ^a, Benjamin Noël ^b, Anthony Bretaudeau ^{cd}, Karine
5 Labadie ^e, Matéo Boudet ^{cd}, Nachida Tadrent ^b, Benjamin Istace ^b, Salima Kritli ^b,
6 Corinne Cruaud ^e, Robert Olaso ^f, Jean-François Deleuze ^f, Maarten Voordouw ^g,
7 Caroline Hervet ^a, Olivier Plantard ^a, Aya Zamoto-Niikura ^h, Thomas Chertemps ⁱ,
8 Martine Maïbèche ⁱ, Frédérique Hilliou ^j, Gaëlle Le Goff ^j, Jindrich Chmelar ^k, Vilém
9 Mazák ^k, Mohammed Amine Jmel ^l, Michalis Kotsyfakis ^{lm}, José María Medina ^{no},
10 Michael Hackenberg ^{no}, Ladislav Šimo ^p, Fotini A. Koutroumpa ^q, Patrick Wincker ^b, Petr
11 Kopacek ^l, Jan Perner ^l, Jean-Marc Aury ^b, Claude Rispe ^a *

12
13 ^a Oniris, INRAE, BIOEPAR, route de Gachet, 44300, Nantes, France. ^b Génomique
14 Métabolique, Genoscope, Institut François Jacob, CEA, CNRS, Univ Evry, Université
15 Paris-Saclay, Evry, 91057, France. ^c BIPAA, IGEPP, INRAE, Institut Agro, University of
16 Rennes, Rennes, France. ^d University of Rennes, INRIA, CNRS, IRISA, Rennes,
17 France. ^e Genoscope, Institut François Jacob, CEA, CNRS, Univ Evry, Université Paris-
18 Saclay, Evry, 91057, France. ^f Centre National de Recherche en Génomique Humaine
19 (CNRGH), Institut de Biologie François Jacob, CEA, Université Paris-Saclay, Evry,
20 France. ^g Department of Veterinary Microbiology, Western College of Veterinary
21 Medicine, University of Saskatchewan, Saskatoon, Canada. ^h Management Department
22 of Biosafety, Laboratory Animal, and Pathogen Bank National Institute of Infectious
23 Diseases 4-7-1 Gakuen, Musashimurayama, Tokyo 208-0011, Japan. ⁱ Institut
24 d'Ecologie et des Sciences de l'Environnement de Paris, Sorbonne Université, INRAE,
25 CNRS, IRD, UPEC, Paris, France. ^j Université Côte d'Azur, INRAE, CNRS, ISA, F-
26 06903 Sophia Antipolis, France. ^k Department of Medical Biology, Faculty of Science,
27 University of South Bohemia in České Budějovice, Branišovská 31, 37005, České
28 Budějovice, Czechia. ^l Institute of Parasitology, Biology Centre, Czech Academy of
29 Sciences, Branisovska 1160/31, 37005, Ceske Budejovice, Czech Republic. ^m Institute
30 of Molecular Biology and Biotechnology, Foundation for Research and Technology-
31 Hellas, N. Plastira 100, 70013, Heraklion, Crete, Greece. ⁿ Dpto. de Genética, Facultad
32 de Ciencias, Universidad de Granada, Campus de Fuentenueva s/n, 18071, Granada,
33 Spain. ^o Lab. de Bioinformática, Centro de Investigación Biomédica, PTS, Instituto de
34 Biotecnología, Avda. del Conocimiento s/n, 18100, Granada, Spain. ^p ANSES, INRAE,
35 Ecole Nationale Vétérinaire d'Alfort, UMR BIPAR, Laboratoire de Santé Animale, 22 rue
36 Pierre et Marie Curie, Maisons-Alfort, France. ^q INRAE, Université de Tours, UMR1282
37 Infectiologie et Santé Publique, 37380 Nouzilly, France.

38 * Corresponding author Claude Rispe: claude.rispe@inrae.fr

39 Abstract

40 Ticks, hematophagous acari, pose a significant threat by transmitting various pathogens
41 to their vertebrate hosts during feeding. Despite advances in tick genomics, high-quality
42 genomes were lacking until recently, particularly in the genus *Ixodes*, which includes the
43 main vectors of Lyme disease. Here, we present the complete genome sequences of
44 four tick species, derived from a single female individual, with a particular focus on the
45 European species *Ixodes ricinus*, achieving a chromosome-level assembly. Additionally,
46 draft assemblies were generated for the three other *Ixodes* species, *I. persulcatus*, *I.*
47 *pacificus* and *I. hexagonus*. The quality of the four genomes and extensive annotation
48 of several important gene families have allowed us to study the evolution of gene
49 repertoires at the level of the genus *Ixodes* and of the tick group. We have determined
50 gene families that have undergone major amplifications during the evolution of ticks,
51 while an expression atlas obtained for *I. ricinus* reveals striking patterns of specialization
52 both between and within gene families. Notably, several gene family amplifications are
53 associated with a proliferation of single-exon genes. The integration of our data with
54 existing genomes establishes a solid framework for the study of gene evolution,
55 improving our understanding of tick biology. In addition, our work lays the foundations
56 for applied research and innovative control targeting these organisms.

57 Introduction

58 Ticks are one of a few groups of arthropods that have independently evolved a unique
59 lifestyle of blood-feeding on vertebrates. Present in most terrestrial ecosystems, they
60 represent a threat to companion and farm animals and to humans by transmitting
61 diverse pathogens and parasites (Jongejan & Uilenberg 2004). For example, ticks in the
62 genus *Ixodes* transmit the spirochetes that cause Lyme borreliosis, which is the most
63 common tick-borne disease in the Northern Hemisphere.

64 Ticks evolved more than 250 million years ago (Mans et al. 2016) and belong to the
65 Parasitiformes, which together with the Acariformes form the Acari (ticks and mites), in
66 the subphylum Chelicerata. Although the Parasitiformes and Acariformes are both
67 monophyletic, the monophyletic status of the Acari has been debated and remains
68 difficult to resolve (Dunlop 2010; Sharma et al. 2014; Lozano-Fernandez et al. 2019;
69 Ballesteros et al. 2019; Zhang et al. 2019; Sharma et al. 2021). Ticks themselves clearly
70 form a monophyletic order (Ixodida), which comprises three families, the Ixodidae (hard
71 ticks), Argasidae (soft ticks) and Nuttalliellidae (Guglielmone et al. 2010; Mans et al.
72 2011, 2012, 2016). The Ixodidae are further subdivided into the Prostriata, which
73 contains the genus *Ixodes*, and the Metastriata, which includes several tick genera.

74 Throughout their history, ticks have evolved remarkable traits to ensure the success of
75 their blood-feeding lifestyle. Molecular level interactions between ticks and their hosts
76 are an essential condition for the success of the blood-feeding strategy of ticks. These
77 interactions principally take place at two host-tick interfaces, represented by the feeding
78 site in the host skin (Mans 2019) and by the ingested blood meal in the tick midgut.
79 Molecules of hosts and ticks interact at these interfaces; for example, tick compounds
80 neutralize host immune and haemostatic responses and thus facilitate tick attachment
81 and blood-feeding on the host (Medina, Jmel, et al. 2022). Tick saliva is mainly produced
82 by the tick salivary glands and facilitates tick-host interactions at the feeding site (Šimo
83 et al. 2017) whereas the tick midgut is the main organ responsible for the digestion of
84 host blood components. These two interfaces represent points of interactions between
85 tick genomes and the hemostatic and immune responses of their vertebrate hosts,
86 exerting a strong selective pressure on ticks and driving a diversification of the tick
87 genetic toolbox.

88 Gene duplication is believed to shape the major innovations in tick biology, and the
89 duplicate genes would facilitate the evolution of the metabolic potential of these
90 organisms (Mans et al. 2017). To understand the evolution of tick gene repertoires and
91 the importance of tick-specific duplications in particular, a comprehensive comparative
92 study of tick genomes is necessary, which is now possible thanks to the growing number
93 of available genome sequences both in ticks and in other Chelicerata. In comparison
94 with insects, tick genomics has developed late, due to the relatively large genome sizes
95 in this group (several times larger than most insects) (Geraci et al. 2007). The first

96 complete tick genome was published for *Ixodes scapularis* in 2016 (Gulia-Nuss et al.
97 2016), followed by the genomes of six other tick species, including *Ixodes persulcatus*
98 and five species belonging to a monophyletic group of non-*Ixodes* hard tick species,
99 known as the Metastriata (Jia et al. 2020). Two high quality genome sequences of *I.*
100 *scapularis* have been published recently (De et al. 2023; Nuss et al. 2023) that used the
101 newer generation of long-read high-throughput sequencing.

102 The purpose of our study was to improve our knowledge of tick genomics, especially in
103 the genus *Ixodes* which includes some of the most important vectors of tick-borne
104 disease in Europe, North America, and Asia. We therefore generated the genome
105 sequences and gene catalogs of four species, *I. ricinus*, *I. pacificus*, *I. persulcatus*, and
106 *I. hexagonus*. *Ixodes ricinus*, *I. pacificus*, *I. persulcatus*, and *I. scapularis* are closely
107 related to each other and are part of the *Ixodes ricinus* species complex, whereas *I.*
108 *hexagonus* represents an outgroup (Charrier et al. 2019; Keirans et al. 1999; Xu et al.
109 2003). The following species have distinct distributions: *I. scapularis* (Eastern USA), *I.*
110 *pacificus* (West-coast USA), *I. persulcatus* (Eurasian) and *I. ricinus* (Europe). This
111 ensemble could thus represent an example of vicariant species, corresponding to
112 species that have diverged from a common ancestor in different regions, where they
113 have conserved similar ecological characteristics, as found for the tick genus *Hyalomma*
114 (Sands et al. 2017). Our comprehensive study of the tick gene repertoires in a
115 comparative and phylogenetic framework provides insight into the major aspects that
116 shaped the evolution of tick genomes in the genus *Ixodes* and ticks in general, pointing
117 gene families that have evolved and expanded differently from the rest of Chelicerata,
118 or between different branches within the tick group.

119

120 Results

121 Genome assembly and annotation

122 To enhance our understanding of the genomic characteristics of ticks, particularly in the
123 genus *Ixodes*, we sequenced and assembled the genome of four species: *I. ricinus*, *I.*
124 *pacificus*, *I. persulcatus* and *I. hexagonus*. The genome sequencing for these four
125 species involved the use of linked reads (10X Genomics library sequence with Illumina
126 short-reads), and for *I. ricinus*, we also incorporated Hi-C libraries to achieve
127 chromosome-level assembly.

128 In the case of *I. ricinus*, we identified fourteen major scaffolds corresponding to 13
129 autosomes and the X sex chromosome, which totalled 93% of the total assembly (Hi-C
130 map of interaction, Fig. 1 A). This result is consistent with the established haploid
131 chromosome count of 14 for this species, as in *I. scapularis* (Oliver 1977). We therefore
132 assume that the 14 largest scaffolds of the *I. ricinus* genome, accounting for 95.2% of
133 the assembly size and 98.2% of the predicted genes, represent these 14 chromosomes.

134 By comparison, the 14 largest scaffolds of the *I. scapularis* genome (De et al. 2023)
135 represented 87.0% of the assembly size and 88.2% of the predicted genes, indicating a
136 slightly more fragmented assembly. The genome assemblies of the other three species
137 were organized by aligning them with the chromosomal structure of *I. ricinus*. Standard
138 metrics of the four *Ixodes* genome assemblies sequenced in the present study are given
139 in Table 1.

140 The four genome assemblies were annotated, and genes were predicted by using
141 homologies with proteins of closely related species and RNA-Seq data. Manual curation
142 was performed exclusively for *I. ricinus* resulting in the OGS1.1 gene catalog, which
143 resulted in the correction of 1,569 genes (see supplementary Table S1). The most
144 notable change was the prediction of 500 entirely new gene models (supplementary
145 Table S2). The completeness (% of complete BUSCOs) of the four new gene catalogs
146 generated in this study fell within the range of recently sequenced tick genomes as
147 shown in Table 2. Completeness was lowest in *I. pacificus* (81%), and highest in *I.*
148 *ricinus* and *I. hexagonus* (about 91%), which is somewhat lower than the 98% observed
149 for the recently improved genome of *I. scapularis* (De et al. 2023). For *I. pacificus*, we
150 also note a relatively high percentage of “duplicated” genes in the BUSCO analysis,
151 suggesting that heterozygosity might have not been fully resolved and that our assembly
152 still contains duplicate alleles, which is supported by the higher heterozygosity estimate
153 for this genome (supplementary Fig. S1). Finally, two tick genomes from another study
154 (Jia et al. 2020), *Hyalomma asiaticum* and *Haemaphysalis longicornis*, showed
155 significantly lower completeness (65% and 56% of complete BUSCOs, respectively),
156 whereas the completeness for *I. persulcatus* in that study was lower compared to our
157 study (79.6% versus 88.0%). For subsequent analyses involving *I. persulcatus*, we
158 utilized our assembly as the reference genome.

159

160 **Transposable elements in ticks**

161 In *I. ricinus*, *I. hexagonus*, *I. pacificus* and *I. persulcatus*, repeated elements represented
162 between 57.3% (*I. ricinus*) and 67.9% (*I. hexagonus*) of the genome, the majority being
163 transposable elements (Table 3). Most of the transposable elements (TEs) identified are
164 unclassified (79.83% of the total elements, and covering ~43% of the tick genomes).
165 The most abundant TEs found in these tick species were long interspersed nuclear
166 elements (LINEs), with 397,287 elements on average (~7% of the elements identified).
167 Interspersed sequences represented only 9.5% of the genome of *Amblyomma*
168 *maculatum* (Ribeiro et al. 2023), whereas they accounted for over 50% of the genome
169 of all *Ixodes* ticks. However, the relative frequencies of each TE family were similar
170 between the genomes of *A. maculatum* (Jose M. C. Ribeiro et al. 2023) and *I. scapularis*
171 (De et al. 2023). For example, the Gypsy/DIRS family in the long terminal repeat (LTR)
172 class has one of the highest coverages in both *A. maculatum* (Ribeiro et al 2023) and *I.*

173 *scapularis*, (Nuss et al 2023, De et al 2023), and represent ~5% of the genome in the
174 four *Ixodes* species sequenced in the present study.

175 Interestingly, Bov-B LINE retrotransposons were found in our tick genomes: 160
176 elements in *I. persulcatus*, 155 in *I. ricinus*, 1 in *I. pacificus*, and none in *I. hexagonus*
177 (see Discussion).

178

179 **Macro-syntenies between hard ticks**

180 The genomes of *I. ricinus* and *I. scapularis* were found to be largely syntenic (Fig. 1 B).
181 Comparison of these two tick species suggests very little gene shuffling (homologous
182 genes remained in the same blocks). However, the length of the largest scaffolds
183 (chromosomes) varied between the two species and their ranking in size was slightly
184 different. These differences may be due to different amounts of repeated elements,
185 and/or to the state of assembly of these elements. We note that the sequence
186 NW_0240609873.1 representing the 15th largest scaffold in *I. scapularis* was included
187 in scaffold 7 of *I. ricinus*. Conversely, scaffold 15 from *I. ricinus* matched with
188 NW_0240609883.1, the 8th largest scaffold from *I. scapularis*). In both species, the
189 smaller scaffolds that were not included in the 14 putative chromosomes were relatively
190 gene poor and could correspond to regions with a high proportion of repeated elements,
191 which are difficult to assemble. The plot comparing the two genome assemblies
192 (supplementary Fig. S2 A) indicated several inversions (especially for scaffolds 1 and 6
193 of *I. ricinus*). It was not possible to determine whether these inversions are real or the
194 result of post-assembly errors. The comparison between *I. ricinus* and *Dermacentor*
195 *silvarum* also revealed the correspondence of major scaffolds between the two
196 assemblies (supplementary Fig. S2 B). *Dermacentor silvarum* has 11 major scaffolds,
197 which corresponds to its chromosomal number. Despite a low level of micro-synteny,
198 there was a substantial proportion of shared content in the chromosomes, with eight
199 exact matches between chromosomes of these two tick species. In addition, scaffold
200 NC_051157.2 of *D. silvarum* had non-overlapping matches with scaffolds 3 and 14 of *I.*
201 *ricinus*, *D. silvarum* scaffold NC_051154.1 matched with scaffolds 6 and 12 of *I. ricinus*,
202 and *D. silvarum* scaffold NC_051155.1 matched with scaffolds 7 and 11 of *I. ricinus*.
203 Thus, depending on the ancestral karyotype, there were only three chromosome fission
204 or fusion events in the two branches leading from a common ancestor to the two extant
205 species, after which macro-synteny remained remarkably stable. In the two comparisons
206 (*I. ricinus* versus *I. scapularis* and *I. ricinus* versus *D. silvarum*) we did not observe
207 evidence of multiple regions from one species matching two different regions from the
208 other species. This indirectly suggests that no large-scale duplication events occurred
209 in a common ancestor of ticks.

210

211 **Gene families in ticks and the Chelicerata**

212 Analysis of 497,214 protein sequences from 21 species of Chelicerata, including 11 tick
213 species, resulted in 11,331 gene families comprising a total of 332,365 protein
214 sequences (supplementary Table S3). For some gene families, we found unexpected
215 large differences in gene abundance even among closely related tick species. These
216 gene families with differential gene abundance were associated with gene ontology
217 (GO) terms (or domains, result not shown) typically indicating transposable elements.
218 For example, gene family FAM0000061 had 6,896 genes in the spider *Trichonephila*
219 *clavata* versus 0 genes in some of the Acari genomes, and 1,266 genes in *I. scapularis*
220 but only 113 in *I. ricinus* (supplementary Table S4). Gene annotation strategies may
221 differ among genomes with respect to the masking of repeated regions and hence the
222 putative TEs. For the subsequent analyses on gene family evolution, we therefore
223 masked gene families with typical transposon domains (e.g. reverse transcriptase,
224 transposase, recombination activating gene) and gene families with atypical size
225 variation - families where the number of genes in *I. scapularis* was more than five times
226 that of *I. ricinus*. The resulting distribution of gene families is illustrated in Fig. 2, showing
227 for example that 620 families were present in each of the 21 species analyzed, whereas
228 139 families were present in all 11 tick species, but in none of the other species.

229

230 **Phylogeny based on single copy orthologs**

231 Our phylogenetic tree based on 107 single-copy orthologs (Fig. 3) showed high support
232 for the Acari (Parasitiformes and Acariformes) being a monophyletic group. Whether the
233 Acari are a monophyletic group has been debated in the recent literature (Lozano-
234 Fernandez et al. 2019; Zhang et al. 2019; Van Dam et al. 2019). This question, which
235 was not central to our study, will need more complete sequence data to be fully resolved,
236 especially regarding taxon sampling and filtering of sites/genes. The grouping of the
237 Mesostigmata with the Ixodida, and the monophyletic grouping of ticks were both
238 strongly supported, confirming all previous phylogenetic analyses, and this was the main
239 justification for our comparison of gene family dynamics in ticks. Within the Ixodidae
240 (hard ticks), the phylogenetic relationships in our study are consistent with recent studies
241 based on transcriptomes (Charrier et al. 2019) or whole genomes (Jia et al. 2020). Our
242 study confirms that the group of four species belonging to the *Ixodes ricinus* species
243 complex are very close genetically. Within the genus *Ixodes*, an analysis based on a
244 higher number of shared sequences allowed us to obtain a finer resolution of the
245 phylogenetic relationships (supplementary Fig. S3). The unrooted tree showed that *I.*
246 *ricinus* and *I. persulcatus* are sister clades, as are *I. scapularis* and *I. pacificus*. The first
247 and second species pairs are found in Eurasia and North America, respectively, which
248 suggests a pattern of phylogeographic divergence. We note however that these four
249 species diverged at nearly the same time.

250

251 **Dynamics of gene family expansions in ticks**

252 To analyze gene gain/loss dynamics across Chelicerata species, we ran CAFE5 (v5.0),
253 using a lambda of 0.451 predicted from a first round of Base model. This program filtered
254 gene families not present at the root of the tree, and retained 4,525 gene families, of
255 which 497 gene families were found to be either significantly expanded or contracted
256 during the evolution of the Chelicerata. Gene family expansions and contractions were
257 quantified on each branch of the phylogenetic tree of Chelicerata (Fig. 4 and Fig. 5).

258 Expanded gene families in the *Ixodidae* included were involved in lipid metabolism and
259 xenobiotic detoxification (Fig. 5 C). The principal GO terms for molecular functions
260 associated with tick expansions were heme binding, transferase, hydrolase,
261 oxidoreductase, metalloendopeptidase/protease and transmembrane transporter
262 activities. The list of the significantly expanded gene families in ticks (supplementary
263 Table S5) shows that some of the most important expansions during the evolution of
264 ticks concern genes associated with detoxification processes, for example cytosolic
265 sulfotransferases (SULTs), carboxylesterases, and Glutathione S-transferases (see
266 below for more detailed analyses). Other important gene family expansions include
267 genes known for their importance in tick metabolism such as metallopeptidases, or
268 serpins. Other gene family expansions were unexpected and not previously described,
269 such as acylcoA synthases and fatty acid elongases.

270 The number of gene families gained per branch was also estimated by summing all gene
271 families present in a specific clade but absent from species outside of this clade. We
272 identified 406 gene families that were gained in the common ancestor of ticks (i.e., these
273 gene families were absent in all other Chelicerata, Fig. 5 B). These results must be
274 interpreted with caution; we noted that the largest gene family in this category,
275 FAM007521, contains genes annotated as tumor necrosis factor receptor (TNFR)-
276 associated factors (TRAF), which are widespread in the Metazoa. Tick genes from this
277 family show a low level of conservation since best hits have ~25% identities in BlastP
278 comparisons with non-tick organisms. This suggests that this gene family contains
279 highly divergent genes and would explain why this gene family did not have any potential
280 orthologs in the Chelicerata.

281

282 **Structure of genes, importance of mono-exonic genes**

283 As many as 20.7% of genes in *I. ricinus* were predicted to be mono-exonic. This result
284 is interesting because in eukaryotic genomes mono-exonic genes are usually at much
285 lower frequencies. The percentage of mono-exonic genes was high in gene families
286 tagged as putative TEs (35% on average in families containing > 10 genes in *I. ricinus*),
287 but with a large range (0% to 86%). The percentage of mono-exonic genes was also

288 high in other gene families (18% for families containing > 10 genes in *I. ricinus*), again
289 with a large range (0% to 100%). Some of the gene families with high a percentage of
290 mono-exonic genes corresponded to the most expanded gene families in ticks, such as
291 the fatty acid elongases (FAM002111, 82%), cytosolic sulfotransferases (FAM000226,
292 52%), serpins (FAM001806, 45%), and M13 metallopeptidases (FAM000666, 34%),
293 suggesting that a proliferation of mono-exonic genes contributed to tick-specific gene
294 family expansions. However, other large gene families had few or no mono-exonic
295 copies, such as the MFS transporters (FAM000149).

296

297 **Structural and regulatory non-coding elements**

298 Extensive analysis to identify and annotate putative structural and regulatory non-coding
299 elements in the *I. ricinus* genome revealed a total of 21,792 non-coding RNAs (ncRNAs)
300 and cis-regulatory elements, including small nuclear RNAs, small nucleolar RNAs,
301 ribosomal RNAs, long non-coding RNAs (lncRNAs), transfer RNAs, microRNAs,
302 ribozymes or riboswitches, among others (Table 4). Annotating the lncRNAs was difficult
303 due to the paucity of information on lncRNAs in the species studied here and the lack of
304 previous complete annotation of lncRNAs in *I. ricinus*. To accurately annotate the
305 lncRNAs, we used a published lncRNA dataset that included both putative and
306 consensus lncRNAs for *I. ricinus* (Medina, Abbas, et al. 2022). Consensus lncRNAs
307 from this dataset were considered as high-confidence annotations. Before aligning the
308 putative lncRNAs to our *I. ricinus* genome, we confirmed their non-coding properties.
309 We identified 13,287 lncRNAs with alignment scores above 90, indicating significant
310 matches with the genome. To ensure the reliability of our results, we deleted 2,591
311 lncRNAs that showed overlap with coding RNAs. As a result, we annotated a total of
312 10,696 lncRNAs in the *I. ricinus* genome, of which 2,433 were classified as high
313 confidence lncRNAs. Our annotation and characterization of ncRNAs and cis-regulatory
314 elements in the *I. ricinus* genome therefore contributes to a comprehensive view of the
315 structural and regulatory non-coding elements of this species.

316

317 **Neuropeptides in the *I. ricinus* genome**

318 A total of 41 different orthologs of invertebrate neuropeptide genes were found in the *I.*
319 *ricinus* genome (supplementary Table S6). Including protein isoforms, 45 neuropeptide
320 precursors contain more than 100 active peptide forms (supplementary Fig. S4). Most
321 of the neuropeptides identified in *I. ricinus* have clear counterparts in other hard tick
322 species (Donohue et al. 2010; Waldman et al. 2022), whereas agotoxin-like peptide and
323 IDLSRF-like peptide were identified for the first time in ticks in the current study.
324 Interestingly, the precursors of ecdysis triggering hormone, which occurs in the tick
325 *Rhipicephalus microplus* (Waldman et al. 2022) and neuropeptide F found in some hard

326 ticks were not detected in the genome of *I. ricinus*. Similarly, the pigment dispersing
327 factor (PDF), which is common in insects and some Chelicerata, was not identified.

328

329 **Tick cystatins and Kunitz-domain proteins**

330 The cystatins are a family of cysteine protease inhibitors. Iristatin has been
331 characterized as a secreted immunomodulator from tick salivary glands found at the
332 tick-host interface (PMID: 30747251, (Kotál et al. 2019)). Our phylogenetic analysis of
333 these gene families (supplementary Fig. S5) found independent expansions of cystatins
334 in *I. scapularis* (ISCP_027970 clade) and *I. hexagonus* (Ihex00005714 clade) and
335 expansions of iristatins in both *I. pacificus* and *I. ricinus*, suggesting that these gene
336 family expansions were important for the biology of these species. In terms of gene
337 structure, the cystatins and iristatins have a typical three-exon structure, and they are
338 principally clustered in two genomic regions on scaffold 3 and scaffold 9, respectively
339 (detailed list provided in supplementary Table S7A). Cystatins correspond to family
340 FAM006825 in the SiLiX analysis, which expanded significantly in the common ancestor
341 of ticks, but not in branches deriving from this node (supplementary Table S5). Iristatins
342 have high expression either in hemocytes, or in ovaries, malpighian tissues, salivary
343 glands, and synganglion respectively (supplementary Fig. S6).

344 Tick Kunitz-domain proteins constitute a major group of serine protease inhibitors that
345 function in blood feeding (Jmel et al. 2023). Kunitz-type inhibitors are divided into
346 subgroups based on the number of Kunitz domains, which varies from one to five and
347 defines the monolaris, bilaris, trilaris, tetralaris and penthalaris groups, respectively. The
348 numbers of Kunitz-type inhibitors in each category were quite variable (detailed list in
349 supplementary Table S7 B), even among closely related species within the genus
350 *Ixodes* (supplementary Table S7 C). The most and least abundant categories were the
351 monolaris and trilaris, respectively. Several species-specific expansion events in the
352 monolaris family (supplementary Fig. S7 A) were observed in the genomes of *I.
353 scapularis* and *I. ricinus*, and to a lesser extent in the other species. The bilaris family,
354 which is the second most abundant group, and includes two well-studied genes
355 *Boophilin* and *Ixolaris*, showed few species-specific expansions (supplementary Fig. S7
356 B), with the exception of an expansion of *Ixolaris*-like genes in *I. scapularis*. *Ixolaris* has
357 been characterized as a tick salivary anticoagulant localized at the tick-host interface
358 (Francischetti et al. 2002; Nazareth et al. 2006; De Paula et al. 2019), and our phylogeny
359 indicates that *I. scapularis* has five similar gene copies in its genome. Phylogenies for
360 the trilaris, tetralaris, and penthalaris groups are available in supplementary Fig. S7 C,
361 D, E). By contrast with other gene groups analyzed in this study, determining groups of
362 orthologs for Kunitz-domain proteins within the genus *Ixodes* was difficult, due to a
363 patchy representation of arthropod species in each gene family, and unequal patterns
364 of gene duplication. This could be explained by highly dynamic evolution of this gene

365 family, and high sequence divergence. Alternatively, incomplete annotation in the
366 different arthropod species could also be a factor, given the structure of these genes;
367 most sequences (especially in the monolaris group) are short with ~80 residues and
368 have a typical 4-exon structure with some of the exons being very short). For the three
369 species that were not manually curated in our study or for other tick species, annotation
370 might not be complete and correct. Finally, we note that the automatic clustering by
371 SiLiX assigned most of the Kunitz peptides from the five groups into a single family
372 (FAM000015), which significantly expanded in *Ixodes* ticks, but not in their common
373 ancestor. In summary, Kunitz-domain proteins exhibit dynamic evolution in ticks and
374 other groups in the Chelicerata.

375

376 **Serpins**

377 Serpins are protease inhibitors involved in the regulation of many physiological
378 processes in vertebrates and invertebrates (Huntington 2011), and even viruses
379 (Spence et al. 2021). In ticks, serpins are salivary components responsible for anti-
380 hemostatic, anti-inflammatory and immunomodulatory effects in the vertebrate host
381 (Abbas et al. 2022). Serpins from *I. ricinus* can be divided into two groups, Iripins (*I.*
382 *ricinus* serpins) and IRIS-like serpins, which refers to the first described tick serpin IRIS
383 (Leboulle et al. 2002). Iripins bear signal peptides and are secreted from the cell,
384 whereas IRIS-like serpins are most likely intracellular or secreted non-canonically. A
385 total of 61 Iripins and 21 IRIS-like serpin sequences were found in the genome of *I.*
386 *ricinus*. Gene expression differed among tick tissues and the number of exons ranged
387 from 1 to 7 (supplementary Table S8). Serpins were generally classified in the same
388 SiLiX family (FAM001806), which was significantly expanded in the common tick
389 ancestor. Our phylogenetic analysis found several clades of Iripins and one clade of
390 IRIS genes (Fig. 6 B), in agreement with a previous phylogenetic study (Spence et al.
391 2021). Several serpins form clusters of closely related genes in the genome, suggesting
392 they have arisen through tandem duplication (e.g., a cluster of 22 Iripins within a region
393 of 600 Kbp on scaffold 14 of the *I. ricinus* genome, whereas most IRIS serpins form a
394 cluster on scaffold 9). Mono-exonic genes were common in the Iripins (53% were
395 intronless), whereas three other Iripins only had two exons, the first one being 5'
396 untranslated region (UTR) only. This gene structure suggests initial events of
397 retroposition, followed by re-exonization of some genes, in addition to tandem
398 duplication. Some serpins are expressed constitutively, while others are upregulated or
399 downregulated by the blood meal (Fig. 6 A). Many serpin genes, especially mono-exonic
400 ones, had no or negligible levels of gene expression, which could explain why they were
401 not found in transcriptomic studies. By contrast, the most highly expressed serpins, such
402 as Iripin-01, -02, -03, -05 and -08 and IRIS-1, have been previously studied and
403 characterized as anti-hemostatic, anti-inflammatory and/or immunomodulatory proteins
404 (Leboulle et al. 2002; Chmelar et al. 2011; Chlastáková et al. 2021, 2023; Kascakova et

405 al. 2021, 2023; Kotál et al. 2021). High numbers of silent serpins located in clusters on
406 the tick genome suggest high rates of gene duplication and gene recombination for this
407 gene family. Highly dynamic gene families can generate new gene copies that are
408 redundant with older ones and that will ultimately be eliminated by selection. Such a
409 scenario would fit with low or no gene expression, and we tagged 14 of the serpins as
410 potential pseudogenes, based on the absence of expression and their incomplete gene
411 model. However, some of the newly generated serpin copies may undergo mutations,
412 be positively selected, and lead to new serpins with novel functions.

413

414 **Incomplete heme pathways and heme-independent iron inter-tissue trafficking**

415 Heme is an essential molecule for living organisms, involved in multiple processes, and
416 necessary for successful reproduction in ticks (Perner, Sobotka, et al. 2016). The *I.*
417 *ricinus* genome only contains genes coding for the last three enzymes of the heme
418 biosynthetic pathway: *cpxo*, *ppox*, and *fech*, which code for coproporphyrinogen
419 oxidase, protoporphyrinogen oxidase, and ferrochelatase, respectively. Ticks from the
420 Metastriata group have lost the *cpxo* gene (Fig. 7, supplementary Fig. S8). Finally, soft
421 ticks in the genus *Ornithodoros* have *cpxo*, *ppbox* and *fetch* but also carry the conserved
422 genes *pbgs* and *urod*, which code for porphobilinogen synthase and uroporphyrinogen
423 decarboxylase (supplementary Table S9 and supplementary Fig. S8). The absence of
424 several genes in the heme pathway strongly suggests a loss of heme biosynthetic
425 activity in all ticks, implying they only obtain haem from the blood meal, which agrees
426 with previous studies on *I. ricinus* and other tick species (Perner, Sobotka, et al. 2016;
427 Perner, Provažník, et al. 2016; Perner et al. 2019; Jia et al. 2020). The heme pathway
428 genes *cpxo*, *ppox*, and *fech*, have tissue-specific patterns of expression (Perner,
429 Sobotka, et al. 2016), suggesting functional transcripts. The function of these three
430 proteins remains elusive, but the retention of their mitochondrial target sequence
431 indicates a function in mitochondrial biology (Fig. 7). Finally, no sequence homologous
432 to heme oxygenase was found in ticks, nor in other Chelicerata, as shown by the
433 metabolic pathway reconstructed for porphyrin metabolism (supplementary Fig. S8).

434 Ferritins are an essential actor of iron metabolism in ticks. Unlike in other arthropods,
435 the absence of heme oxygenase in ticks means that iron homeostasis is indeed
436 decoupled from haem homeostasis, and is only ensured by these cytosolic proteins that
437 store iron. Our study confirms previous findings that ticks genomes contain two ferritin
438 genes (Hajdusek et al. 2009) that respectively encode for intracellular Ferritin 1 (without
439 a signal peptide) and secretory Ferritin 2 (with a signal peptide). The sequence of the
440 *ferritin 1* gene is preceded (5'UTR to the gene sequence) by a regulatory region called
441 the iron responsive element (IRE) (Kopáček et al. 2003) (Fig. 7). Both tick ferritins fold
442 into conserved four-helix bundle monomers that self-assemble into higher-order 24-
443 homomeric structures (Fig. 7). The mechanisms of cellular export of tick Ferritin 2

444 nanocages (Oh & Jung 2023) or their uptake by peripheral tissues remains unknown.
445 The presence of two types of ferritin, allows ticks to store intracellular iron in tissues
446 using Ferritin 1, and traffic non-haem iron between tissues using Ferritin 2 (Perner et al.
447 2022). Binding of the iron regulatory protein to the IRE prevents expression of Ferritin 1
448 under low iron conditions (Perner, Sobotka, et al. 2016; Hajdusek et al. 2009). While
449 these ferritin cages are often several nanometers in diameter, the secretory Ferritin 2
450 was identified within larger (~ 100 nm) hemolymphatic extracellular vesicles in
451 *Rhipicephalus haemaphysaloides* and *Hya. asiaticum* ticks (Xu et al. 2023).

452

453 **Metallopeptidases**

454 The M13 metalloproteases are ubiquitous in bacteria and animals, indicating their
455 evolutionary significance. Mammalian M13 metalloproteases, exemplified by neprilysin,
456 consist of a short N-terminal cytoplasmic domain, a single transmembrane helix, and a
457 larger C-terminal extracellular domain containing the active site. Invertebrate M13
458 metalloproteases include transmembrane proteins, and secreted soluble proteins
459 (Meyer et al. 2021). Some invertebrate genomes have expanded gene copies for M13
460 metalloproteases, but most of them are secreted and catalytically inactive (Meyer et al.
461 2021; Bland et al. 2008). We screened the *I. ricinus* genome to assess the expansion
462 history of the M13 metalloprotease-encoding genes. We identified 88 genes, which is
463 one of the largest recorded expansions of this gene family. The M13 gene family
464 (FAM000666 according to the SiLix clustering) was the second most-expanded gene
465 family in ticks compared to other Chelicerata and was identified as significantly
466 expanded (CAFE analysis) in both the common ancestor of all ticks, and in the common
467 ancestor of the Metastriata. This reflects even larger numbers of gene copies in the non-
468 *Ixodes* species of hard ticks (~130 in *Rhipicephalus*, and ~220 in *Dermacentor* versus
469 ~90 in *Ixodes* species). The genes display diverse exon arrangements (supplementary
470 Fig. S9); most of the multi-exonic genes are expressed in salivary glands or synganglia,
471 whereas most of the mono-exonic genes are transcribed in tick ovaries (supplementary
472 Fig. S9). To predict conservation of protein functions, we searched for protein motifs
473 known to be important for zinc ion binding (HExxH), protein folding (CxxW), and
474 substrate binding (NA(F/K)Y) (Meyer et al. 2021). The very diverse combinations of
475 conserved/substituted residues among the whole collection of sequences present in the
476 *I. ricinus* genome suggests a full spectrum of proteins with diverse functions, including
477 neo-functionalized proteins, possible scavengers and inactive enzymes. The
478 conservation of the zinc-binding motif is always coupled with a secretion signal peptide,
479 and not with transmembrane domains. Also, proteins containing conserved active
480 domains often have low expression in the tick tissues, suggesting that these proteins
481 play discrete functions across multiple tissues. The functions of highly expressed,
482 possibly inactive, M13 homologs in ticks are currently unknown.

483

484 **Gustatory receptors and ionotropic receptors for chemosensation**

485 Non-insect arthropods, including ticks, use two major gene families for chemosensation,
486 gustatory receptors (GRs) (Robertson et al. 2003) and ionotropic receptors (IRs) (Rytz
487 et al. 2013). The IRs are involved in the perception of both volatile odorants and tastes
488 (Joseph & Carlson 2015). Ticks possess olfactory receptors that are part of the IR family
489 and gustatory receptors that are part of either the IR family or the distinct GR family.
490 Insects possess a third family of chemoreceptors, odorant receptors (ORs), which
491 probably evolved in ancient insects from GRs (Missbach et al. 2014). While ticks seem
492 to lack homologs of the insect ORs, their IRs and GRs are related to the insect IRs and
493 GRs, respectively (Eyun et al. 2017). Arthropod chemosensory receptors are
494 characterized by high sequence divergence, gene duplication, and gene loss
495 (Robertson et al. 2003; Robertson & Wanner 2006; McBride 2007; McBride & Arguello
496 2007). This has been well demonstrated in insect groups for which a large number of
497 species genomes have been sequenced and annotated. For this reason, annotation of
498 tick chemoreceptors also requires careful curation, which we performed here for *I.*
499 *ricinus*.

500 The *I. ricinus* genome contains 159 IR and 71 GR genes, whereas 125 IR and 63 GR
501 genes have been described for *I. scapularis* (Josek et al. 2018) (Table 5). For *I. ricinus*,
502 65 of the 90 full-length IRs (72.2%), and 10 of the 51 full-length GRs (19.6%) were
503 intronless. Acari GRs are highly divergent including the most functionally and genetically
504 conserved GRs in insects, such as the receptors that detect sugar, fructose, carbon
505 dioxide (CO₂) and bitter taste (Kent & Robertson 2009; Shim et al. 2015; Kumar et al.
506 2020). Consequently, our phylogenetic studies only included sequences from the
507 closely related *I. scapularis*, and the predatory phytoseid mite, *Galendromus*
508 *occidentalis*. We identified three clades of GRs in the Acari (Fig. 8 A), one clade was
509 specific to *G. occidentalis* and another to ticks, and both clades showed relatively large
510 group-specific gene expansions. A third clade contained sequences from both mites and
511 ticks, suggesting that it represents more conserved sequences. Several (but not all) of
512 the *I. ricinus* gene copies in this third clade were intronless, suggesting retroposition
513 events. The fact that the *G. occidentalis* homologs are all multi-exonic in this clade
514 suggests that the multi-exonic status was ancestral, and that independent retroposition
515 events occurred repeatedly in *I. ricinus*. For both GRs and IRs, we most often identified
516 co-orthologs between *I. ricinus* and *I. scapularis*, although some expected orthologs
517 were absent, or there were specific amplifications (e.g., there were 6 copies of a gene
518 in *I. ricinus* that was co-orthologous to IscaGR13F in *I. scapularis*). We note that these
519 differences may result from incomplete annotation in either species.

520 The phylogenetic study of IRs also found several clades based on gene structure and
521 conservation (Fig. 8 B). A large clade of sequences was found only in *Ixodes* spp., all of

522 which were intronless. A second large clade contained sequences from both the mite
523 *G. occidentalis* and *Ixodes* spp. (all multi-exonic). Another 5 IR sequences of *I. ricinus*
524 were found in clades more conserved between insects and Acari. In a separate
525 phylogenetic analysis, we compared only these 'conserved' IRs between insects and
526 Acari (supplementary Fig. S10), which allowed us to identify orthologs in *I. ricinus* for two
527 IR coreceptors, IR25a and IR93a, which are conserved in all arthropods. Interestingly,
528 IR25a and IR93a were co-linear in the genomes of arachnids, such as *I. ricinus*, *I.*
529 *scapularis*, *G. occidentalis* (mite), and *Argiope bruennichi* (spider), but not in
530 Lepidopteran insects, such as *Spodoptera littoralis* (Meslin et al. 2022) and *Heliconius*
531 *melpomene* (van Schooten et al. 2016) (not shown). We also found a pair of closely
532 related sequences, IR101 and IR102, which cluster with the IR93a and IR76b clades
533 (being basal to this group of sequences), and could therefore function as co-receptors
534 in ticks. Finally, another sequence, IR103, was distantly related to the *D. melanogaster*
535 IR proteins that detect humidity, heat, ammonia or amines (Min et al. 2013; Hussain et
536 al. 2016; Knecht et al. 2016, 2017). These stimuli are known attractants for
537 hematophagous (blood feeding) arthropods and are potentially important for the biology
538 of *I. ricinus*. We note that homologs of IR103 in *G. occidentalis* have undergone multiple
539 duplications. Due to their fast evolution, our SiLiX clustering divided the IR and GR
540 families into several gene families, and some of these contained only tick sequences.
541 This was especially the case for the more divergent mono-exonic clades (e.g.
542 FAM013836, FAM015933, FAM021535 for IRs). However, the majority of multi-exonic
543 IR sequences were contained in one gene family (FAM000240), which was classified as
544 significantly expanded in the tick common ancestor. In summary, we found strong
545 evidence of expansion of GR and IR genes in ticks. Detailed lists for GRs and IRs are
546 given in supplementary Tables S10 and S11, respectively.

547

548 **Defensins**

549 Defensins are small cationic antimicrobial peptides (AMPs) that are part of the innate
550 immune system in both hard and soft tick species (Kopácek et al. 2010; Wu et al. 2022).
551 A characteristic feature of these secreted effector molecules is their small molecular size
552 of about 4 kDa and the conserved pattern of six cysteine residues forming three
553 intrachain disulfide bridges (Wang & Zhu 2011). Two types of defensin-related genes
554 were considered, prepro-defensins and defensin-like peptides. Prepro-defensins were
555 defined using three criteria for canonical tick defensins: (i) conserved pattern of cysteine
556 residues in the C-terminal part of the molecule, (ii) presence of the furin cleavage motif
557 (R)VRR, and (iii) mature peptide of ~4 kDa. Sequences that differed in any of these
558 criteria were termed defensin-like peptides. With these criteria, we identified 14 genes
559 encoding prepro-defensins 1-14 (def1-14), and 8 defensin-like peptides (DLP1-8). Most
560 prepro-defensins (def1-12) were located in a cluster (range 28 Mbp) on scaffold 7, while
561 the two remaining sequences (def13-14) were on scaffold 9, and adjacent. For the

562 DLPs, 3 sequences (DLP1-3) were located on scaffold 7, in the same cluster as def1-
563 12, while the other DLPs were located on scaffold 6 (supplementary Table S12). The
564 absence of intron-less copies in this gene family suggests repeated tandem duplications
565 without retroposition events, unlike other gene families. This is also supported by the
566 fact that closely related sequences in our phylogeny are genes that are physically close
567 in the genome as for example DLP4-8 (supplementary Fig. S11). Ortholog groups within
568 *Ixodes* species were not easy to determine from our phylogeny because there were
569 many 'gaps' (subclades where one or more of the five *Ixodes* species were missing),
570 which could be explained by either gene loss/expansion or incomplete annotation (an
571 increased risk for these very short peptides, with a three- or four-exon structure). The
572 predicted mature peptides of DLP1 and DLP2 have only four conserved cysteine
573 residues, while *DLP3* encodes a mature defensin with an extended C-terminal portion,
574 and the *DLP8* gene sequence is longer due to an internal insertion (Fig. 9 A). The
575 sequences of DLP4-7 lack furin cleavage motifs, but both canonical defensins and DLPs
576 contain an N-terminal signal peptide, indicating that they are secreted peptides.
577 Defensins def1 and def3 (which have identical amino acid sequences) were by far the
578 most expressed genes in this family, especially in the hemocytes and midgut of fed ticks
579 (Fig. 9 B). Most defensins were more expressed in the hemocytes than in other tick
580 tissues. Exceptions included def2 and def4 (which differ only in their prepro-domains but
581 have identical mature sequences) that were preferentially expressed in the fat body-
582 trachea complex, def13 was more expressed in the salivary glands of fed ticks, DLP3
583 was more expressed in the ovaries of fed ticks, and DLP1,2 and 7 were more expressed
584 in the synganglion of males.

585

586 **Tick gene repertoires for detoxification**

587 Ticks, like other arthropods, have developed a variety of mechanisms to cope with a
588 wide range of endogenous or exogenous compounds. Detoxification processes occur in
589 three main phases (Després et al. 2007). In phase 1, toxic substances are chemically
590 modified to make them more reactive. In phase 2, metabolites are conjugated to
591 hydrophilic molecules to facilitate their excretion. In phase 3, conjugated metabolites are
592 transported out of the cells. Phase 1 typically involves cytochromes P450 (CYPs) and
593 carboxylesterases (CCEs), while phase 2 mainly involves glutathione S-transferases
594 (GSTs), UDP-glycosyltransferases (UGTs) and cytosolic sulfotransferases (SULTs).
595 Phase 3 is carried out by cellular transporters, such as ATP-binding cassette (ABC)
596 transporters, which use the energy from ATP breakdown to transport molecules across
597 lipid membranes. CYPs and CCEs are involved in various physiological processes such
598 as digestion, reproduction, behavioral regulation, hormone biosynthesis, xenobiotic
599 detoxification, and insecticide and acaricide resistance (Oakeshott et al. 2005; Rewitz
600 et al. 2006; Beugnet & Franc 2012; Nauen et al. 2022). Of note, in *I. ricinus*, transcripts

601 for several phase 2 detoxification enzymes were shown to be regulated by ingested
602 heme from the host blood meal (Perner, Provažník, et al. 2016).

603 The *I. ricinus* genome contains all components of the classical three-phase
604 detoxification system. We did not find homologs for UGTs in the tick genomes, which
605 agrees with the demonstrated loss of this gene family in the common ancestor of the
606 Chelicerata (Ahn et al. 2014). A summary of gene counts is given in Table 6 and detailed
607 lists of genes are given for CYPs, CCEs, GSTs, SULTs, and ABCs (supplementary
608 Tables S13 and S17, respectively).

609

610 **Cytochrome P450s:** A total of 194 CYP genes were identified in *I. ricinus*, including
611 131 complete open reading frames (ORFs). The IricCYPs were all named following the
612 Nelson nomenclature (Dr D. Nelson, University of Tennessee Health Science Center,
613 Memphis). The number of IricCYPs and their distribution into five clans is similar to that
614 of *I. scapularis* (Dermauw et al. 2020), in line with the fact that many of the genes are
615 one-to-one orthologs in both species (supplementary Fig. S12). Three members of the
616 mitochondrial clan (CYP302A, CYP314A and CYP315A) involved in ecdysteroid
617 biosynthesis have orthologs in mites and ticks as well as in insects and crustaceans
618 (Dermauw et al. 2020). In mites and ticks, clan 2 genes have been implicated in pesticide
619 detoxification, especially when expressed in the midgut (De Rouck et al. 2023). In *I.*
620 *ricinus*, four CYP families (3001B, 3001M, 3001N and 3003A) of clan 2 are clustered in
621 tandem duplications, each at different locations, that are also rich in other detoxification
622 gene families (CCEs, SULTs, ABCs). A cluster of 21 CYPs from clan 3 was found on
623 scaffold 13 with genes from CYP3009 (A, B and D) and from CYP3006 (E, F and G),
624 some of which are highly expressed in the midgut of unfed ticks, whereas other groups
625 of genes had high gene expression in other tissues or stages, especially eggs or larvae
626 (supplementary Fig. S13). Six SULT genes were also found at this location on scaffold
627 13, as well as 2 ABC transporters, suggesting a possible role of this cluster in xenobiotic
628 detoxification. The CYPs essentially corresponded to the SiLiX family FAM000045,
629 which was found to be significantly expanded in several species of ticks, but only in the
630 terminal branches of the evolutionary tree and not in the common ancestor of ticks. This
631 can be explained by other independent large expansions of CYPs in other species of
632 Chelicerata.

633

634 **Carboxylesterases:** A total of 104 IricCCEs were identified in *I. ricinus*, including 73
635 complete ORFs. This count is similar to that of *I. scapularis* (Gulia-Nuss et al. 2016; De
636 et al. 2023) indicating that these genes also have one-to-one orthology between the two
637 species. Insect CCEs have been classified into three main functional groups
638 (Claudianos et al. 2006), including the dietary/detoxification group, for which we found
639 no genes in ticks or other Acari (supplementary Table S14, sheet B), and the

640 hormonal/semiochemical group represented by a single gene both in *I. ricinus* and *I.*
641 *scapularis*. In contrast, the third group of neurodevelopmental CCEs was highly
642 developed in ticks (Fig. 10 A), with a strong expansion of two new clades closely related
643 to AChEs, as already observed in mites (Grbić et al. 2011; Bajda et al. 2015). Similar to
644 the CYPs, we observed a strong differentiation of expression profiles within this gene
645 family and a relatively large number of genes were highly expressed in larvae
646 (supplementary Fig. S14). The CCEs essentially corresponded to the SiLiX family
647 FAM000444, which was significantly expanded in the common ancestor of ticks, and
648 also in the common ancestors of Metastriata and of *Ixodes* species, respectively.

649

650 **Glutathione S-transferases:** A total of 49 GST sequences were identified for both *I.*
651 *ricinus* and *I. scapularis*. Interestingly, more than half of the IricGSTs - including the
652 heme-responsive GST, here named GSTD2/IricT00009278 (Perner et al. 2018) - are
653 located on scaffold 2, a cluster already identified in *I. scapularis* (De et al. 2023). This
654 distribution of GSTs may reflect numerous clade-specific duplication events at the root
655 of GST diversity. Our phylogenetic analysis indicated some patterns of lineage-specific
656 duplication within ticks; for example, several duplications in the Zeta class were specific
657 to the genus *Ixodes*, and several duplications in the Epsilon class were specific to the
658 Metastriata (supplementary Fig. S15 A). Similar to the CYPs and CCEs, several clusters
659 of GSTs were well characterized by distinct gene expression profiles (supplementary
660 Fig. S15 B). The GSTs corresponded almost exactly to FAM000927 in the SiLix
661 clustering, which was found to be significantly expanded in the common ancestor of
662 ticks, and also in the common ancestor of the *I. ricinus* species complex, this GST family
663 had more genes in these four *Ixodes* species compared to *I. hexagonus* or the
664 Metastriata ticks.

665

666 **Cytosolic sulfotransferases:** The SULT family is one of the most expanded gene
667 families in ticks with ~200 genes in *I. scapularis* and *I. ricinus*, and was found to be
668 significantly expanded in both the common ancestor of ticks and in the internal nodes of
669 the tick evolutionary tree (i.e., in the common ancestor of the Metastriata and of *Ixodes*
670 species, respectively, and also in the ancestor of the *I. ricinus* species complex - SiLiX
671 family FAM000226, supplementary Table S5). This suggests a continuous trend of gene
672 family expansion. Our phylogenetic analysis (Fig.11 A) allowed us to distinguish three
673 clades in the SULT gene family. Clades A and B contain sequences found in the
674 Chelicerata and in other Metazoa including humans and houseflies. These two clades
675 have few or no duplications in the Chelicerata. For clade A, only one tick sequence was
676 identified (SFT-142), which was homologous to the four *D. melanogaster* sequences
677 (dmel-St1-4) and to the human ST4A1 sequence. Clade B also contained a single tick
678 sequence (SFT-7), which was homologous to three human sequences (ST1A1, ST2A1
679 and ST6B1), but no sequences from *D. melanogaster*. Clades A and B have high

680 bootstrap support, so we tentatively propose that an ancient duplication in the common
681 ancestor of arthropods and vertebrates gave rise to these two clades. This would have
682 been followed by secondary gene duplications or gene loss (e.g., loss of the clade B
683 ortholog for *D. melanogaster*). All other SULT sequences form clade C, and are
684 exclusively found in the Chelicerata. Several independent gene expansions occurred
685 within clade C, especially in ticks. While SULT genes in clades A and B have a similar
686 structure and a similar number of exons (6 or 7), the SULT genes in clade C have a
687 much lower number of exons. Most of the SULT genes in clade C are indeed mono-
688 exonic, or have only two exons, the first one often non-coding (i.e., entirely 5' UTR). In
689 addition, genes with introns are nested between clades of intron-less copies. This
690 suggests an initial retroposition event, which would have generated an intron-less copy,
691 at the origin of clade C - and thus probably in the common ancestor of Chelicerata -
692 followed by a process of re-exonization of some of the copies. A particularly large SULT
693 gene expansion in *I. ricinus* indicates tandem duplication events, as shown by several
694 clusters of adjacent copies. Intriguingly, the conserved multi-exonic copy SFT-7 (clade
695 B) is embedded within a cluster of mono-exonic genes on scaffold 9, although these
696 copies are phylogenetically distant (they belong to clade C) and structurally different.
697 This arrangement is unexpected if it reflects an ancient local duplication event, as
698 tandemly arranged genes are not supposed to arise through retroposition (Pan & Zhang
699 2008). Finally, the distribution of SULT gene sequences among many different
700 chromosomes or chromosomal regions indicate that additional retroposition events have
701 also occurred.

702 Further evidence that SULTs are a particularly dynamic gene family in tick genomes are
703 the traces of many partial gene copies. However, the absence of complete ORFs or
704 transcript support led us to not annotate these additional hits as *bona fide* genes, and
705 they were not included in our gene counts. With respect to gene expression (Fig.11 B),
706 the conserved copies (SFT-7 and SFT-142) are preferentially expressed in the ovaries
707 of half-fed ticks, whereas many of the other SULTs were dominantly expressed in either
708 the Malpighian tubules of unfed ticks, in larvae, or in salivary glands, with a generally
709 low level of gene expression for the strictly mono-exonic copies.

710

711 **ATP-binding cassette transporters:** We identified 104 genes encoding IricABCs in *I.*
712 *ricinus* (the same number as in *I. scapularis*), while 103 genes were found in the red
713 spider mite *Tetranychus urticae* (Dermauw et al. 2013). While most ABC genes in the
714 two *Ixodes* tick species were one-to-one orthologs, the distribution within gene
715 subfamilies was different between ticks and *T. urticae*. ABCs are grouped into 8
716 subfamilies (A to H) based on similarities in the ATP-binding domain. In *T. urticae*, the
717 most important lineage-specific expansions were found in subfamilies C, G and H,
718 whereas in *I. ricinus* they were found in subfamilies A and C (supplementary Fig. S16).
719 Automatic clustering grouped the B and C subfamilies into a family FAM000065, which

720 was significantly expanded in the genus *Ixodes* and in the common ancestor of the *I.*
721 *ricinus* species complex, but not in the common ancestor of ticks. This result agrees with
722 the high abundance of ABC genes in other Chelicerata, probably due to independent
723 expansion, and with higher gene counts in *Ixodes* species than in the Metastriata. A
724 second gene family, FAM000381, included the A and G subfamilies, and was found to
725 be significantly expanded in the common ancestor of ticks and in the Metastriata
726 (FAM000381 being more abundant in the Metastriata than the *Ixodes* genus).

727 Similar to other large gene families, there was strong differentiation in the gene
728 expression profiles of ABCs (supplementary Fig. S17), and the two largest groups of
729 genes were preferentially expressed in eggs and larvae. Mono-exonic copies were
730 found in less than 20 of 104 ABC genes of *I. ricinus*. A group of 11 mono-exonic copies
731 belonging to the C subfamily formed a physical cluster located on scaffold 10, the other
732 9 intronless copies were dispersed on seven different scaffolds.

733

734

735 Discussion

736 Importance of transposable elements in tick genomes, and definition of cellular 737 genes

738 Our analysis of transposable elements (TEs) shows that they constitute a large
739 proportion of the genomes in four *Ixodes* tick species, which is typical of large eukaryotic
740 genomes. Interestingly, we identified Bov-B LINEs in the genome of *I. ricinus*, a subclass
741 of retrotransposons abundant in vertebrates, which have also been found in the
742 genomes of reptile ticks, with evidence of horizontal gene transfer between vertebrates
743 and ticks (Walsh et al. 2013; Puinongpo et al. 2020). The presence of Bov-B LINE
744 sequences in several species of *Ixodes* could therefore reflect independent acquisitions
745 of transposons from vertebrate hosts. A recent study of the variation in gene presence-
746 absence in tick genomes showed that most *de novo* genes and genes that are not
747 consistently shared between species are TE-related (Rosani et al. 2023). Due to the
748 unique dynamics of TEs, it is common practice to distinguish TEs from the core genome.
749 However, our comparative study of the Chelicerata genomes found that many of the
750 predicted cellular genes, which sometimes belonged to large gene families, were
751 actually TEs. The number of TEs was high in some genomes, in particular in *I. scapularis*
752 and *Trichonephila clavata* (Joro spider). Following best practices for comparative
753 genomics, we removed these genes from our analyses. Although the role of these TEs
754 is not clear, the acquisition of introns and the high levels of tissue-specific gene
755 expression for some of these genes suggest that they have a functional role in tick
756 biology. More studies are needed to determine whether the large differences in the

757 number of TEs among tick species (including closely related ones) is due to annotation
758 strategies, or to true differences in transposon dynamics.

759

760 **Mechanisms of duplication, importance of intronless copies**

761 Gene duplication can result from different mechanisms, with both small-scale events,
762 such as tandem duplications and retropositions, and larger-scale events, such as
763 segmental duplications or whole genome duplication (WGD) (Wolfe & Shields 1997;
764 Kuzmin et al. 2022). In the Chelicerata, previous studies have shown that WGD has
765 occurred independently in the Xiphosura (horseshoe crabs) (Kenny et al. 2016) and in
766 the common ancestor of scorpions and spiders (Schwager et al. 2017; Aase-Remedios
767 et al. 2023), whereas there is currently no evidence of WGD in ticks. A previous study
768 based on the genetic distances between paralogs (Van Zee et al. 2016) suggested that
769 large-scale duplications may have occurred in ancestral ticks. However, the absence of
770 duplicated Hox genes in ticks (Schwager et al. 2017) and our analyses of macro-synteny
771 between tick genomes both suggest that large-scale duplications have not occurred in
772 tick genomes.

773 Our study identified several large gene families in ticks, often with physical clusters of
774 closely related copies, suggesting that they arose through tandem duplications.
775 Strikingly, many gene families also harbor a high percentage of intronless genes.
776 Intronless copies result from the retroduplication of poly-exonic genes where the mRNA
777 of the ancestral poly-exonic gene is reverse transcribed into DNA and then inserted back
778 elsewhere into the genome (Long et al. 2003; Ohno 1970). Retroposed genes were
779 typically considered as secondary and accidental events, because they generate copies
780 that lack regulatory sequences (and are therefore expected to be eliminated by
781 selection) and because of their small number. However, it has been shown that these
782 retroposed genes can re-acquire new exons, typically in the 5' untranslated region
783 (UTR), allowing the restoration of a promoter sequence (Fablet et al. 2009;
784 Vinckenbosch et al. 2006). This mechanism could “stabilize” duplicated genes and
785 facilitate their retention in the genome (Micheli & Camilloni 2022). We observed this
786 phenomenon in several gene families, indicating secondary exon acquisition in initially
787 retroposed gene copies. Mono-exonic genes often had low or null levels of expression
788 (with some exceptions), whereas the expression of genes with secondarily acquired
789 introns was in the range of the multi-exonic copies. Thus, our study suggests a high
790 gene duplication rate in tick genomes, driven by a combination of transposon-based
791 retroposition events and tandem duplication. While most duplicate gene copies are
792 probably destined for elimination (e.g., as shown by the many expressionless partial
793 copies for the serpins or SULTs), some copies may be retained by selection and acquire
794 new functions.

795

796 **Functional importance of gene expansions**

797 Gene duplication is a major force in the evolution of genomes and in the adaptative
798 potential of organisms (Ohno 1970; Lynch 2002). Although most duplicated genes are
799 eliminated, some new genes undergo sub-functionalization or acquire new functions
800 (Lynch & Conery 2000; Kuzmin et al. 2022). Ticks are no exception and are expected
801 to show specific gene duplications linked with the constraints and particularities of their
802 parasitic life-style. In hematophagous (blood feeding) arthropods, genes involved in
803 host-parasite interactions and blood processing (e.g., salivary gland proteins and
804 proteases) are more likely to show gene expansion (Arcà et al. 2017; Mans et al. 2017;
805 Ruzzante et al. 2019). Ticks possess multigene families involved in various physiological
806 processes, such as detoxification of host molecules, evasion of host immune defenses,
807 and sensory perception (Mans et al. 2017). The co-evolutionary arms race between ticks
808 and their vertebrate hosts exerts particularly strong selection on the tick genes involved
809 in searching for a host, attachment to the host, and blood-feeding. Many of these host-
810 tick interaction genes are expressed in the tick salivary glands, which produce a complex
811 mixture of proteins that have anti-hemostatic, anti-inflammatory, and anti-immunity
812 functions in addition to facilitating tick attachment and tick blood feeding. Thus, the
813 duplication of the tick salivary gland genes contributes to the diversification of these
814 functionally important genes in the frame of the co-evolutionary arms race with their
815 hosts (Chmelař et al. 2016; Francischetti et al. 2008).

816

817 Our comparative genomics analysis allowed us to identify important expansions of gene
818 families in tick genomes. Genes associated with detoxification processes showed high
819 expansions in tick genomes (especially in the tick common ancestor) compared to the
820 other Chelicerata. For example, the high number of GST genes identified in tick species
821 may be related to specific adaptations during the rapid evolution of this group towards
822 its modern avian and mammalian hosts (Parola & Raoult 2001), but may also
823 compensate for the absence of UDP-glycosyltransferases in ticks (Ahn et al. 2014). In
824 ticks and mites, several genes of the ABC sub-family C (ABCC) have been shown to
825 confer acaricide resistance (Shakya et al. 2023, Wu et al. 2023). With 55 genes
826 encoding for ABCCs, *I. ricinus* appears to be well equipped to evolve resistance to
827 acaricides, although these genes are probably also involved in physiological processes.
828 For example, the ABC transporter of *R. microplus* (RmABC10) mediates the transport
829 of dietary acquired heme across cell membranes, and is being studied as an acaricidal
830 target (Lara et al. 2015).

831 We observed expansions of several gene families that encode metalloproteases, in
832 particular for the M13 metalloprotease family. Metalloproteases are the most abundant
833 protease class in ticks (Ali et al. 2015); they are secreted in tick saliva at the tick host
834 interface (Francischetti et al. 2003; Perner et al. 2020), and are recognised as

835 immunogens inherent to blood feeding (Decrem et al. 2008; Becker et al. 2015; Ali et al.
836 2015; Jarmey et al. 1995; Perner et al. 2020). However, most of the members of the
837 M13 gene family lack SignalP prediction and only some are expressed by the tick
838 salivary glands. It is therefore tempting to speculate that these proteases play multiple
839 functions including regulation of physiological processes, development, and modulation
840 of bioactive regulatory peptides, and that they are important for the tick parasitic lifestyle.

841 The most spectacular gene family expansion concerned the family of cytosolic
842 sulfotransferases (SULTs). The research on SULTs is relatively new compared to the
843 research on detoxification enzymes like cytochrome P450s and UGTs (Suiko et al.
844 2017). The characterization of SULTs in model organisms like humans, zebrafish, and
845 the house fly has shown the importance of these enzymes in the detoxification of
846 exogenous compounds, and in the sulfation of key endogenous compounds. The
847 number of tick SULTs (~130 genes in Metastriata, and ~200 genes in *Ixodes*) was
848 considerably higher compared to any other Chelicerata species, vertebrates (~20
849 genes), and the housefly (4 genes), suggesting that these genes have acquired an
850 important function in tick biology. As discussed above, this expansion of the SULT genes
851 in ticks appears to result from a combination of retroposition and tandem duplications,
852 as observed in other tick gene families. Our observations of many additional SULT gene
853 fragments (i.e., genes that were not annotated due to partial sequences and no
854 transcription support) shows that SULT gene duplication is highly dynamic, is possibly
855 mediated by nearby transposable elements, and often leads to the degradation of the
856 gene copy. This observation agrees with an analysis of presence-absence variation
857 (PAV) (Rosani et al. 2023) based on tick genomes sequenced in another study (Jia et
858 al. 2020). The study of Rosani et al. identified sulfotransferases among sequences with
859 a strong signal of PAV, along with transposable elements. We hypothesize that with
860 such a dynamic SULT toolbox, ticks may differ at the population level or even at the
861 individual level in the number of SULT copies. Different SULT genes may be adapted to
862 detoxify different substrates, such as the host molecules ingested with the blood. Thus,
863 the function of SULTs could be the digestion and/or detoxification of these vertebrate
864 host blood components. Alternatively, the function of SULTs could be the modification
865 and enhancement of some of the compounds in the tick saliva, creating a cocktail of
866 molecules that modulates the host immune response. We also observed tissue-specific
867 gene expression of SULTs; many SULT genes had higher expression in the Malpighian
868 tubules, an excretory organ that has several functions in ticks, such as the excretion of
869 nitrogenous wastes, osmoregulation, water balance, and detoxification. Other groups of
870 SULT copies were primarily expressed in eggs or larvae, indicating also specialization
871 of SULT gene expression by tick developmental stage.

872
873 Ticks do not synthesize juvenile hormone (JH), although JHs and their precursors play
874 crucial roles in molting and reproduction in insects and crustaceans. The last enzyme in

875 the JH pathway, CYP15A1, is absent from tick genomes. It is therefore surprising that a
876 study in *I. scapularis* found a large gene expansion of juvenile hormone acid
877 methyltransferases (JHAMTs), which are the preceding enzymes in the JH pathway
878 (Julia-Nuss 2016). Another study on *I. scapularis* found that Gln-14 and Trp-120, which
879 are residues critical for interactions with farnesoic acid and JH acid, respectively, were
880 absent (Zhu et al. 2016). Another study found that methyl farnesoate (MF) does not
881 occur in ticks (Neese et al. 2000). Together, these data raise doubts whether these
882 sequences actually function as JHAMTs in ticks. Our study found that this gene family
883 has one of the largest expansions in ticks (with ~40 genes in Metastriata tick, and ~80
884 genes in the *I. ricinus* species complex), although curation showed that a substantial
885 proportion of these gene copies are incomplete and might be non-functional. In contrast
886 with the study of Zhu et al. (2016) our alignment of 45 curated JHAMT sequences in the
887 *I. ricinus* genome showed that Gln-14 and Trp-120 were conserved in the majority of the
888 tick sequences (data not shown). Interestingly, independent expansions of JHAMTs
889 have been recorded in spiders (Yang et al. 2021), and the presence of a transcript of
890 *CYP15A1* may indicate the presence of juvenile hormone and/or methyl farnesoate in
891 this group (Nicewicz et al. 2021). JH synthesis occurs in the corpora allata in insects,
892 and tick synganglia are partly homologous to this tissue (Zhu et al 2016). However, the
893 expression profiles of the JHAMT genes in *I. ricinus* do not show synganglion specificity;
894 most JHAMT genes are more expressed in eggs, larvae, and ovaries, while a few genes
895 have a broad pattern of expression. In conclusion, although ticks lack JH, they have kept
896 most genes of the JH pathway and the large expansion of JHAMTs could indicate that
897 MF is produced by ticks. More studies are needed to elucidate the processes that control
898 molting in ticks, and if tick molting still relies on the JH biosynthesis pathway and on JH
899 precursors.

900

901 **Conclusions**

902 In conclusion, our comparative analysis of the genomes of four species within the genus
903 *Ixodes*, namely *I. ricinus*, *I. pacificus*, *I. persulcatus*, and *I. hexagonus*, shed new light
904 on the genomic characteristics of ticks. Through genome sequencing and assembly,
905 and by emphasizing the chromosome-level assembly in *I. ricinus*, we achieved a
906 detailed understanding of the genomic architecture in *Ixodes* ticks. The macro-syntenic
907 analysis highlighted the conservation of genomic organization between *I. ricinus* and *I.*
908 *scapularis*, with few structural rearrangements. Our annotation efforts, including manual
909 curation for *I. ricinus*, revealed that a high proportion of tick genes have an unusual,
910 intronless structure, indicating frequent retroposition events. We have highlighted the
911 significant role of gene family expansions in the evolution of tick genomes which have
912 undergone highly dynamic gains and losses of genes, alongside expansions and
913 contractions of gene families, showcasing a remarkable adaptation to their parasitic

914 lifestyle. Our comprehensive analysis of the genomes of four *Ixodes* species offers a
915 rich understanding of tick genomics and sets the stage for future functional studies.

916

917 **Materials and Methods**

918 **Tick sampling** For *I. ricinus*, we used a laboratory population originally derived from
919 wild ticks in the region of Neuchâtel, Switzerland, and maintained in the laboratory since
920 1980. This population was maintained in small numbers (~30 adults) and sexual
921 reproduction was conducted on an annual basis, conditions expected to have favored
922 inbreeding. Unfed adult females were isolated for sequencing. For *I. pacificus*, ticks were
923 collected from the vegetation on November 9, 2017 in Del Valle Regional Park California
924 (37° 48' 15.71" N, 122° 16' 16.0" W). Adult female ticks were put in RNAlater and
925 shipped to the Nantes laboratory under cold conditions (~4°C) for DNA extraction. Ticks
926 from the species *I. persulcatus* were sampled in the Tokachi district, Hokkaido, Japan.
927 Adult female ticks were fed on Mongolian gerbils, and their salivary glands (SG) were
928 dissected. *Ixodes hexagonus* ticks were isolated from a live hedgehog collected at
929 Oudon, France (47° 20' 50" N, 1° 17' 09" W) and sent to a wildlife recovery center
930 (CVFSE, Oniris, Nantes, France). Fully engorged *I. hexagonus* nymphs were collected,
931 and maintained in the lab until they molted into adult ticks.

932

933 **DNA extraction** For the four species of *Ixodes*, a single adult female was used for
934 genome sequencing. For *I. persulcatus*, DNA from salivary glands (SGs) was extracted
935 following a standard SDS/ProK and phenol/isopropanol protocol, and stored at -30°C.
936 For the three other tick species, DNA extraction of the whole body was performed
937 following the salting-out protocol recommended for DNA extraction from single insects
938 by 10X Genomics.

939

940 **10X library preparation and sequencing** For each species, linked read sequencing
941 libraries were constructed using the Chromium Gel Bead and Library Kit (10X
942 Genomics, Pleasanton, CA, USA) and the Chromium instrument (10X Genomics)
943 following the manufacturer's instructions. Prior to DNA library construction, tick DNA
944 fragments were size-selected using the BluePippin pulsed field electrophoresis system
945 (Sage Science, Beverly, MA, USA); size selection was adjusted according to the initial
946 size of the extracted DNA fragments (ranging in size from 20 to 80 Kb). Approximately
947 1 ng of high molecular weight (HMW) genomic DNA (gDNA) was used as input for
948 Chromium Genome library preparation (v1 and v2 chemistry), which was added on the
949 10X Chromium Controller to create Gel Bead in-Emulsions (GEMs). The Chromium
950 controller partitions and barcodes each HMW gDNA fragment. The resulting genome

951 GEMs underwent isothermal incubation to generate 10X barcoded amplicons from
952 which an Illumina library was constructed. The resulting 10X barcoded sequencing
953 library was then quantified by Qubit Fluorometric Quantitation; the insert size was
954 checked using an Agilent 2100, and finally quantified by qPCR (Kapa Biosystems,
955 Wilmington, MA, USA). These libraries were sequenced with 150 bp paired-end reads
956 on an Illumina HiSeq 4000 or NovaSeq 6000 instrument (Illumina, San Diego, CA, USA).

957

958 **Hi-C library preparation and sequencing** Chicago and Hi-C libraries were prepared
959 by Dovetail Genomics (Dovetail Genomics, Scotts Valley, CA, USA) and sequenced at
960 the Genoscope on a HiSeq 4000 instrument (Illumina, San Diego, CA, USA).

961

962 **Illumina short-reads filtering** Short Illumina reads were bioinformatically post-
963 processed as previously described (Aury et al. 2008; Alberti et al. 2017) to filter out low
964 quality data. Low-quality nucleotides ($Q < 20$) were discarded from both read ends,
965 Illumina sequencing adapters and primer sequences were removed, and only reads \geq
966 30 nucleotides were retained. These filtering steps were done using an in-house-
967 designed software based on the FastX package
968 (<https://www.genoscope.cns.fr/fastxtend/>). Genomic reads were then mapped to the
969 phage phiX genome and aligned reads were identified and discarded using SOAP
970 aligner (Li et al. 2008) (default parameters) and the Enterobacteria phage PhiX174
971 reference sequence (GenBank: NC_001422.1). Standard metrics for sequencing data
972 are available in supplementary Table S18).

973

974 **Genome sizes and heterozygosity rate** Genome sizes and heterozygosity rates were
975 estimated using Genomescope2 (Ranallo-Benavidez et al. 2020) with a kmer size of 31
976 (supplementary Fig. S17). Genome size ranged between 1.8 Gbp (*I. pacificus*) and 2.6
977 Gbp (*I. ricinus* and *I. hexagonus*). Heterozygosity rates varied between 0.82% (*I. ricinus*)
978 and 3.17% (*I. pacificus*).

979

980 **Tick genome assemblies (10X Genomics) and scaffolding** Genomes were
981 assembled using the Supernova software from 10X Genomics. *I. ricinus* was assembled
982 using the 1.2.0 version while *I. hexagonus*, *I. pacificus* and *I. persulcatus* were
983 assembled with the 2.1.1 version of the assembler. Hi-C scaffolding of the *I. ricinus*
984 genome assembly was performed by Dovetail using both Chicago and Hi-C libraries.
985 The RagTag (Alonge et al. 2022) software (version 1.0.1) was used to scaffold the
986 genomes of *I. hexagonus*, *I. pacificus* and *I. persulcatus* by using the chromosome-scale

987 assembly of *I. ricinus* as an anchor. RagTag was launched with default options and with
988 Minimap 2.17 (Li 2018) for the mapping step.

989

990 **Gene prediction** The genome assemblies of *I. ricinus*, *I. hexagonus*, *I. pacificus* and *I.*
991 *persulcatus* were masked using RepeatMasker (<http://repeatmasker.org/>, default
992 parameters) with Metazoa transposable elements from Repbase (version 20150807
993 from RepeatMasker package) and RepeatModeler (Flynn et al. 2020) with default
994 parameters (version v2.0.1). The proteomes of *Varroa destructor*, *Centruroides*
995 *sculpturatus* and *Stegodyphus mimosarum* were used to detect conserved genes in the
996 four tick genome assemblies. In addition, a translated pan-transcriptome of 27 tick
997 species (Charrier et al. 2019) was aligned on the four tick genome assemblies. The
998 proteomes were aligned against genome assemblies in two steps. BLAT (Kent 2002)
999 with default parameters was used to efficiently delineate a genomic region
1000 corresponding to the given protein. The best match and matches with a score $\geq 90\%$ of
1001 the best match score were retained and alignments were refined using Genewise
1002 (Birney et al. 2004) with default parameters, which allows for accurate detection of
1003 intron/exon boundaries. Alignments were kept if more than 50% of the length of the
1004 protein was aligned to the genome.

1005 We also used RNA-Seq data to allow the prediction of expressed and/or specific genes.
1006 Two transcriptome libraries of synganglia (Rispe et al. 2022) from *I. ricinus*
1007 (PRJEB40724), a library from the whole body of *I. ricinus* (GTVZ00000000.1), and a
1008 pan-transcriptome of 27 different tick species (Charrier et al. 2019) were aligned on the
1009 four genome assemblies. As for protein sequences, these transcripts were first aligned
1010 with BLAT where the best match (based on the alignment score) was selected.
1011 Alignments were then refined within previously identified genomic regions using
1012 Est2Genome (Mott 1997) to define intron/exon boundaries. Alignments were retained if
1013 more than 80% of the transcript length was aligned to the genome with a minimum
1014 percent identity of 95%.

1015 Genes were predicted on the four genome assemblies by integrating protein and
1016 transcript alignments as well as *ab initio* predictions using a combiner called Gmove
1017 (Dubarry et al. 2016). Single-exon genes with a CDS length smaller or equal to 100
1018 amino acids were filtered out. Additionally, putative transposable elements (TEs) were
1019 removed from the predicted genes using three different approaches: (i) genes that
1020 contain a TE domain from InterPro; (ii) transposon-like genes detected using
1021 TransposonPSI (<http://transposonpsi.sourceforge.net/>, default parameters); (iii) and
1022 genes overlapping repetitive elements. Finally, InterProScan (Jones et al. 2014) (version
1023 v5.41-78.0, with default parameters) was used to detect conserved protein domains in
1024 predicted genes. Predicted genes without conserved domains and covered by at least
1025 90% of their cumulative exonic length by repeats, or matching TransposonPSI criteria
1026 or selected IPR domains, were removed from the gene set.

1027

1028 **Genomic web portal, Apollo server and manual curation** A genomic portal was set
1029 up at the BIPAA platform (<https://bipaa.genouest.org/>), providing access to raw data and
1030 to a set of web tools facilitating data exploration and analysis (BLAST application
1031 (Camacho et al. 2009), including a JBrowse genome browser (Buels et al. 2016),
1032 GeneNoteBook (Holmer et al. 2019)). Automatic functional annotation of genes was
1033 performed using Diamond 2.0.13 (Buchfink et al. 2021) against the nr databank (2022-
1034 12-11), EggNog-Mapper 2.1.9 (Cantalapiedra et al. 2021), InterProScan 5.59-91.0
1035 (Jones et al. 2014) and Blast2Go 1.5.1 (2021.04 database) (Götz et al. 2008). Results
1036 were then made available into GeneNoteBook. The BIPAA Apollo (Dunn et al. 2019)
1037 server was also used in order to improve the annotation for *I. ricinus*, based on expert
1038 knowledge of several functional groups of gene. Based on the automatic annotation,
1039 alignments of RNA-Seq data (reads of selected libraries and contigs of reference
1040 transcriptomes), localization of TEs, and of non-coding RNAs, experts were able to
1041 perform manual curation of the annotation (gene model edition and functional annotation
1042 refinement, including gene naming). Manual curation data was merged with OGS 1.0
1043 (automatic annotation) to produce a new reference annotation named OGS1.1. This
1044 merging was performed using ogs_merge (<https://github.com/genouest/ogs-tools>
1045 version 0.1.2). The OGS1.1 was functionally annotated using the same procedure as
1046 OGS1.0 and made available into GeneNoteBook.

1047

1048 **Synteny analysis** Synteny analyses between *I. scapularis* and *I. ricinus* were performed
1049 using CHRonicle (January 2015) and SynChro (January 2015) (Drillon et al. 2014),
1050 which use protein similarity to determine syntenic blocks across these two genomes.
1051 The results were parsed and then plotted into chromosomes using chromoMap R
1052 package (v0.4.1 (Anand & Rodriguez Lopez 2022)). Parity plots were built using a
1053 homemade R script (R version v4.2.2) based on hit tables, for two comparisons: *I. ricinus*
1054 versus *I. scapularis*, and *I. ricinus* versus *D. silvarum*. Hit tables were generated using
1055 BlastP (NCBI Blast+ v2.13.0 (Camacho et al. 2009)) with the following options: e-value
1056 cutoff = 1e-5, max HSPs = 1 and max target sequences = 1.

1057

1058 **Transposable element annotation** Repeated elements (REs) and transposable
1059 elements (TEs) were first annotated by RepeatModeler (v 2.0.2a) (Smit, AFA, Hubley,
1060 R. *RepeatModeler Open-1.0*. 2008-2015 <http://www.repeatmasker.org>) using NCBI
1061 BLAST for alignment. Predicted TEs or REs matching with gene sequences from the
1062 OGS1.1 prediction were removed from the RepeatModeler results. Finally, a second
1063 round of annotation was performed by RepeatMasker (v 4.1.1) (Smit, AFA, Hubley, R &
1064 Green, P. *RepeatMasker Open-4.0*. 2013-2015, <http://www.repeatmasker.org>) using the

1065 filtered results of RepeatModeler combined with sequences from arthropods contained
1066 in the Dfam database (from RepeatMasker v 4.1.1).

1067 For Bov-B LINEs, sequences annotated as RTE/Bov-B by RepeatModeler were
1068 extracted and blasted by tblastx against curated Bov-B LINE sequences contained in
1069 the Dfam database (downloaded on 5 December 2023). Only hits with an e-value lower
1070 than 1e-3 were kept and sequences aligning with curated Bov-B sequences were
1071 considered as BovB LINE retrotransposons.

1072

1073 **Gene clustering, definition of gene families** In addition to the four genomes newly
1074 sequenced, the genomes of other tick species and other arachnids were included for a
1075 study of phylogeny and evolutionary dynamics of gene repertoires, as listed in
1076 supplementary Table S19. Genome completeness was assessed by BUSCO (v5.4.4)
1077 for each species (Manni et al. 2021), using the Arachnida database (OrthoDB10)
1078 (Kriventseva et al. 2019), with an e-value threshold of 1e-5. For each species, the
1079 longest protein isomorph of each gene was extracted using AGAT tools (v0.8.1,
1080 <https://zenodo.org/records/5834795>) in order to retain a single sequence per gene.
1081 Three clustering methods were then compared, using several well-annotated gene
1082 families as benchmark tests. We found that SiLiX (v1.2.11) (Miele et al. 2011) generated
1083 larger gene families that typically matched well the curated gene families, whereas
1084 OrthoMCL (v2.0.9) (Li et al. 2003) and OrthoFinder (v2.5.2) (Emms & Kelly 2019)
1085 defined gene families at a much smaller grain (clades with fewer genes, of more closely
1086 related sequences, as shown for two examples of gene families in supplementary Fig.
1087 S18). We therefore decided to use SiLiX for the clustering. Pairwise comparisons
1088 between all arthropod species were carried out using BlastP (NCBI Blast+ v2.13.0
1089 (Camacho et al. 2009). Parameters for clustering were a minimum percentage identity
1090 of 0.30 and a minimum length of 75 residues. The SiLiX output was then parsed to obtain
1091 a contingency table, while a BlastP search against the Swiss-Prot database (12th of
1092 January 2023 download), using an e-value threshold of 1e-5, was performed to attribute
1093 gene ontology (GO) terms to each gene family.

1094

1095 **Phylogeny of the Chelicerata** The SiLiX output was then parsed to obtain a
1096 contingency table, while a BlastP search against the Swiss-Prot database (12th of
1097 January 2023 download), using an e-value threshold of 1e-5, was performed to attribute
1098 GO terms to each gene family. For gene families containing a single gene sequence in
1099 each species, protein sequences were aligned using MAFFT (v7.487 (Kuraku et al.
1100 2013)) with the "genafpair" alignment algorithm and 1000 iterations. The generated
1101 alignments were trimmed with TrimAI (v1.4.1 (Capella-Gutiérrez et al. 2009a)), using a
1102 gap threshold of 0.6, and concatenated using goalign (v0.3.2 (Lemoine & Gascuel 2021,
1103 NAR Genomics and Bioinformatics)). A phylogenetic tree was then generated with IQ-

1104 TREE (v2.1.3) (Minh et al. 2020). The best model was identified by the software using
1105 BIC and branch supports were estimated with 1000 bootstrap replicates and SH-like
1106 approximate likelihood ratio tests. Non-concatenated alignments were also used to
1107 construct trees for each family in order to check branch length and topology for all single-
1108 copy families. Owing to the low completeness of the *Hae. longicornis* and *Hya. asiaticum*
1109 genomes, illustrated by BUSCO metrics and lower number of gene families compared
1110 to other ticks (see Results), we removed these species from further analyses. Our
1111 phylogeny thus included 107 shared single-copy orthologs, for 19 species of
1112 Chelicerata.

1113 To further evaluate the phylogenetic relationships among *Ixodes* species included in our
1114 data set, some of them being very closely related, the nucleotide sequences of the
1115 single-copy genes of the five species included in our study were aligned using MAFFT
1116 (with the "genafpair" alignment algorithm, 1000 iterations and using the LOSUM 80
1117 matrix). Aligned sequences were trimmed with TrimAI (using a gap threshold of 0.8)
1118 before being concatenated with goalign. Finally, a phylogenetic tree was built with IQ-
1119 TREE. As described previously, the best model was identified by IQ-TREE using BIC
1120 and branch supports were estimated with 1000 bootstrap replicates and SH-like
1121 approximate likelihood ratio tests.

1122

1123 **Global study of the evolutionary dynamics of gene families** To analyze changes in
1124 gene family size across the phylogeny, CAFE5 (v5.0) (Mendes et al. 2021) was run
1125 using the previously generated contingency table and the species phylogenetic tree,
1126 rooted and previously transformed into an ultrametric tree using phytools (v 1.5-1)
1127 (Revell 2012) and the ape R packages (v5.7-1) (Paradis & Schliep 2019) with R version
1128 v4.2.2. The horseshoe crab, *Limulus polyphemus*, was used as an outgroup to root the
1129 tree. The error model was estimated before running the base model with a dataset
1130 cleaned of highly divergent families. The base model predicted a lambda value of 0.451,
1131 which was used for a second run of CAFE5 with the full family dataset. This second run
1132 was then used to predict gene family expansion/contraction.

1133

1134 **Metabolic pathways** KEGG orthology (KO) numbers were assigned to each protein
1135 sequence of the Chelicerata species used in this study using eggNOG-mapper (v2.1.10)
1136 (Cantalapiedra et al. 2021). KO numbers of each species were regrouped into five
1137 taxonomic groups (*Ixodes* spp., Metastriata ticks, Mesostigmata+Acariformes, spiders
1138 and finally a group including *C. sculpturatus* and *L. polyphemus*). Assessment of gene
1139 presence/absence was made based on a majority rule in each group (a gene being
1140 considered present in each group if present in the majority of its species), to avoid both
1141 the effects of incomplete or spurious annotation, or of contamination. Metabolic maps
1142 and reactions were then reconstructed using the Reconstruct tool of KEGG Mapper

1143 (Kanehisa & Sato 2020). Maps and detailed patterns of presence/absence in each
1144 species are available in the BIPAA webpage for the *I. ricinus* genome (see
1145 https://bipaa.genouest.org/sp/ixodes_ricinus/download/).

1146

1147 **Expression atlas** Transcriptomic data of *I. ricinus* were downloaded from the NCBI SRA
1148 archive (see supplementary Table S20 for detailed information) using the SRAtoolkit
1149 (v3.0.0 (<https://trace.ncbi.nlm.nih.gov/Traces/sra/sra.cgi?view=software>))). A
1150 preliminary study of read quality, quantity, and homogeneity between replicates was first
1151 conducted, which led us to retain only a sample of the many data sets already published
1152 for this species. Whenever possible, we retained two replicates for a given combination
1153 of tissue and condition (typically either unfed ticks, or half-replete ticks), to include a
1154 minimal level of replication. The transcriptome datasets were filtered and trimmed using
1155 Trimmomatic (v0.39) (Bolger et al. 2014). To filter rRNA sequences from the datasets,
1156 paired-reads were mapped on an RNA-Seq contig from *I. ricinus* described previously
1157 (Charrier et al. 2018); this sequence of 7,065 bp was found to represent a cluster with
1158 complete 18S, 5.8S and 28S subunits of rRNA. Mapping was performed with Hisat2
1159 (v2.2.1) (Kim et al. 2019). Unmapped paired-reads (non-rRNA) were extracted using
1160 bamUtil (v1.0.14) (Jun et al. 2015) and Samtools (v1.16.1) (Danecek et al. 2021) and
1161 read quality was checked using MultiQC (v1.14) (Ewels et al. 2016) on FastQC (v0.11.7)
1162 outputs. Another run of Trimmomatic was then performed on the retained reads, which
1163 were then mapped on the *I. ricinus* genome with Hisat2. Mapped reads were finally
1164 sorted with Samtools and the number of mapped reads per gene was retrieved by the
1165 FeatureCount R function contained in the Rsubread package (v3.16) (Liao et al. 2019).
1166 Counts were then converted into Transcripts per million (TPMs) - supplementary Table
1167 S21. The Spearman correlation heatmap was built for each gene family using the
1168 heatmap.2 function (gplots packages v3.1.3) and tree/gene model/heatmap figures
1169 were built using a homemade script using treeio (v1.22.0) (Wang et al. 2020), ggtree
1170 (v3.6.2) (Yu et al. 2017) and ggplot2 (v3.4.2 ((Wickham 2016)
1171 <https://ggplot2.tidyverse.org>) packages.

1172

1173 **Annotation of structural and regulatory non-coding elements** To ensure reliable
1174 and accurate annotation of structural and regulatory non-coding elements, we used
1175 several approaches, software and databases. Initially, we used Infernal and the latest
1176 version of the Rfam database to identify ncRNAs and cis-regulatory elements in the *I.*
1177 *ricinus* genome (Nawrocki & Eddy 2013; Kalvari et al. 2021). Subsequently, we used
1178 tRNAscan-SE to annotate transfer RNAs in the *I. ricinus* genome (Chan & Lowe 2019)
1179 and sRNAbench to identify the most accurate set of miRNAs and their genomic positions
1180 (Aparicio-Puerta et al. 2019).

1181 For the annotation of long non-coding RNAs (lncRNAs), we relied on the lncRNA dataset
1182 compiled and analyzed by Medina et al. (Medina, Jmel, et al. 2022; Medina, Abbas, et
1183 al. 2022). These studies resulted in a consensus set of lncRNAs, which we considered
1184 to be high confidence lncRNAs. First, we confirmed the absence of coding properties in
1185 these lncRNAs using CPC2 (Kang et al. 2017). Next, we aligned the lncRNAs to the *I.*
1186 *ricinus* genome using Blat and retained alignments with a score above 90. Finally, to
1187 eliminate potential assembly artifacts and avoid interference with the set of coding
1188 RNAs, we used gffcompare to remove any lncRNAs that overlapped with coding RNAs
1189 (Pertea & Pertea 2020).

1190

1191 **Annotation and phylogeny of protease inhibitors in *I. ricinus*** To annotate proteins
1192 containing the Kunitz domain (KDCP) and cystatins, we combined *I. ricinus* mRNA
1193 sequences from different sources: our initial prediction of coding sequences for the *I.*
1194 *ricinus* genome (version OGS1.0), the National Center for Biotechnology Information
1195 (NCBI), and the transcriptome assembled by Medina et al. (Medina, Jmel, et al. 2022).
1196 We used TransDecoder to extract coding sequences (CDSs) from the mRNA
1197 sequences. To eliminate redundancy, we used CD-HIT (Fu et al. 2012): sequences with
1198 a CDS showing 98% identity and at least 70% coverage were identified as redundant,
1199 and the longer sequence in each cluster was chosen. Next, InterProScan and BlastP
1200 were used to identify proteins belonging to the Cystatin and Kunitz families (Jones et al.
1201 2014; Blum et al. 2021; Altschul et al. 1990). These sequences were then aligned with
1202 the *I. ricinus* genome using Blat (Kent 2002). The automatic annotation was then
1203 manually curated on the basis of expression and junction data using the Apollo
1204 annotation platform (Lee et al. 2013), the result of all our annotations being present in
1205 the OGS1.1 version of the genome prediction.

1206 For phylogenetic analysis, we included gene sequences from *I. scapularis* (De et al.
1207 2023), as well as from the four genomes sequenced in the present study. For the three
1208 species other than *I. ricinus* sequenced in our study, cystatins and Kunitz domain-
1209 containing proteins were annotated using the same method as described for *I. ricinus*,
1210 but no manual curation was performed. SignalP was used to identify the signal peptide
1211 of cystatins and Kunitz domain-containing proteins (Almagro Armenteros et al. 2019).
1212 Clustal Omega was then used to perform a multiple sequence alignment of the mature
1213 protein sequence (Sievers et al. 2011). Spurious sequences and misaligned regions
1214 from the multiple alignment were removed using trimAI (Capella-Gutiérrez et al. 2009b).
1215 The phylogenetic tree was then constructed using FastME (Lefort et al. 2015), and
1216 visualized with the R software ggtree (Yu et al. 2017). Detailed lists of KDCPs and
1217 cystatins are given in Supplementary Table 7.

1218

1219 **Serpins** The search for serpins in the genome was performed by BLAST, either with
1220 blastn algorithm (protein query against translated nucleotide sequences) or tblastn
1221 (translated nucleotides query against translated nucleotide sequences), and sequences
1222 from the original prediction were manually curated. Sequences were aligned and edited
1223 as proteins by using the ClustalW algorithm and Maximum likelihood method and the
1224 JTT matrix-based model and bootstrap method with 1000 replications was used to
1225 calculate the reliability of tree branches.

1226

1227 **Metallobiology and Ferritins** The search for heme synthesis and degrading enzymes
1228 in the *I. ricinus* genome was performed by BLAST, with the tblastn or blastp algorithms,
1229 using the sequences of *Dermanyssus gallinae* (Ribeiro et al. 2023) as queries. The
1230 Alphafold2 algorithm was used to predict the monomeric structure of ferritin-1 and
1231 ferritin-2 identified in the *I. ricinus* genome. The resulting PDB files were used for Swiss
1232 Homology Modelling (Waterhouse et al. 2018) to predict the structure of their multimeric
1233 assemblies, using human Ferritin heavy chain as a template (3ajo.1.A; seq identity 67%,
1234 CMQE 0.89). Measures of the external diameters of the protein multimers were
1235 performed in PyMol.

1236

1237 **Chemoreceptors: annotation and phylogenetic study** The annotation of the two
1238 major chemosensory gene families of *I. ricinus* was based on known sequences from
1239 the closely related species *I. scapularis* (Josek et al. 2018). The *I. ricinus* scaffolds with
1240 significant blast hits (cutoff value 1e-30) were retrieved to generate a subset of the
1241 genome for each chemosensory gene family. Gene models were obtained after amino
1242 acid sequences were aligned to this subset of the genome using Exonerate (Slater &
1243 Birney 2005). All gene models thus generated were manually validated or corrected via
1244 Apollo. Based on homology with *I. scapularis* sequences, matching parts were joined
1245 when located on different scaffolds. The classification of deduced proteins and their
1246 integrity were verified using blastp against the nonredundant (NR) GenBank database.
1247 When genes were suspected to be split on different scaffolds, protein sequences were
1248 merged for further analyses.

1249 Following alignment and phylogenetic proximity, *I. ricinus* sequences were named after
1250 their *I. scapularis* orthologs according to Josek et al. 2018. The abbreviations Iric and
1251 Isca are used before the gene names to clarify the species, *I. ricinus* and *I. scapularis*,
1252 respectively. The gene family was defined by IR or GR for ionotropic or gustatory
1253 receptors, respectively and were followed by a number designating a different gene
1254 sequence. A supplementary number was given for closely related sequences. For
1255 example, if a receptor was named IscaIRX for *I. scapularis* the closest *I. ricinus* receptor
1256 was named IricIRX. If other sequences were closely related they were named IricIRX-
1257 1, IricIRX-2 etc. The IRs and GRs of the phytoseid predatory mite, *G. occidentalis* (Hoy

1258 et al. 2016), were ultimately added to the phylogenetic analysis as well as the *Drosophila*
1259 *melanogaster* IRs. On the GR dendrogram we used the Mocc abbreviations while for
1260 the IR dendrogram we did not display the name abbreviations for reasons of clarity.
1261 Finally, for the phylogenetic analysis of the conserved IRs, we included the two *Ixodes*
1262 spp. (Ir and Is), *G. occidentalis* (Mo), *D. melanogaster* (Dm), *Spodoptera littoralis* (Sp)
1263 and *Heliconius melpomene* (Hm).

1264 Multiple sequence alignment was performed by MAFFT v7 (Katoh & Standley 2013) and
1265 maximum-likelihood phylogenies were built using the Smart Model Selection (Lefort et
1266 al. 2015) in PhyML 3.0 (Guindon et al. 2010) (<http://www.atgc-montpellier.fr/phym/>)
1267 which automatically selects the best substitution model. Node support was estimated
1268 using the approximate likelihood ratio test via SH-like aLRT (Anisimova & Gascuel
1269 2006). Trees were retrieved with FigTree v1.4.4 (<https://github.com/rambaut/figtree>) and
1270 images were edited with PowerPoint software.

1271

1272 **Defensins** Identification of genes encoding defensins in the *I. ricinus* genome was
1273 performed by tBlastn search (default parameter) using annotated *I. ricinus* prepro-
1274 defensin transcripts from a variety of *I. ricinus* transcriptomes deposited in GenBank
1275 (NCBI) as queries.

1276 Phylogenetic analysis of the prepro-defensins and defensin-like proteins (DLPs) of *I.*
1277 *ricinus* was performed using sequences including other *Ixodes* sp. (*I. scapularis*, *I.*
1278 *persulcatus*, *I. hexagonus*, *I. pacificus*) and constructed as above for Kunitz-type and
1279 cystatin protease inhibitors

1280

1281 **Detoxification** We used different sets of tick CYP, CCE, GST, and ABC transporter
1282 proteins from published studies (for *I. scapularis*) or from the NCBI website automatic
1283 annotation databases to search the *I. ricinus* genome using TBLASTN with Galaxy
1284 (Giardine et al. 2005), Exonerate and Scipio to align protein sequences to the genome
1285 and define intron/exon boundaries (Keller et al. 2008). All generated gene models were
1286 manually validated or corrected in WebApollo based on homology with other tick
1287 sequences and aligned with RNA-seq data when available. In addition, a direct search
1288 was performed using the keyword search on the NCBI website to search for specific
1289 protein domains in the databases as well as a search in the automated annotation for *I.*
1290 *ricinus*. The classification of the deduced proteins and their integrity were checked using
1291 BlastP against the non-redundant GenBank database. When genes were suspected to
1292 be split into different scaffolds, the protein sequences were merged for further analysis.
1293 All active sites were confirmed using the NCBI CD search program. Phylogenetic trees
1294 were constructed using PhyML (Guindon et al. 2010) based on the best substitution
1295 model determined by the SMS server (Lefort et al. 2017), and both SPR (Subtree-

1296 Pruning-Regrafting) and NNI (Nearest-Neighbor-Interchange) methods were applied to
1297 improve tree topology. Branch supports were estimated by a Bayesian transformation
1298 of aLRT (aBayes) (Anisimova et al. 2011). Dendograms were constructed and edited
1299 using the FigTree software (<http://tree.bio.ed.ac.uk/software/figtree/>). RNA-Seq data, as
1300 described on the expression atlas section, were used to construct heatmaps for each
1301 enzyme family using TBtools (Chen et al. 2020).

1302 Manual curation of cytosolic sulfo-transferases (SULTs) was carried out for *I. ricinus*,
1303 adding several new genes that had not been predicted in the initial automatic annotation,
1304 in particular, mono-exonic genes. For a phylogenetic study of this expanded gene family,
1305 we included sequences from the horseshoe crab *P. polyphemus* and a spider,
1306 *Parasteatoda tepidariorum*, as well as from two model organisms where SULTs have
1307 been well characterized, humans and the housefly (sult1-4). For human sequences, we
1308 chose one sequence in each of the major clades of SULTs, as previously characterized
1309 (Suiko et al. 2017). Sequences assumed to be incomplete based on the predicted gene
1310 model and sequence length were discarded. Sequences were aligned with Muscle. The
1311 alignment was cleaned with Gblocks, using the following options: -b2=112 -b3=20 -b4=2
1312 -b5=h, implying a low-stringency (small blocks and gaps in up to half of the sequences
1313 being allowed). A ML phylogenetic tree was obtained with IQ-tree (Nguyen et al. 2015),
1314 using Model Finder to determine the best model of substitution (Kalyaanamoorthy et al.
1315 2017). Branch support was assessed using 1000 ultrafast bootstrap replicates (Hoang
1316 et al. 2018) and the resulting tree was graphically edited with iTOL (Letunic & Bork
1317 2019).

1318

1319 **Ethical statement**

1320 For the feeding of *I. persulcatus* ticks on gerbils, animal experimentation was carried out
1321 according to the Laboratory Animal Control Guidelines of National Institute of Infectious
1322 Diseases (institutional permission no. 215038).

1323

1324 **Data availability**

1325 Illumina and Hi-C data, assemblies and annotations are available in the European
1326 Nucleotide Archive under the following project PRJEB67793. A genome page for each
1327 of the four species of this study is available at
1328 https://bipaa.genouest.org/sp/ixodes_ricinus/: it contains blast forms, a GeneNoteBook
1329 page providing detailed information on each individual gene, a genome browser, and
1330 gives the possibility to download sequences, annotation files, expression data (RNA-
1331 Seq based atlas, for *I. ricinus*) and maps of metabolic pathways.

1332

1333 Acknowledgements

1334 We thank Olivier Lambert from the Centre Vétérinaire de la Faune Sauvage et des
1335 Écosystèmes (CVFSE) at Oniris, Nantes, France, for providing rescued hedge-hogs, on
1336 which we sampled *I. hexagonus* ticks.

1337 Thanks to Joyce Kleinjan (U. Berkeley, USA) for providing *I. pacificus* samples.

1338 Thanks to the Genotoul platform for access to its bioinformatics and calculation
1339 resources, and Fabrice Legeai (INRAE, BIPAA) for help with the Apollo database.

1340 We thank Céline Baulard from the Centre National de Recherche en Génomique
1341 Humaine (CNRGH) at Evry, France, for providing help with the preparation of 10X
1342 libraries.

1343

1344 Funding

1345 This work was supported by the Genoscope, the Commissariat à l'Énergie Atomique et
1346 aux Énergies Alternatives (CEA) and France Génomique (ANR-10-INBS-09–08). JP
1347 was funded by the Czech Science Foundation 22-18424M.

1348

1349 References

1350 Aase-Remedios ME, Janssen R, Leite DJ, Sumner-Rooney L, McGregor AP. 2023. Evolution of the
1351 Spider Homeobox Gene Repertoire by Tandem and Whole Genome Duplication. *Mol. Biol. Evol.*
1352 40:msad239. doi: 10.1093/molbev/msad239.

1353 Abbas MN et al. 2022. Serpins in Tick Physiology and Tick-Host Interaction. *Front. Cell. Infect. Microbiol.*
1354 12:892770. doi: 10.3389/fcimb.2022.892770.

1355 Ahn S-J, Dermauw W, Wybouw N, Heckel DG, Van Leeuwen T. 2014. Bacterial origin of a diverse family
1356 of UDP-glycosyltransferase genes in the *Tetranychus urticae* genome. *Insect Biochem. Mol. Biol.*
1357 50:43–57. doi: 10.1016/j.ibmb.2014.04.003.

1358 Alberti A et al. 2017. Viral to metazoan marine plankton nucleotide sequences from the Tara Oceans
1359 expedition. *Sci. Data.* 4:170093. doi: 10.1038/sdata.2017.93.

1360 Ali A et al. 2015. Probing the functional role of tick metalloproteases. *Physiol. Entomol.* 40:177–188. doi:
1361 10.1111/phen.12104.

1362 Almagro Armenteros JJ et al. 2019. SignalP 5.0 improves signal peptide predictions using deep neural
1363 networks. *Nat. Biotechnol.* 37:420–423. doi: 10.1038/s41587-019-0036-z.

1364 Alonge M et al. 2022. Automated assembly scaffolding using RagTag elevates a new tomato system for
1365 high-throughput genome editing. *Genome Biol.* 23:258. doi: 10.1186/s13059-022-02823-7.

1366 Altschul SF, Gish W, Miller W, Myers EW, Lipman DJ. 1990. Basic local alignment search tool. *J. Mol.*
1367 *Biol.* 215:403–410. doi: 10.1016/S0022-2836(05)80360-2.

1368 Anand L, Rodriguez Lopez CM. 2022. ChromoMap: an R package for interactive visualization of multi-
1369 omics data and annotation of chromosomes. *BMC Bioinformatics.* 23:33. doi: 10.1186/s12859-
1370 021-04556-z.

1371 Anisimova M, Gascuel O. 2006. Approximate likelihood-ratio test for branches: A fast, accurate, and
1372 powerful alternative. *Syst. Biol.* 55:539–552. doi: 10.1080/10635150600755453.

1373 Aparicio-Puerta E et al. 2019. sRNAbench and sRNAtoolbox 2019: intuitive fast small RNA profiling and
1374 differential expression. *Nucleic Acids Res.* 47:W530–W535. doi: 10.1093/nar/gkz415.

1375 Arcà B, Lombardo F, Struchiner CJ, Ribeiro JMC. 2017. Anopheline salivary protein genes and gene
1376 families: an evolutionary overview after the whole genome sequence of sixteen *Anopheles*
1377 species. *BMC Genomics.* 18:153. doi: 10.1186/s12864-017-3579-8.

1378 Aury J-M et al. 2008. High quality draft sequences for prokaryotic genomes using a mix of new sequencing
1379 technologies. *BMC Genomics.* 9:603. doi: 10.1186/1471-2164-9-603.

1380 Bajda S et al. 2015. Transcriptome profiling of a spirodiclofen susceptible and resistant strain of the
1381 European red mite *Panonychus ulmi* using strand-specific RNA-seq. *BMC Genomics.* 16:974.
1382 doi: 10.1186/s12864-015-2157-1.

1383 Ballesteros JA, Santibáñez López CE, Kováč L, Gavish-Regev E, Sharma PP. 2019. Ordered
1384 phylogenomic subsampling enables diagnosis of systematic errors in the placement of the
1385 enigmatic arachnid order Palpigradi. *Proc. R. Soc. B Biol. Sci.* 286:20192426. doi:
1386 10.1098/rspb.2019.2426.

1387 Becker M et al. 2015. Application of M13 phage display for identifying immunogenic proteins from tick
1388 (*Ixodes scapularis*) saliva. *BMC Biotechnol.* 15:43. doi: 10.1186/s12896-015-0167-3.

1389 Beugnet F, Franc M. 2012. Insecticide and acaricide molecules and/or combinations to prevent pet
1390 infestation by ectoparasites. *Trends Parasitol.* 28:267–279. doi: 10.1016/j.pt.2012.04.004.

1391 Birney E, Clamp M, Durbin R. 2004. GeneWise and Genomewise. *Genome Res.* 14:988–995. doi:
1392 10.1101/gr.1865504.

1393 Bland ND, Pinney JW, Thomas JE, Turner AJ, Isaac RE. 2008. Bioinformatic analysis of the neprilysin
1394 (M13) family of peptidases reveals complex evolutionary and functional relationships. *BMC Evol.*
1395 *Biol.* 8:16. doi: 10.1186/1471-2148-8-16.

1396 Blum M et al. 2021. The InterPro protein families and domains database: 20 years on. *Nucleic Acids Res.*
1397 49:D344–D354. doi: 10.1093/nar/gkaa977.

1398 Bolger AM, Lohse M, Usadel B. 2014. Trimmomatic: a flexible trimmer for Illumina sequence data.
1399 *Bioinformatics.* 30:2114–2120. doi: 10.1093/bioinformatics/btu170.

1400 Buchfink B, Reuter K, Drost H-G. 2021. Sensitive protein alignments at tree-of-life scale using DIAMOND.
1401 *Nat. Methods.* 18:366–368. doi: 10.1038/s41592-021-01101-x.

1402 Buels R et al. 2016. JBrowse: a dynamic web platform for genome visualization and analysis. *Genome*
1403 *Biol.* 17:66. doi: 10.1186/s13059-016-0924-1.

1404 Camacho C et al. 2009. BLAST+: architecture and applications. *BMC Bioinformatics.* 10:421. doi:
1405 10.1186/1471-2105-10-421.

1406 Cantalapiedra CP, Hernández-Plaza A, Letunic I, Bork P, Huerta-Cepas J. 2021. eggNOG-mapper v2:
1407 Functional Annotation, Orthology Assignments, and Domain Prediction at the Metagenomic
1408 Scale. *Mol. Biol. Evol.* 38:5825–5829. doi: 10.1093/molbev/msab293.

1409 Capella-Gutiérrez S, Silla-Martínez JM, Gabaldón T. 2009a. trimAl: a tool for automated alignment
1410 trimming in large-scale phylogenetic analyses. *Bioinformatics.* 25:1972–1973. doi:
1411 10.1093/bioinformatics/btp348.

1412 Capella-Gutiérrez S, Silla-Martínez JM, Gabaldón T. 2009b. trimAl: a tool for automated alignment
1413 trimming in large-scale phylogenetic analyses. *Bioinformatics.* 25:1972–1973. doi:
1414 10.1093/bioinformatics/btp348.

1415 Chan PP, Lowe TM. 2019. tRNAscan-SE: Searching for tRNA genes in genomic sequences. *Methods*
1416 *Mol. Biol.* Clifton NJ. 1962:1–14. doi: 10.1007/978-1-4939-9173-0_1.

1417 Charrier NP et al. 2019. A transcriptome-based phylogenetic study of hard ticks (Ixodidae). *Sci. Rep.* 9.
1418 doi: 10.1038/s41598-019-49641-9.

1419 Charrier NP et al. 2018. Whole body transcriptomes and new insights into the biology of the tick *Ixodes*
1420 *ricinus*. *Parasit. Vectors.* 11:364. doi: 10.1186/s13071-018-2932-3.

1421 Chen C et al. 2020. TBtools: An Integrative Toolkit Developed for Interactive Analyses of Big Biological
1422 Data. *Mol. Plant.* 13:1194–1202. doi: 10.1016/j.molp.2020.06.009.

1423 Chlastáková A et al. 2023. Iripin-1, a new anti-inflammatory tick serpin, inhibits leukocyte recruitment in
1424 vivo while altering the levels of chemokines and adhesion molecules. *Front. Immunol.*
1425 14:1116324. doi: 10.3389/fimmu.2023.1116324.

1426 Chlastáková A et al. 2021. Iripin-3, a New Salivary Protein Isolated From *Ixodes ricinus* Ticks, Displays
1427 Immunomodulatory and Anti-Hemostatic Properties In Vitro. *Front. Immunol.* 12:626200. doi:
1428 10.3389/fimmu.2021.626200.

1429 Chmelar J et al. 2011. A tick salivary protein targets cathepsin G and chymase and inhibits host
1430 inflammation and platelet aggregation. *Blood.* 117:736–744. doi: 10.1182/blood-2010-06-293241.

1431 Chmelař J et al. 2016. Sialomes and Mialomes: A Systems-Biology View of Tick Tissues and Tick–Host
1432 Interactions. *Trends Parasitol.* 32:242–254. doi: 10.1016/j.pt.2015.10.002.

1433 Claudio C et al. 2006. A deficit of detoxification enzymes: pesticide sensitivity and environmental
1434 response in the honeybee. *Insect Mol. Biol.* 15:615–636. doi: 10.1111/j.1365-2583.2006.00672.x.
1435 Danecek P et al. 2021. Twelve years of SAMtools and BCFtools. *GigaScience.* 10:giab008. doi:
1436 10.1093/gigascience/giab008.
1437 De Paula VS et al. 2019. NMR structure determination of Ixolaris and factor X(a) interaction reveals a
1438 noncanonical mechanism of Kunitz inhibition. *Blood.* 134:699–708. doi:
1439 10.1182/blood.2018889493.
1440 De Rouck S, İnak E, Dermauw W, Van Leeuwen T. 2023. A review of the molecular mechanisms of
1441 acaricide resistance in mites and ticks. *Insect Biochem. Mol. Biol.* 159:103981. doi:
1442 10.1016/j.ibmb.2023.103981.
1443 De S et al. 2023. A high-quality *Ixodes scapularis* genome advances tick science. *Nat. Genet.* 55:301–
1444 311. doi: 10.1038/s41588-022-01275-w.
1445 Decrem Y et al. 2008. The impact of gene knock-down and vaccination against salivary metalloproteases
1446 on blood feeding and egg laying by *Ixodes ricinus*. *Int. J. Parasitol.* 38:549–560. doi:
1447 10.1016/j.ijpara.2007.09.003.
1448 Dermauw W, Van Leeuwen T, Feyereisen R. 2020. Diversity and evolution of the P450 family in
1449 arthropods. *Insect Biochem. Mol. Biol.* 127:103490. doi: 10.1016/j.ibmb.2020.103490.
1450 Després L, David J-P, Gallet C. 2007. The evolutionary ecology of insect resistance to plant chemicals.
1451 *Trends Ecol. Evol.* 22:298–307. doi: 10.1016/j.tree.2007.02.010.
1452 Donohue KV et al. 2010. Neuropeptide signaling sequences identified by pyrosequencing of the American
1453 dog tick synganglion transcriptome during blood feeding and reproduction. *Insect Biochem. Mol.*
1454 *Biol.* 40:79–90. doi: 10.1016/j.ibmb.2009.12.014.
1455 Drillon G, Carbone A, Fischer G. 2014. SynChro: A Fast and Easy Tool to Reconstruct and Visualize
1456 Synteny Blocks along Eukaryotic Chromosomes. *PLOS ONE.* 9:e92621. doi:
1457 10.1371/journal.pone.0092621.
1458 Dubarry M et al. 2016. <p>Gmove a tool for eukaryotic gene predictions using various evidences</p>. *F1000Research.* 5. doi: 10.7490/f1000research.1111735.1.
1460 Dunlop JA. 2010. Geological history and phylogeny of Chelicerata. *Arthropod Struct. Dev.* 39:124–142.
1461 doi: 10.1016/j.asd.2010.01.003.
1462 Dunn NA et al. 2019. Apollo: Democratizing genome annotation. *PLOS Comput. Biol.* 15:e1006790. doi:
1463 10.1371/journal.pcbi.1006790.
1464 Emms DM, Kelly S. 2019. OrthoFinder: phylogenetic orthology inference for comparative genomics.
1465 *Genome Biol.* 20:238. doi: 10.1186/s13059-019-1832-y.
1466 Ewels P, Magnusson M, Lundin S, Käller M. 2016. MultiQC: summarize analysis results for multiple tools
1467 and samples in a single report. *Bioinformatics.* 32:3047–3048. doi:
1468 10.1093/bioinformatics/btw354.
1469 Eyun S et al. 2017. Evolutionary History of Chemosensory-Related Gene Families across the Arthropoda.
1470 *Mol. Biol. Evol.* 34:1838–1862. doi: 10.1093/molbev/msx147.
1471 Fablet M, Bueno M, Potrzebowski L, Kaessmann H. 2009. Evolutionary Origin and Functions of Retogene
1472 Introns. *Mol. Biol. Evol.* 26:2147–2156. doi: 10.1093/molbev/msp125.
1473 Flynn JM et al. 2020. RepeatModeler2 for automated genomic discovery of transposable element families.
1474 *Proc. Natl. Acad. Sci.* 117:9451–9457. doi: 10.1073/pnas.1921046117.
1475 Francischetti IMB et al. 2008. An insight into the sialome of the soft tick, *Ornithodoros parkeri*. *Insect*
1476 *Biochem. Mol. Biol.* 38:1–21. doi: 10.1016/j.ibmb.2007.09.009.
1477 Francischetti IMB, Mather TN, Ribeiro JMC. 2003. Cloning of a salivary gland metalloprotease and
1478 characterization of gelatinase and fibrin(ogen)lytic activities in the saliva of the Lyme disease tick
1479 vector *Ixodes scapularis*. *Biochem. Biophys. Res. Commun.* 305:869–875. doi: 10.1016/S0006-
1480 291X(03)00857-X.
1481 Francischetti IMB, Valenzuela JG, Andersen JF, Mather TN, Ribeiro JMC. 2002. Ixolaris, a novel
1482 recombinant tissue factor pathway inhibitor (TFPI) from the salivary gland of the tick, *Ixodes*
1483 *scapularis*: identification of factor X and factor Xa as scaffolds for the inhibition of factor VIIa/tissue
1484 factor complex. *Blood.* 99:3602–3612. doi: 10.1182/blood-2001-12-0237.
1485 Fu L, Niu B, Zhu Z, Wu S, Li W. 2012. CD-HIT: accelerated for clustering the next-generation sequencing
1486 data. *Bioinformatics.* 28:3150–3152. doi: 10.1093/bioinformatics/bts565.
1487 Geraci NS, Spencer Johnston J, Paul Robinson J, Wikle SK, Hill CA. 2007. Variation in genome size of
1488 argasid and ixodid ticks. *Insect Biochem. Mol. Biol.* 37:399–408. doi: 10.1016/j.ibmb.2006.12.007.
1489 Götz S et al. 2008. High-throughput functional annotation and data mining with the Blast2GO suite.
1490 *Nucleic Acids Res.* 36:3420–3435. doi: 10.1093/nar/gkn176.
1491 Grbić M et al. 2011. The genome of *Tetranychus urticae* reveals herbivorous pest adaptations. *Nature.*
1492 479:487–492. doi: 10.1038/nature10640.

1493 Guglielmone AA et al. 2010. **The Argasidae, Ixodidae and Nuttalliellidae (Acari: Ixodida) of the**

1494 world: a list of valid species names. Zootaxa. 2528:1–28. doi:

1495 10.11646/zootaxa.2528.1.1.

1496 Guindon S et al. 2010. New Algorithms and Methods to Estimate Maximum-Likelihood Phylogenies:

1497 Assessing the Performance of PhyML 3.0. Syst. Biol. 59:307–321. doi: 10.1093/sysbio/syq010.

1498 Giulia-Nuss M et al. 2016. Genomic insights into the *Ixodes scapularis* tick vector of Lyme disease. Nat.

1499 Commun. 7:10507. doi: 10.1038/ncomms10507.

1500 Hajdusek O et al. 2009. Knockdown of proteins involved in iron metabolism limits tick reproduction and

1501 development. Proc. Natl. Acad. Sci. 106:1033–1038. doi: 10.1073/pnas.0807961106.

1502 Hoang DT, Chernomor O, von Haeseler A, Minh BQ, Vinh LS. 2018. UFBoot2: Improving the Ultrafast

1503 Bootstrap Approximation. Mol. Biol. Evol. 35:518–522. doi: 10.1093/molbev/msx281.

1504 Holmer R et al. 2019. GeneNoteBook, a collaborative notebook for comparative genomics. Bioinformatics.

1505 35:4779–4781. doi: 10.1093/bioinformatics/btz491.

1506 Hoy MA et al. 2016. Genome Sequencing of the Phytoseiid Predatory Mite *Metaseiulus occidentalis*

1507 Reveals Completely Atomized Hox Genes and Superdynamic Intron Evolution. Genome Biol.

1508 Evol. 8:1762–1775. doi: 10.1093/gbe/evw048.

1509 Huntington JA. 2011. Serpin structure, function and dysfunction. J. Thromb. Haemost. 9:26–34. doi:

1510 10.1111/j.1538-7836.2011.04360.x.

1511 Hussain A et al. 2016. Ionotropic Chemosensory Receptors Mediate the Taste and Smell of Polyamines.

1512 PLOS Biol. 14:e1002454. doi: 10.1371/journal.pbio.1002454.

1513 Jarmey JM, Riding GA, Pearson RD, McKenna RV, Willadsen P. 1995. Carboxydipeptidase from

1514 *Boophilus microplus*: A “concealed” antigen with similarity to angiotensin-converting enzyme.

1515 Insect Biochem. Mol. Biol. 25:969–974. doi: 10.1016/0965-1748(95)00038-W.

1516 Jia N et al. 2020. Large-Scale Comparative Analyses of Tick Genomes Elucidate Their Genetic Diversity

1517 and Vector Capacities. Cell. 182:1328–1340.e13. doi: 10.1016/j.cell.2020.07.023.

1518 Jmel MA et al. 2023. Tick Salivary Kunitz-Type Inhibitors: Targeting Host Hemostasis and Immunity to

1519 Mediate Successful Blood Feeding. Int. J. Mol. Sci. 24:1556. doi: 10.3390/ijms24021556.

1520 Jones P et al. 2014. InterProScan 5: genome-scale protein function classification. Bioinformatics.

1521 30:1236–1240. doi: 10.1093/bioinformatics/btu031.

1522 Jongejan F, Uilenberg G. 2004. The global importance of ticks. Parasitology. 129:S3–S14. doi:

1523 10.1017/S0031182004005967.

1524 Josek T, Walden KKO, Allan BF, Alleyne M, Robertson HM. 2018. A foreleg transcriptome for *Ixodes*

1525 *scapularis* ticks: Candidates for chemoreceptors and binding proteins that might be expressed in

1526 the sensory Haller’s organ. Ticks Tick-Borne Dis. 9:1317–1327. doi: 10.1016/j.ttbdis.2018.05.013.

1527 Joseph RM, Carlson JR. 2015. Drosophila Chemoreceptors: A Molecular Interface Between the Chemical

1528 World and the Brain. Trends Genet. 31:683–695. doi: 10.1016/j.tig.2015.09.005.

1529 Jun G, Wing MK, Abecasis GR, Kang HM. 2015. An efficient and scalable analysis framework for variant

1530 extraction and refinement from population-scale DNA sequence data. Genome Res. 25:918–925.

1531 doi: 10.1101/gr.176552.114.

1532 Kalvari I et al. 2021. Rfam 14: expanded coverage of metagenomic, viral and microRNA families. Nucleic

1533 Acids Res. 49:D192–D200. doi: 10.1093/nar/gkaa1047.

1534 Kalyaanamoorthy S, Minh BQ, Wong TKF, von Haeseler A, Jermiin LS. 2017. ModelFinder: fast model

1535 selection for accurate phylogenetic estimates. Nat. Methods. 14:587–589. doi:

1536 10.1038/nmeth.4285.

1537 Kanehisa M, Sato Y. 2020. KEGG Mapper for inferring cellular functions from protein sequences. Protein

1538 Sci. 29:28–35. doi: 10.1002/pro.3711.

1539 Kang Y-J et al. 2017. CPC2: a fast and accurate coding potential calculator based on sequence intrinsic

1540 features. Nucleic Acids Res. 45:W12–W16. doi: 10.1093/nar/gkx428.

1541 Kascakova B et al. 2023. Conformational transition of the *Ixodes ricinus* salivary serpin Iripin-4. Acta

1542 Crystallogr. Sect. Struct. Biol. 79:409–419. doi: 10.1107/S2059798323002322.

1543 Kascakova B et al. 2021. Structural and biochemical characterization of the novel serpin Iripin-5 from

1544 *Ixodes ricinus*. Acta Crystallogr. Sect. Struct. Biol. 77:1183–1196. doi:

1545 10.1107/S2059798321007920.

1546 Katoh K, Standley DM. 2013. MAFFT Multiple Sequence Alignment Software Version 7: Improvements in

1547 Performance and Usability. Mol. Biol. Evol. 30:772–780. doi: 10.1093/molbev/mst010.

1548 Keirans JE, Needham GR, Oliver Jr JR. 1999. The *Ixodes ricinus* complex worldwide: diagnosis of the

1549 species in the complex, hosts and distribution. In: Acarology IX: Symposia. Columbus, Ohio pp.

1550 341–347.

1551 Kenny NJ et al. 2016. Ancestral whole-genome duplication in the marine chelicerate horseshoe crabs.

1552 Heredity. 116:190–199. doi: 10.1038/hdy.2015.89.

1553 Kent LB, Robertson HM. 2009. Evolution of the sugar receptors in insects. *BMC Evol. Biol.* 9:41. doi:
1554 10.1186/1471-2148-9-41.
1555 Kent WJ. 2002. BLAT—The BLAST-Like Alignment Tool. *Genome Res.* 12:656–664. doi:
1556 10.1101/gr.229202.
1557 Kim D, Paggi JM, Park C, Bennett C, Salzberg SL. 2019. Graph-based genome alignment and genotyping
1558 with HISAT2 and HISAT-genotype. *Nat. Biotechnol.* 37:907–915. doi: 10.1038/s41587-019-0201-
1559 4.
1560 Knecht ZA et al. 2016. Distinct combinations of variant ionotropic glutamate receptors mediate
1561 thermosensation and hygrosensation in *Drosophila* Ramaswami, M, editor. *eLife*. 5:e17879. doi:
1562 10.7554/eLife.17879.
1563 Knecht ZA et al. 2017. Ionotropic Receptor-dependent moist and dry cells control hygrosensation in
1564 *Drosophila* Ramaswami, M, editor. *eLife*. 6:e26654. doi: 10.7554/eLife.26654.
1565 Kopáček P et al. 2003. Molecular cloning, expression and isolation of ferritins from two tick species—
1566 *Ornithodoros moubata* and *Ixodes ricinus*. *Insect Biochem. Mol. Biol.* 33:103–113. doi:
1567 10.1016/S0965-1748(02)00181-9.
1568 Kopáček P, Hajdusek O, Buresová V, Daffre S. 2010. Tick innate immunity. *Adv. Exp. Med. Biol.* 708:137–
1569 162.
1570 Kotál J et al. 2021. *Ixodes ricinus* Salivary Serpin Iripin-8 Inhibits the Intrinsic Pathway of Coagulation and
1571 Complement. *Int. J. Mol. Sci.* 22:9480. doi: 10.3390/ijms22179480.
1572 Kotál J et al. 2019. The structure and function of Iristatin, a novel immunosuppressive tick salivary cystatin.
1573 *Cell. Mol. Life Sci.* 76:2003–2013. doi: 10.1007/s00018-019-03034-3.
1574 Kriventseva EV et al. 2019. OrthoDB v10: sampling the diversity of animal, plant, fungal, protist, bacterial
1575 and viral genomes for evolutionary and functional annotations of orthologs. *Nucleic Acids Res.*
1576 47:D807–D811. doi: 10.1093/nar/gky1053.
1577 Kumar A et al. 2020. Contributions of the Conserved Insect Carbon Dioxide Receptor Subunits to Odor
1578 Detection. *Cell Rep.* 31:107510. doi: 10.1016/j.celrep.2020.03.074.
1579 Kuraku S, Zmasek CM, Nishimura O, Katoh K. 2013. aLeaves facilitates on-demand exploration of
1580 metazoan gene family trees on MAFFT sequence alignment server with enhanced interactivity.
1581 *Nucleic Acids Res.* 41:W22–W28. doi: 10.1093/nar/gkt389.
1582 Kuzmin E, Taylor JS, Boone C. 2022. Retention of duplicated genes in evolution. *Trends Genet.* 38:59–
1583 72. doi: 10.1016/j.tig.2021.06.016.
1584 Lara FA et al. 2015. ATP Binding Cassette Transporter Mediates Both Heme and Pesticide Detoxification
1585 in Tick Midgut Cells. *PLOS ONE*. 10:e0134779. doi: 10.1371/journal.pone.0134779.
1586 Leboulle G et al. 2002. Characterization of a Novel Salivary Immunosuppressive Protein from *Ixodes*
1587 *ricinus* Ticks *. *J. Biol. Chem.* 277:10083–10089. doi: 10.1074/jbc.M111391200.
1588 Lee E et al. 2013. Web Apollo: a web-based genomic annotation editing platform. *Genome Biol.* 14:R93.
1589 doi: 10.1186/gb-2013-14-8-r93.
1590 Lefort V, Desper R, Gascuel O. 2015. FastME 2.0: A Comprehensive, Accurate, and Fast Distance-Based
1591 Phylogeny Inference Program. *Mol. Biol. Evol.* 32:2798–2800. doi: 10.1093/molbev/msv150.
1592 Letunic I, Bork P. 2019. Interactive Tree Of Life (iTOL) v4: recent updates and new developments. *Nucleic*
1593 *Acids Res.* 47:W256–W259. doi: 10.1093/nar/gkz239.
1594 Li H. 2018. Minimap2: pairwise alignment for nucleotide sequences Birol, I, editor. *Bioinformatics*.
1595 34:3094–3100. doi: 10.1093/bioinformatics/bty191.
1596 Li L, Stoeckert CJ, Roos DS. 2003. OrthoMCL: identification of ortholog groups for eukaryotic genomes.
1597 *Genome Res.* 13:2178–2189. doi: 10.1101/gr.1224503.
1598 Li R, Li Y, Kristiansen K, Wang J. 2008. SOAP: short oligonucleotide alignment program. *Bioinformatics*.
1599 24:713–714. doi: 10.1093/bioinformatics/btn025.
1600 Liao Y, Smyth GK, Shi W. 2019. The R package Rsubread is easier, faster, cheaper and better for
1601 alignment and quantification of RNA sequencing reads. *Nucleic Acids Res.* 47:e47. doi:
1602 10.1093/nar/gkz114.
1603 Long M, Betrán E, Thornton K, Wang W. 2003. The origin of new genes: glimpses from the young and
1604 old. *Nat. Rev. Genet.* 4:865–875. doi: 10.1038/nrg1204.
1605 Lozano-Fernandez J et al. 2019. Increasing species sampling in chelicerate genomic-scale datasets
1606 provides support for monophyly of Acari and Arachnida. *Nat. Commun.* 10:2295. doi:
1607 10.1038/s41467-019-10244-7.
1608 Lynch M. 2002. Gene Duplication and Evolution. *Science*. 297:945–947. doi: 10.1126/science.1075472.
1609 Lynch M, Conery JS. 2000. The Evolutionary Fate and Consequences of Duplicate Genes. *Science*.
1610 290:1151–1155. doi: 10.1126/science.290.5494.1151.
1611 Manni M, Berkeley MR, Seppey M, Simão FA, Zdobnov EM. 2021. BUSCO Update: Novel and
1612 Streamlined Workflows along with Broader and Deeper Phylogenetic Coverage for Scoring of

1613 Eukaryotic, Prokaryotic, and Viral Genomes. *Mol. Biol. Evol.* 38:4647–4654. doi: 10.1093/molbev/msab199.

1614 Mans BJ et al. 2016. Ancestral reconstruction of tick lineages. *Ticks Tick-Borne Dis.* 7:509–535. doi: 10.1016/j.ttbdis.2016.02.002.

1615 Mans BJ. 2019. Chemical Equilibrium at the Tick–Host Feeding Interface: A Critical Examination of Biological Relevance in Hematophagous Behavior. *Front. Physiol.* 10. <https://www.frontiersin.org/journals/physiology/articles/10.3389/fphys.2019.00530> (Accessed February 21, 2024).

1616 Mans BJ, Featherston J, de Castro MH, Pienaar R. 2017. Gene Duplication and Protein Evolution in Tick–Host Interactions. *Front. Cell. Infect. Microbiol.* 7. <https://www.frontiersin.org/articles/10.3389/fcimb.2017.00413> (Accessed November 17, 2023).

1617 Mans BJ, Klerk D de, Pienaar R, Castro MH de, Latif AA. 2012. The Mitochondrial Genomes of *Nuttalliella namaqua* (Ixodoidea: Nuttalliellidae) and *Argas africolumbae* (Ixodoidea: Argasidae): Estimation of Divergence Dates for the Major Tick Lineages and Reconstruction of Ancestral Blood-Feeding Characters. *PLOS ONE.* 7:e49461. doi: 10.1371/journal.pone.0049461.

1618 Mans BJ, Klerk D de, Pienaar R, Latif AA. 2011. *Nuttalliella namaqua*: A Living Fossil and Closest Relative to the Ancestral Tick Lineage: Implications for the Evolution of Blood-Feeding in Ticks. *PLOS ONE.* 6:e23675. doi: 10.1371/journal.pone.0023675.

1619 McBride CS. 2007. Rapid evolution of smell and taste receptor genes during host specialization in *Drosophila sechellia*. *Proc. Natl. Acad. Sci.* 104:4996–5001. doi: 10.1073/pnas.0608424104.

1620 McBride CS, Arguello JR. 2007. Five *Drosophila* Genomes Reveal Nonneutral Evolution and the Signature of Host Specialization in the Chemoreceptor Superfamily. *Genetics.* 177:1395–1416. doi: 10.1534/genetics.107.078683.

1621 Medina JM, Jmel MA, et al. 2022. Transcriptomic analysis of the tick midgut and salivary gland responses upon repeated blood-feeding on a vertebrate host. *Front. Cell. Infect. Microbiol.* 12. <https://www.frontiersin.org/articles/10.3389/fcimb.2022.919786> (Accessed June 21, 2023).

1622 Medina JM, Abbas MN, Bensaoud C, Hackenberg M, Kotsyfakis M. 2022. Bioinformatic Analysis of *Ixodes ricinus* Long Non-Coding RNAs Predicts Their Binding Ability of Host miRNAs. *Int. J. Mol. Sci.* 23:9761. doi: 10.3390/ijms23179761.

1623 Mendes FK, Vanderpool D, Fulton B, Hahn MW. 2021. CAFE 5 models variation in evolutionary rates among gene families. *Bioinformatics.* 36:5516–5518. doi: 10.1093/bioinformatics/btaa1022.

1624 Meslin C et al. 2022. *Spodoptera littoralis* genome mining brings insights on the dynamic of expansion of gustatory receptors in polyphagous noctuidae. *G3 GenesGenomesGenetics.* 12:jkac131. doi: 10.1093/g3journal/jkac131.

1625 Meyer H et al. 2021. Identification and bioinformatic analysis of neprilysin and neprilysin-like metalloendopeptidases in *Drosophila melanogaster*. *MicroPublication Biol.* 2021. doi: 10.17912/micropub.biology.000410.

1626 Micheli G, Camilloni G. 2022. Can Introns Stabilize Gene Duplication? *Biology.* 11:941. doi: 10.3390/biology11060941.

1627 Miele V, Penel S, Duret L. 2011. Ultra-fast sequence clustering from similarity networks with SiLiX. *BMC Bioinformatics.* 12:116. doi: 10.1186/1471-2105-12-116.

1628 Min S, Ai M, Shin SA, Suh GSB. 2013. Dedicated olfactory neurons mediating attraction behavior to ammonia and amines in *Drosophila*. *Proc. Natl. Acad. Sci.* 110:E1321–E1329. doi: 10.1073/pnas.1215680110.

1629 Minh BQ et al. 2020. IQ-TREE 2: New Models and Efficient Methods for Phylogenetic Inference in the Genomic Era. *Mol. Biol. Evol.* 37:1530–1534. doi: 10.1093/molbev/msaa015.

1630 Missbach C et al. 2014. Evolution of insect olfactory receptors Jékely, G, editor. *eLife.* 3:e02115. doi: 10.7554/eLife.02115.

1631 Mott R. 1997. EST_GENOME: a program to align spliced DNA sequences to unspliced genomic DNA. *Comput. Appl. Biosci.* 13:477–478. doi: 10.1093/bioinformatics/13.4.477.

1632 Nauen R, Bass C, Feyereisen R, Vontas J. 2022. The Role of Cytochrome P450s in Insect Toxicology and Resistance. *Annu. Rev. Entomol.* 67:105–124. doi: 10.1146/annurev-ento-070621-061328.

1633 Nawrocki EP, Eddy SR. 2013. Infernal 1.1: 100-fold faster RNA homology searches. *Bioinformatics.* 29:2933–2935. doi: 10.1093/bioinformatics/btt509.

1634 Nazareth RA et al. 2006. Antithrombotic properties of Ixolaris, a potent inhibitor of the extrinsic pathway of the coagulation cascade. *Thromb. Haemost.* 96:7–13. doi: 10.1160/TH06-02-0105.

1635 Neese PA, E. Sonenshine D, Kallapur VL, Apperson CS, Roe RM. 2000. Absence of insect juvenile hormones in the American dog tick, *Dermacentor variabilis* (Say) (Acari:Ixodidae), and in *Ornithodoros parkeri* Cooley (Acari:Argasidae). *J. Insect Physiol.* 46:477–490. doi: 10.1016/S0022-1910(99)00134-1.

1673 Nguyen L-T, Schmidt HA, von Haeseler A, Minh BQ. 2015. IQ-TREE: A Fast and Effective Stochastic
1674 Algorithm for Estimating Maximum-Likelihood Phylogenies. *Mol. Biol. Evol.* 32:268–274. doi:
1675 10.1093/molbev/msu300.

1676 Nicewicz AW, Sawadro MK, Nicewicz Ł, Babczyńska AI. 2021. Juvenile hormone in spiders. Is this the
1677 solution to a mystery? *Gen. Comp. Endocrinol.* 308:113781. doi: 10.1016/j.ygcen.2021.113781.

1678 Nuss AB et al. 2023. The highly improved genome of *Ixodes scapularis* with X and Y
1679 pseudochromosomes. *Life Sci. Alliance.* 6. doi: 10.26508/lsa.202302109.

1680 Oakeshott J, Claudianos C, Campbell PM, Newcomb R, Russell RJ. 2005. Biochemical genetics and
1681 genomics of insect esterases. In: *Comprehensive Molecular Insect Science-Pharmacology*.
1682 Elsevier: Amsterdam, The Netherlands pp. 309–381.

1683 Oh HJ, Jung Y. 2023. High order assembly of multiple protein cages with homogeneous sizes and shapes
1684 via limited cage surface engineering. *Chem. Sci.* 14:1105–1113. doi: 10.1039/D2SC02772K.

1685 Ohno S. 1970. *Evolution by Gene Duplication*. Springer: Berlin, Heidelberg doi: 10.1007/978-3-642-
1686 86659-3.

1687 Oliver JH. 1977. Cytogenetics of Mites and Ticks. *Annu. Rev. Entomol.* 22:407–429. doi:
1688 10.1146/annurev.en.22.010177.002203.

1689 Pan D, Zhang L. 2008. Tandemly Arrayed Genes in Vertebrate Genomes. *Comp. Funct. Genomics.*
1690 2008:545269. doi: 10.1155/2008/545269.

1691 Paradis E, Schliep K. 2019. ape 5.0: an environment for modern phylogenetics and evolutionary analyses
1692 in R. *Bioinformatics.* 35:526–528. doi: 10.1093/bioinformatics/bty633.

1693 Parola P, Raoult D. 2001. Ticks and Tickborne Bacterial Diseases in Humans: An Emerging Infectious
1694 Threat. *Clin. Infect. Dis.* 32:897–928. doi: 10.1086/319347.

1695 Perner J, Sobotka R, et al. 2016. Acquisition of exogenous haem is essential for tick reproduction Pal, U,
1696 editor. *eLife.* 5:e12318. doi: 10.7554/eLife.12318.

1697 Perner J et al. 2018. Inducible glutathione S-transferase (*IrGST1*) from the tick *Ixodes ricinus* is a haem-
1698 binding protein. *Insect Biochem. Mol. Biol.* 95:44–54. doi: 10.1016/j.ibmb.2018.02.002.

1699 Perner J, Provažník J, et al. 2016. RNA-seq analyses of the midgut from blood- and serum-fed *Ixodes*
1700 *ricinus* ticks. *Sci. Rep.* 6:36695. doi: 10.1038/srep36695.

1701 Perner J et al. 2020. The Central Role of Salivary Metalloproteases in Host Acquired Resistance to Tick
1702 Feeding. *Front. Cell. Infect. Microbiol.* 10.
1703 https://www.frontiersin.org/articles/10.3389/fcimb.2020.563349 (Accessed February 5, 2024).

1704 Perner J, Gasser RB, Oliveira PL, Kopáček P. 2019. Haem Biology in Metazoan Parasites – ‘The Bright
1705 Side of Haem’. *Trends Parasitol.* 35:213–225. doi: 10.1016/j.pt.2019.01.001.

1706 Perner J, Hajdusek O, Kopáček P. 2022. Independent somatic distribution of heme and iron in ticks. *Curr.*
1707 *Opin. Insect Sci.* 51:100916. doi: 10.1016/j.cois.2022.100916.

1708 Pertea G, Pertea M. 2020. GFF Utilities: GffRead and GffCompare. doi:
1709 10.12688/f1000research.23297.2.

1710 Puinongpo W et al. 2020. Existence of Bov-B LINE Retrotransposons in Snake Lineages Reveals Recent
1711 Multiple Horizontal Gene Transfers with Copy Number Variation. *Genes.* 11:1241. doi:
1712 10.3390/genes11111241.

1713 Ranallo-Benavidez TR, Jaron KS, Schatz MC. 2020. GenomeScope 2.0 and Smudgeplot for reference-
1714 free profiling of polyploid genomes. *Nat. Commun.* 11:1432. doi: 10.1038/s41467-020-14998-3.

1715 Revell LJ. 2012. phytools: an R package for phylogenetic comparative biology (and other things). *Methods*
1716 *Ecol. Evol.* 3:217–223. doi: 10.1111/j.2041-210X.2011.00169.x.

1717 Rewitz KF, Rybczynski R, Warren JT, Gilbert LI. 2006. The Halloween genes code for cytochrome P450
1718 enzymes mediating synthesis of the insect moulting hormone. *Biochem. Soc. Trans.* 34:1256–
1719 1260. doi: 10.1042/BST0341256.

1720 Ribeiro JM et al. 2023. Blood-feeding adaptations and virome assessment of the poultry red mite
1721 *Dermanyssus gallinae* guided by RNA-seq. *Commun. Biol.* 6:517. doi: 10.1038/s42003-023-
1722 04907-x.

1723 Rispe C et al. 2022. Transcriptome of the synganglion in the tick *Ixodes ricinus* and evolution of the cys-
1724 loop ligand-gated ion channel family in ticks. *BMC Genomics.* 23:463. doi: 10.1186/s12864-022-
1725 08669-4.

1726 Robertson HM, Wanner KW. 2006. The chemoreceptor superfamily in the honey bee, *Apis mellifera*:
1727 Expansion of the odorant, but not gustatory, receptor family. *Genome Res.* 16:1395–1403. doi:
1728 10.1101/gr.5057506.

1729 Robertson HM, Warr CG, Carlson JR. 2003. Molecular evolution of the insect chemoreceptor gene
1730 superfamily in *Drosophila melanogaster*. *Proc. Natl. Acad. Sci.* 100:14537–14542. doi:
1731 10.1073/pnas.2335847100.

1732 Rosani U, Sollitto M, Fogal N, Salata C. 2023. Comparative analysis of Presence-Absence gene
1733 Variations in five hard tick species: impact and functional considerations. *Int. J. Parasitol.* doi:
1734 10.1016/j.ijpara.2023.08.004.

1735 Ruzzante L, Reijnders MJMF, Waterhouse RM. 2019. Of Genes and Genomes: Mosquito Evolution and
1736 Diversity. *Trends Parasitol.* 35:32–51. doi: 10.1016/j.pt.2018.10.003.

1737 Rytz R, Croset V, Benton R. 2013. Ionotropic Receptors (IRs): Chemosensory ionotropic glutamate
1738 receptors in *Drosophila* and beyond. *Insect Biochem. Mol. Biol.* 43:888–897. doi:
1739 10.1016/j.ibmb.2013.02.007.

1740 Sands AF et al. 2017. Effects of tectonics and large scale climatic changes on the evolutionary history of
1741 *Hyalomma* ticks. *Mol. Phylogenet. Evol.* 114:153–165. doi: 10.1016/j.ympev.2017.06.002.

1742 van Schooten B, Jiggins CD, Briscoe AD, Papa R. 2016. Genome-wide analysis of ionotropic receptors
1743 provides insight into their evolution in *Heliconius* butterflies. *BMC Genomics.* 17:254. doi:
1744 10.1186/s12864-016-2572-y.

1745 Schwager EE et al. 2017. The house spider genome reveals an ancient whole-genome duplication during
1746 arachnid evolution. *BMC Biol.* 15:62. doi: 10.1186/s12915-017-0399-x.

1747 Sharma PP et al. 2014. Phylogenomic Interrogation of Arachnida Reveals Systemic Conflicts in
1748 Phylogenetic Signal. *Mol. Biol. Evol.* 31:2963–2984. doi: 10.1093/molbev/msu235.

1749 Sharma PP, Ballesteros JA, Santibáñez-López CE. 2021. What is an “arachnid”? Consensus, consilience,
1750 and confirmation bias in the phylogenetics of Chelicerata. *Diversity.* 13:568.

1751 Shim J et al. 2015. The full repertoire of *Drosophila* gustatory receptors for detecting an aversive
1752 compound. *Nat. Commun.* 6:8867. doi: 10.1038/ncomms9867.

1753 Sievers F et al. 2011. Fast, scalable generation of high-quality protein multiple sequence alignments using
1754 Clustal Omega. *Mol. Syst. Biol.* 7:539. doi: 10.1038/msb.2011.75.

1755 Šimo L, Kazimirova M, Richardson J, Bonnet SI. 2017. The Essential Role of Tick Salivary Glands and
1756 Saliva in Tick Feeding and Pathogen Transmission. *Front. Cell. Infect. Microbiol.* 7:281. doi:
1757 10.3389/fcimb.2017.00281.

1758 Slater GSC, Birney E. 2005. Automated generation of heuristics for biological sequence comparison. *BMC
1759 Bioinformatics.* 6:31. doi: 10.1186/1471-2105-6-31.

1760 Spence MA, Mortimer MD, Buckle AM, Minh BQ, Jackson CJ. 2021. A Comprehensive Phylogenetic
1761 Analysis of the Serpin Superfamily. *Mol. Biol. Evol.* 38:2915–2929. doi:
1762 10.1093/molbev/msab081.

1763 Suiko M, Kurogi K, Hashiguchi T, Sakakibara Y, Liu M-C. 2017. Updated perspectives on the cytosolic
1764 sulfotransferases (SULTs) and SULT-mediated sulfation. *Biosci. Biotechnol. Biochem.* 81:63–72.
1765 doi: 10.1080/09168451.2016.1222266.

1766 Van Dam MH, Trautwein M, Spicer GS, Esposito L. 2019. Advancing mite phylogenomics: Designing
1767 ultraconserved elements for Acari phylogeny. *Mol. Ecol. Resour.* 19:465–475. doi: 10.1111/1755-
1768 0998.12962.

1769 Van Zee JP et al. 2016. Paralog analyses reveal gene duplication events and genes under positive
1770 selection in *Ixodes scapularis* and other ixodid ticks. *BMC Genomics.* 17:241. doi:
1771 10.1186/s12864-015-2350-2.

1772 Vinckenbosch N, Dupanloup I, Kaessmann H. 2006. Evolutionary fate of retroposed gene copies in the
1773 human genome. *Proc. Natl. Acad. Sci.* 103:3220–3225. doi: 10.1073/pnas.0511307103.

1774 Waldman J et al. 2022. Neuropeptides in *Rhipicephalus microplus* and other hard ticks. *Ticks Tick-Borne
1775 Dis.* 13:101910. doi: 10.1016/j.ttbdis.2022.101910.

1776 Walsh AM, Kortschak RD, Gardner MG, Bertozi T, Adelson DL. 2013. Widespread horizontal transfer of
1777 retrotransposons. *Proc. Natl. Acad. Sci.* 110:1012–1016. doi: 10.1073/pnas.1205856110.

1778 Wang L-G et al. 2020. Treeio: An R Package for Phylogenetic Tree Input and Output with Richly
1779 Annotated and Associated Data. *Mol. Biol. Evol.* 37:599–603. doi: 10.1093/molbev/msz240.

1780 Wang Y, Zhu S. 2011. The defensin gene family expansion in the tick *Ixodes scapularis*. *Dev. Comp.
1781 Immunol.* 35:1128–1134. doi: 10.1016/j.dci.2011.03.030.

1782 Waterhouse A et al. 2018. SWISS-MODEL: homology modelling of protein structures and complexes.
1783 *Nucleic Acids Res.* 46:W296–W303. doi: 10.1093/nar/gky427.

1784 Watkins PA, Maiguel D, Jia Z, Pevsner J. 2007. Evidence for 26 distinct acyl-coenzyme A synthetase
1785 genes in the human genome. *J. Lipid Res.* 48:2736–2750. doi: 10.1194/jlr.M700378-JLR200.

1786 Wickham H. 2016. *ggplot2*. Springer International Publishing: Cham doi: 10.1007/978-3-319-24277-4.

1787 Wolfe KH, Shields DC. 1997. Molecular evidence for an ancient duplication of the entire yeast genome.
1788 *Nature.* 387:708–713. doi: 10.1038/42711.

1789 Wu J et al. 2022. Defensins as a promising class of tick antimicrobial peptides: a scoping review. *Infect.
1790 Dis. Poverty.* 11:71. doi: 10.1186/s40249-022-00996-8.

1791 Xu G, Fang QQ, Keirans JE, Durden LA. 2003. Molecular phylogenetic analyses indicate that the ixodes
1792 ricinus complex is a paraphyletic group. *J. Parasitol.* 89:452–457. doi: 10.1645/0022-
1793 3395(2003)089[0452:MPAITT]2.0.CO;2.

1794 Xu Z et al. 2023. Proteomic analysis of extracellular vesicles from tick hemolymph and uptake of
1795 extracellular vesicles by salivary glands and ovary cells. *Parasit. Vectors.* 16:125. doi:
1796 10.1186/s13071-023-05753-w.

1797 Yang Z-M et al. 2021. Genomic Identification and Functional Analysis of JHAMTs in the Pond Wolf Spider,
1798 *Pardosa pseudoannulata*. *Int. J. Mol. Sci.* 22:11721. doi: 10.3390/ijms222111721.

1799 Yu G, Smith DK, Zhu H, Guan Y, Lam TT-Y. 2017. ggtree: an r package for visualization and annotation
1800 of phylogenetic trees with their covariates and other associated data. *Methods Ecol. Evol.* 8:28–
1801 36. doi: 10.1111/2041-210X.12628.

1802 Zhang Y-X et al. 2019. Genomic insights into mite phylogeny, fitness, development, and reproduction.
1803 *BMC Genomics.* 20:954. doi: 10.1186/s12864-019-6281-1.

1804 Zhu J et al. 2016. Mevalonate-Farnesal Biosynthesis in Ticks: Comparative Synganglion Transcriptomics
1805 and a New Perspective. *PLoS ONE.* 11:e0141084. doi: 10.1371/journal.pone.0141084.

Figures and Tables Legends

Tables

Table 1: Metrics of genome assemblies of the four *Ixodes* species, and of their gene catalogs. For *I. ricinus*, the metrics are given prior to HiC scaffolding, and gene counts are prior to manual curation (i.e. for the OGS1.0 version of the prediction).

	<i>Ixodes ricinus</i>	<i>Ixodes persulcatus</i>	<i>Ixodes pacificus</i>	<i>Ixodes hexagonus</i>
Estimated genome size	2.6 Gb	2.2 Gb	1.8 Gb	2.7 Gb
Cumulative size	2,266,064,099	2,508,899,395	2,295,733,707	2,627,922,774
# scaffolds	76.37	178.628	199.32	143.052
N50 (L50)	293,124 (1,505)	79,428 (5,227)	32,483 (15,538)	196,001 (2,765)
Average scaffold size	29.672	14.045	11.517	18.37
Max scaffold size	5,276,202	3,084,009	903,275	4,222,030
Mercury score	42.2973	42.9407	42.6649	43.9246
Number of predicted genes (OGS 1.0)	22.486	24.979	29.201	19.511
Average number of exons per gene	5.65	4.67	4.06	5.44
CDS avg/med length (bp)	1,124/789	1,042/732	899/630	1,224/918
Genes av/med length (bp)	30,176/8,214	14,586/3,941	9,526/3,324	21,158/5,354
Introns avg/med length (bp)	5,301/1,665	3,169/1,483	2,474/1,313	3,964/1,851
ENA accession numbers	PRJEB67792	PRJEB67789	PRJEB67791	PRJEB67790

Table 2: Completeness of the species of Chelicerata included in our comparative study. The four *Ixodes* genomes sequenced in this study are in bold character. The search of conserved genes was made using BUSCO with the Arachnida odb_10 database (search of 2934 conserved genes). Group (ticks or other Chelicerata) and species name, Numbers (five next columns) or Percentages (five last columns) of different categories of BUSCO genes, as detailed in the headers.

Group	Species	complete BUSCOs (C)	Complete and single-copy BUSCOs (S)	complete and duplicated BUSCOs (D)	Fragmented BUSCOs (F)	Missing BUSCOs (M)	Percentage C	Percentage S	Percentage D	Percentage F	Percentage M
Ticks	<i>Dermacentor andersoni</i>	2895	2772	123	5	34	98.7	94.5	4.2	0.2	1.1
	<i>Dermacentor silvarum</i>	2885	2717	168	18	31	98.3	92.6	5.7	0.6	1.1
	<i>Hyalomma asiaticum</i>	1907	1835	72	124	903	65.0	62.5	2.5	4.2	30.8
	<i>Haemaphysalis longicornis</i>	1640	1560	80	158	1136	55.9	53.2	2.7	5.4	38.7
	<i>Rhipicephalus microplus</i>	2804	2685	119	16	114	95.6	91.5	4.1	0.5	3.9
	<i>Rhipicephalus sanguineus</i>	2806	2609	197	34	94	95.6	88.9	6.7	1.2	3.2
	<i>Ixodes scapularis</i>	2893	2741	152	7	34	98.6	93.4	5.2	0.2	1.2
	<i>Ixodes hexagonus</i>	2683	2573	110	88	163	91.4	87.7	3.7	3.0	5.6
	<i>Ixodes ricinus</i>	2679	2591	88	78	177	91.3	88.3	3.0	2.7	6.0
	<i>Ixodes pacificus</i>	2403	2059	344	199	332	81.9	70.2	11.7	6.8	11.3
	<i>Ixodes persulcatus</i>	2581	2397	184	121	232	88.0	81.7	6.3	4.1	7.9
Other Chelicerata	<i>Limulus polyphemus</i>	2762	2052	710	77	95	94.1	69.9	24.2	2.6	3.3
	<i>Centruroides sculpturatus</i>	2839	2567	272	55	40	96.8	87.5	9.3	1.9	1.3
	<i>Oedothorax gibbosus</i>	2793	2635	158	31	110	95.2	89.8	5.4	1.1	3.7
	<i>Trichonephila clavata</i>	2817	2355	462	43	74	96.0	80.3	15.7	1.5	2.5
	<i>Parasteotoda tepidariorum</i>	2870	2703	167	31	33	97.8	92.1	5.7	1.1	1.1
	<i>Galendromus occidentalis</i>	2896	2814	82	4	34	98.7	95.9	2.8	0.1	1.2
	<i>Varroa destructor</i>	2897	2861	36	2	35	98.7	97.5	1.2	0.1	1.2
	<i>Sarcoptes scabiei</i>	2724	2686	38	37	173	92.8	91.5	1.3	1.3	5.9
	<i>Oppiella nova</i>	2458	2183	275	123	353	83.8	74.4	9.4	4.2	12.0
	<i>Tetranychus urticae</i>	2771	2589	182	11	152	94.4	88.2	6.2	0.4	5.2

Table 3: Repeated elements in the genomes of the four *Ixodes* species (*I. ricinus*, *I. hexagonus*, *I. pacificus* and *I. persulcatus*). *: Most repeats fragmented by insertions or deletions have been counted as one element.

Element family	<i>Ixodes ricinus</i>		<i>Ixodes hexagonus</i>		<i>Ixodes pacificus</i>		<i>Ixodes persulcatus</i>	
	Number of elements*	Percentage of genome coverage	Number of elements*	Percentage of genome coverage	Number of elements*	Percentage of genome coverage	Number of elements*	Percentage of genome coverage
Retroelements (class I):	467 260	11.74 %	563 828	14.96 %	606 344	14.30 %	677 841	14.45 %
SINEs:	692	0.01 %	795	0.00 %	935	0.01 %	773	0.00 %
LINEs:	318 541	7.14 %	385 768	9.00 %	429 800	9.31 %	455 040	8.53 %
Penelope	68 082	1.10 %	52 969	0.76 %	94 523	1.29 %	74 359	1.04 %
L2/CR1/Rex	158 040	3.39 %	138 618	2.66 %	200 079	4.04 %	227 456	3.98 %
R1/LOA/Jockey	31 715	1.22 %	97 692	3.18 %	55 214	2.22 %	54 525	1.69 %
R2/R4/NeSL	70	0.00 %	0	0.00 %	141	0.00 %	619	0.01 %
RTE/Bov-B	17 064	0.38 %	24 517	0.72 %	24 545	0.56 %	22 648	0.56 %
L1/CIN4	9 668	0.24 %	4 572	0.13 %	6 385	0.14 %	12 171	0.21 %
LTR elements:	148 027	4.60 %	177 265	5.96 %	175 609	4.98 %	222 028	5.91 %
BEL/Pao	6 689	0.23 %	5 431	0.24 %	9 471	0.28 %	11 330	0.27 %
Ty1/Copia	4 200	0.05 %	148	0.00 %	6 571	0.06 %	3 480	0.03 %
Gypsy/DIRS1	125 677	4.10 %	169 153	5.68 %	155 980	4.61 %	198 078	5.52 %
Retroviral	1 721	0.02 %	1 959	0.02 %	809	0.01 %	2 575	0.03 %
DNA transposons (class II):	224 170	3.49 %	349 135	4.94 %	303 130	4.03 %	286 973	3.92 %
TIR elements:								
hobo-Activator	100 154	1.39 %	212 903	2.82 %	143 436	1.65 %	133 077	1.49 %
Tc1-IS630-Pogo	38 954	0.60 %	54 536	0.88 %	49 829	0.65 %	45 241	0.61 %
PiggyBac	1 478	0.03 %	2 492	0.04 %	1 580	0.02 %	2 548	0.07 %
Tourist/Harbinger	9 998	0.14 %	9 633	0.10 %	14 154	0.14 %	18 704	0.36 %
Other (Mirage, P-element, Transib)	26 806	0.55 %	7 947	0.14 %	25 637	0.45 %	30 809	0.39 %
Rolling-circles (Helitrons):	29 289	0.39 %	57 465	0.72 %	75 418	0.51 %	43 503	0.35 %
Unclassified:	3 912 196	40.68 %	4 588 330	46.42 %	4 704 132	44.66 %	4 738 687	43.12 %
Total interspersed repeats:		55.91 %		66.31 %		62.99 %		61.49 %
Small RNA:	38 630	0.37 %	36 622	0.37 %	50 953	0.54 %	32 867	0.31 %
Satellites:	0	0.00 %	4 420	3.00 %	3 946	0.04 %	5 945	0.05 %
Simple repeats:	319 274	0.55 %	250 286	0.41 %	17 318	0.06 %	16 351	0.05 %
Low complexity:	35 265	0.07 %	21 427	0.04 %	0	0.00 %	0	0.00 %
Total	5 026 081	57.30 %	5 871 508	67.88 %	5 761 216	64.14 %	5 802 151	62.25 %

Table 4: Distribution of structural and regulatory non-coding elements in the genome of *I. ricinus*.

Non-coding element	Class	Number
Transfer RNA	Non-coding RNA	9815
Ribosomal RNA	Non-coding RNA	267
Small nuclear RNA	Non-coding RNA	192
Small nucleolar RNA	Non-coding RNA	21
Binding small RNA	Non-coding RNA	1
microRNA	Non-coding RNA	63
Long non-coding RNA	Non-coding RNA	10696
Signal recognition particle	Non-coding RNA	16
Ribozyme	Non-coding RNA	3
Riboswitch	Cis-regulatory element	35
UTR stem-loop	Cis-regulatory element	662
Iron response element	Cis-regulatory element	5
Potassium channel RNA editing signal	Cis-regulatory element	5

Table 5: Number of chemosensory receptor genes for eight Arthropoda species, including *I. ricinus* (genome sequenced and annotated in this study).

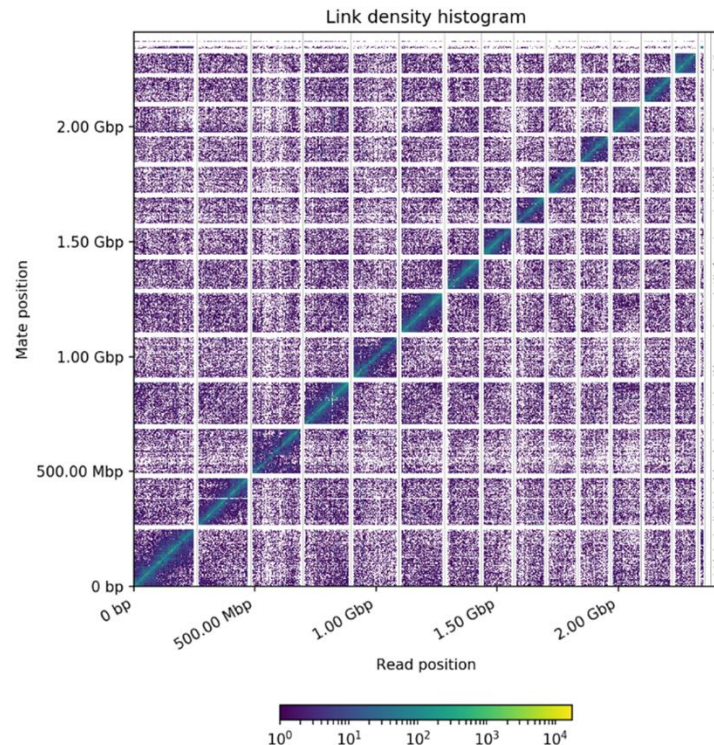
Class	Species	IRs	GRs	ORs
Insect	<i>Drosophila melanogaster</i>	63	68	62
Insect	<i>Bombyx mori</i>	31	76	49
Insect	<i>Tribolium castaneum</i>	22	207	259
Insect	<i>Apis mellifera</i>	10	10	163
Acari	<i>Ixodes ricinus</i>	159	71	0
Acari	<i>Ixodes scapularis</i>	125	63	0
Acari	<i>Galendromus occidentalis</i>	65	64	0
Acari	<i>Tetranychus urticae</i>	18	447	0

Table 6: Gene counts for proteins involved in detoxification processes. Counts are given for two tick species (*I. ricinus* and *I. scapularis*) and another Acari (*T. urticae*). For cytosolic sulfotransferases (SULTs), the numbers given correspond to gene counts in the SiLiX family FAM00226 (pre-manual curation).

Gene families	<i>I. ricinus</i>	<i>I. scapularis</i>	<i>T. urticae</i>
CYP			
clan 2	53	42	48
clan 20	1	1	0
clan 3	105	106	10
clan 4	31	39	23
clan mito	4	4	5
Total CYPs	194	192	86
CCE			
Dietary			
A, B, C	0	0	0
Hormone/semiochemical			
D, E, F, G	0	0	0
F'	1	2	2
Neuro/developmental			
H (glutactin)	0	3	2
I (unkown)	1	1	2
J (AChE)	4	2	1
J'/J1	17	12	34
J"	0	0	22
J2	74	64	1
K (gliotactin)	1	1	1
L (neuroligins)	2	2	5
M (neurotactin)	1	2	1
UN (unkown)	3	2	1
Total CCEs	104	91	72
GSTs			
Microsomal	1	2	0
Kappa	1	2	1
Mu	20	20	12
Omega	5	4	2
Zeta	8	4	1
Epsilon	6	7	0
Delta	8	10	16
Total GSTs	49	49	32
SULTs			
Clade A	1	1	1
Clade B	1	1	1
Clade C	195	207	0
Total SULTs	197*	209*	0
ABCs			
A	22	19	9
B	6	6	4
C	55	57	39
D	3	3	2
E	1	1	1
F	3	3	3
G	11	11	23
H	3	3	22
Total ABCs	104	103	103

Figures

A



B

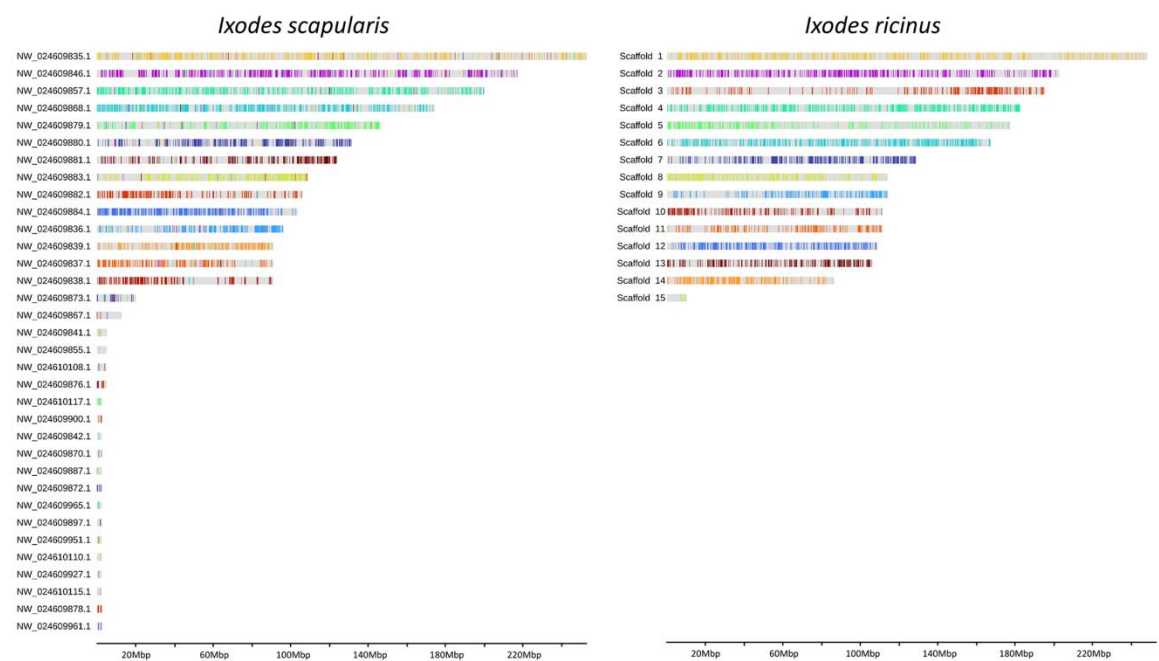


Figure 1: Continuity of the *I. ricinus* genome assembly and synteny with the *I. scapularis* genome. **A** Hi-C map of interactions for the *I. ricinus* genome assembly, showing 14 major scaffolds. The x and y axes give the mapping positions of the first and second read in the read pair respectively, grouped into bins. The color of each square gives the number of read pairs within that bin. Scaffolds less than 1 Mb are excluded. **B** Synteny between the genomes of *I. scapularis* and *I. ricinus*. Horizontal bars represent the major scaffolds of each genome, while syntenies between the two species are indicated by identical colors.

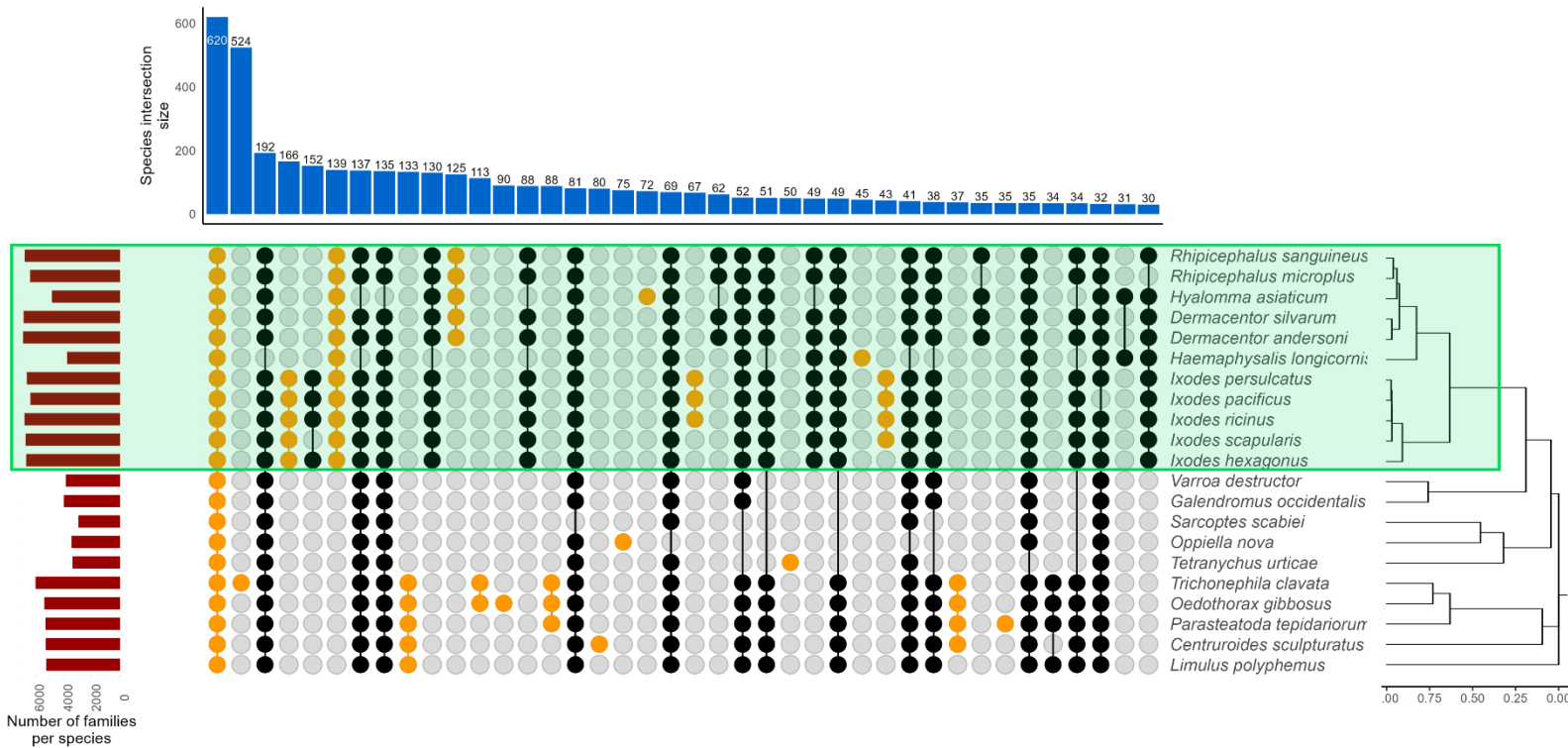


Figure 2: Distribution of gene families among the genomes of twenty-one different species of Chelicerata. Families identified as putative transposable elements were filtered out. The top bar plot represents the number of families shared in a given intersection, the left bar plots gives the number of families per species. Species were ordered according to their phylogeny (right tree) and intersections with a phylogenetic relevance are indicated in orange. Tick (Ixodida) species are highlighted in green

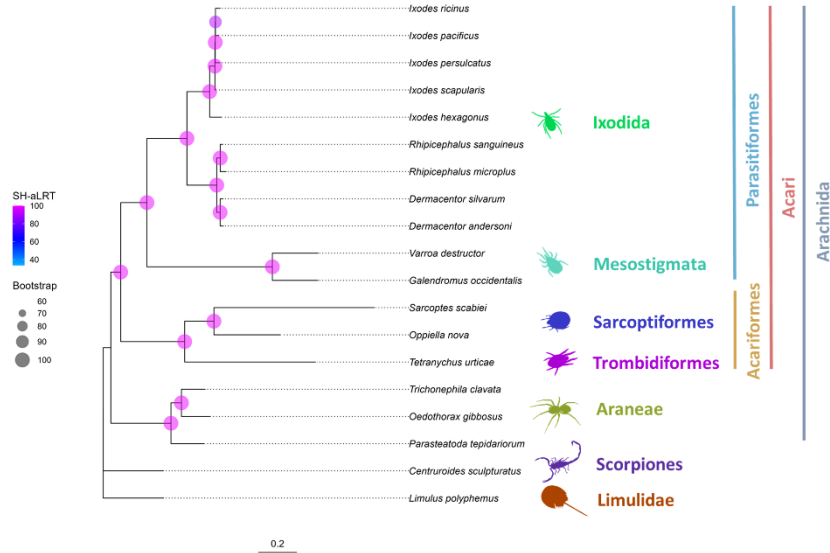


Figure 3: Phylogenetic tree of Chelicerata, based on complete genomes. This analysis was restricted to species with high genome completeness (e.g. without *Hya. marginatum* and *Hae. longicornis*). The tree was built by IQ-TREE 2 using a concatenation of 107 single-copy protein sequences, shared by all represented species. Branch support is shown by bootstrap values and Shimodaira-Hasegawa approximate likelihood ratio test (SH-aLRT) values.

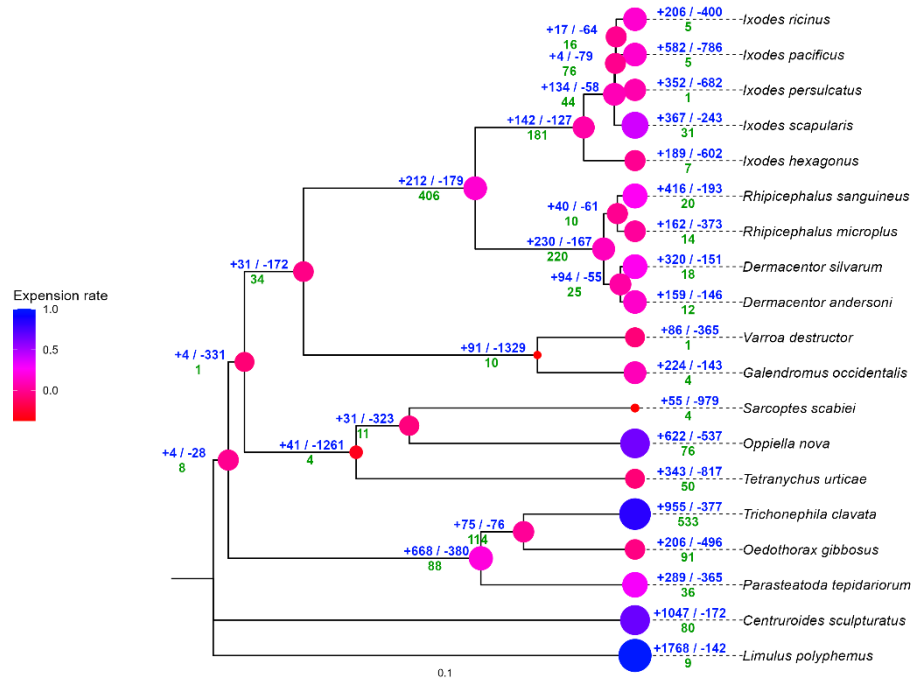


Figure 4: Gene expansion and contraction dynamics in Chelicerata species, analyzed with CAFE. The expansion rate per node is given by the size and the color of the points. The number of expanding (+) or contracting (-) gene families for each node is in blue and above the branches. The number of new families per node is in green. The tree was built by IQ-TREE 2 using 107 protein sequences, before being transformed into an ultrametric tree using phytools and ape R packages.

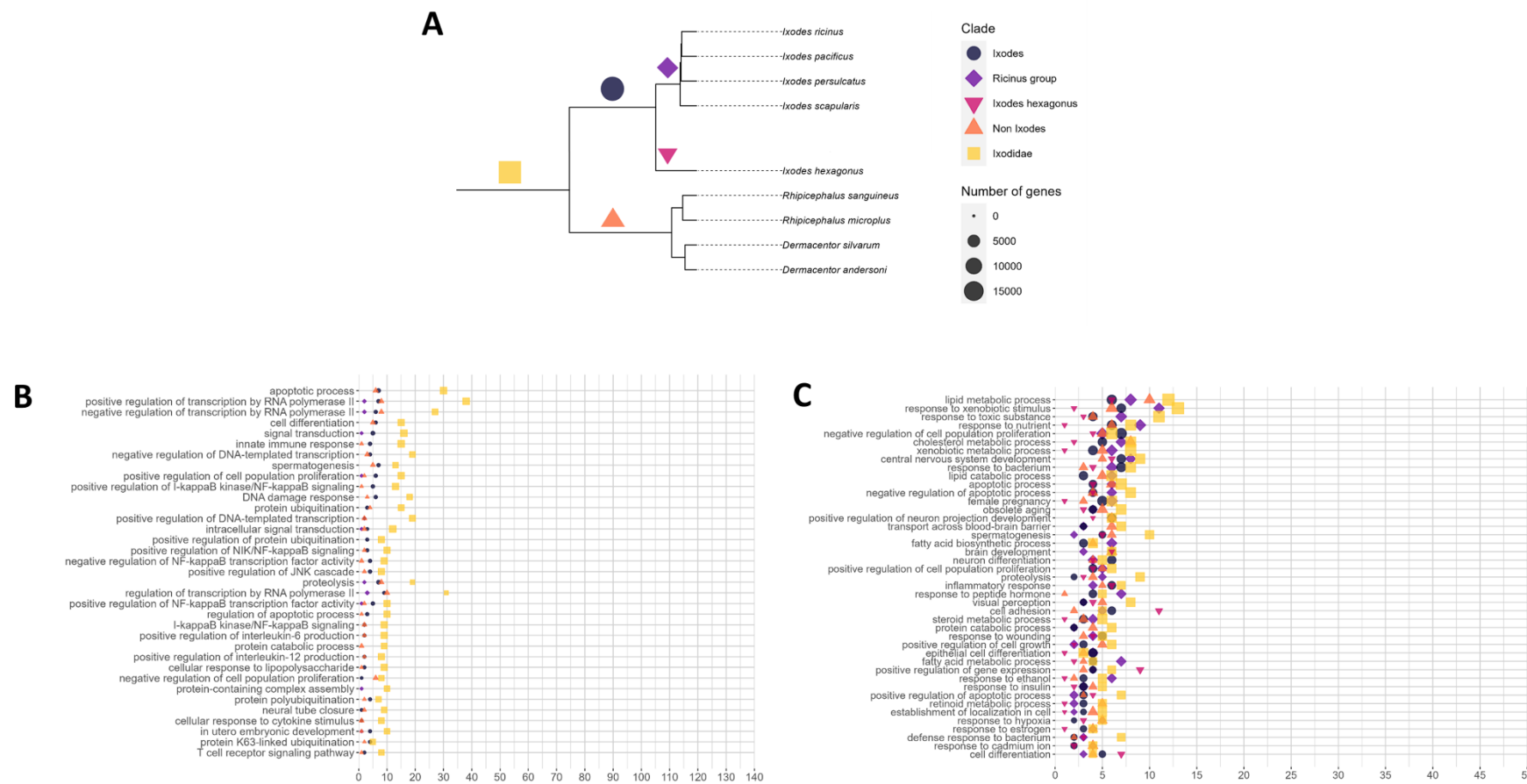
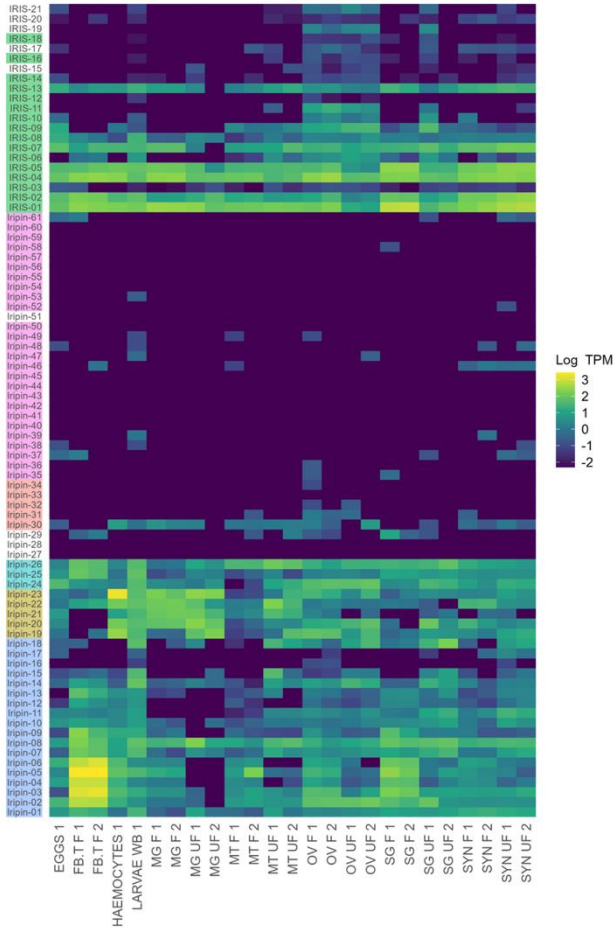


Figure 5: Enriched gene ontology terms (GOs) in gained and expanded families during the evolution of ticks. **A** phylogenetic tree of the tick species (extracted from the complete phylogenetic tree of Chelicerata). The “non *Ixodidae*” clade refers to the Metastriata species. The “ricinus group” is a group of closely related *Ixodes* species. **B** and **C** show the most represented Gene Ontology terms associated with biological processes in gained and expanded families, respectively.

A



B

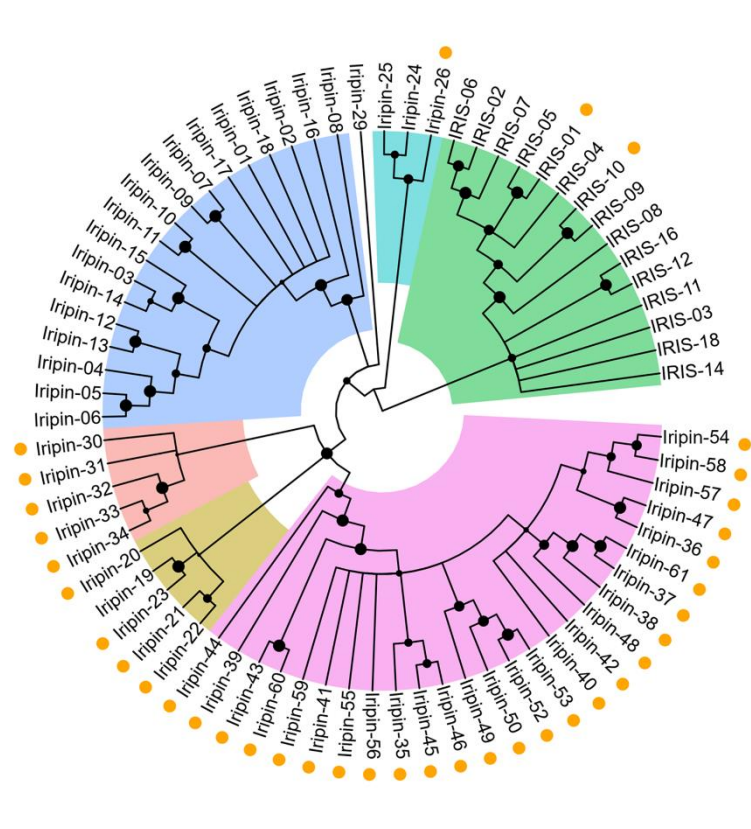


Figure 6: Evolution of serpins in the tick *I. ricinus*. **A** Serpin expression profile. The expression heatmap is based on $\log_{10}(\text{TPM})$ (transcripts per million) calculated for the respective transcriptomes: SYN – synganglion; SG – salivary glands; OV – ovary; MT – Malpighian tubules; MG – midgut; FB.T – fat body/trachea; UF – unfed females; F – fully fed females; WB – whole body. **B** Consensus phylogenetic tree of serpins from *I. ricinus*. Sequences were aligned as proteins, signal peptides and variable reactive center loops were removed before the analysis as well as non-informative positions. Edited protein sequences were analyzed by Maximum likelihood method and JTT matrix-based model and bootstrap method with 1000 replications was used to calculate the reliability of tree branches. Only branches with bootstrap value equal or higher than 50% are shown. Mono-exonic serpins are shown with an orange dot. Specific clades are represented by colored areas in the phylogenetic tree, using the same background color for sequence labels in the heatmap.

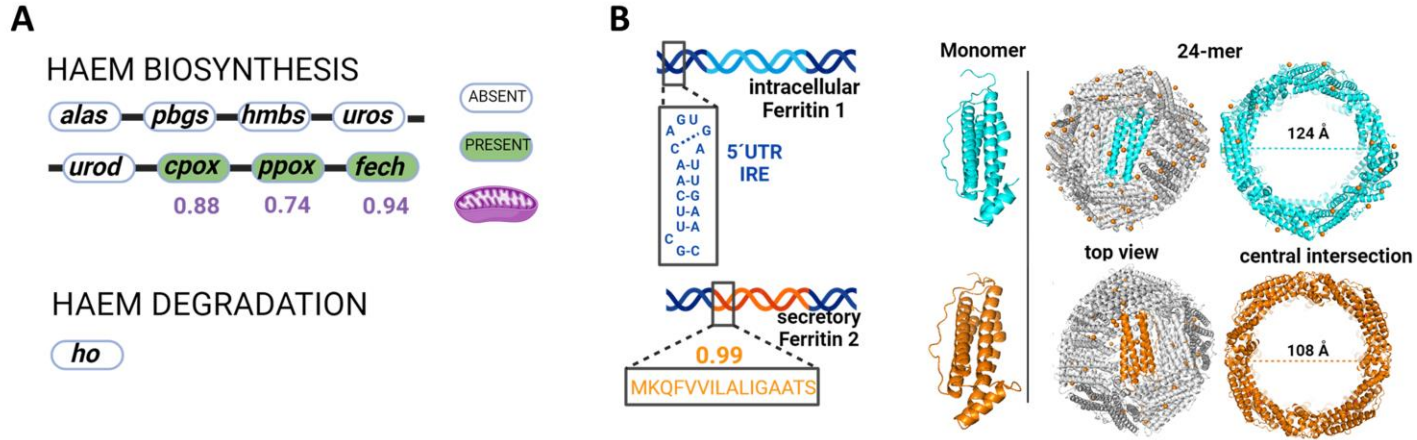
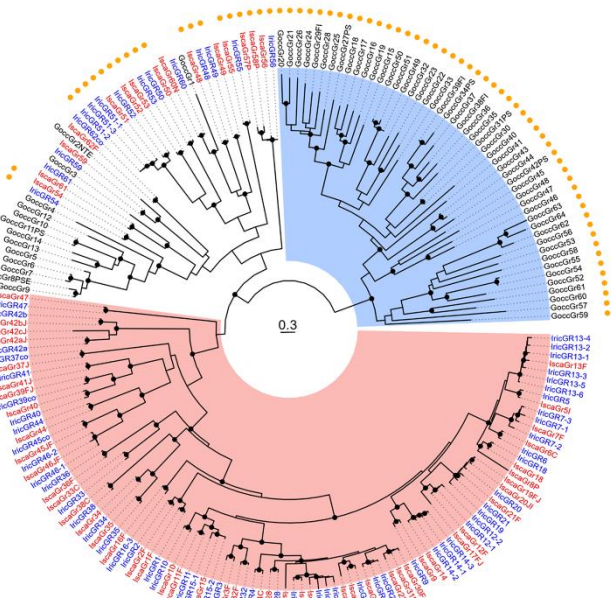


Figure 7: Genomic prediction for heme and iron biology. **A** Gene loss in the heme biosynthesis pathway in the genome of *I. ricinus*. The green color indicates the presence of the homologous gene in the *I. ricinus* genome, with predicted mitochondrial targeting of their protein products (DeepLoc8 prediction values in purple are shown below the enzyme name). **B** Two ferritin genes have been identified in the *I. ricinus* genome: ferritin 1 contains 5'UTR iron-responsive element with the “head” part of the stem-loop structure and complementary bases forming the stem (the blue inset), while ferritin 2 contains a signal peptide (the orange inset) with high SignalP9 probability (shown above the inset). The 3-D reconstruction confirms the conservation of monomeric folding and assembly towards a 24-mer multimers of > 10 nm in external diameter.

A



B

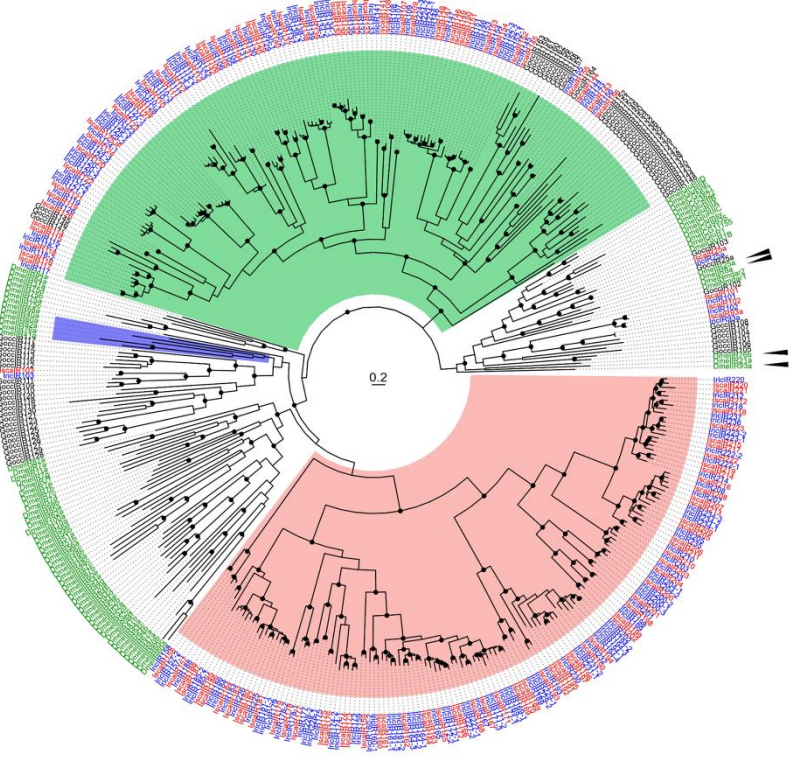
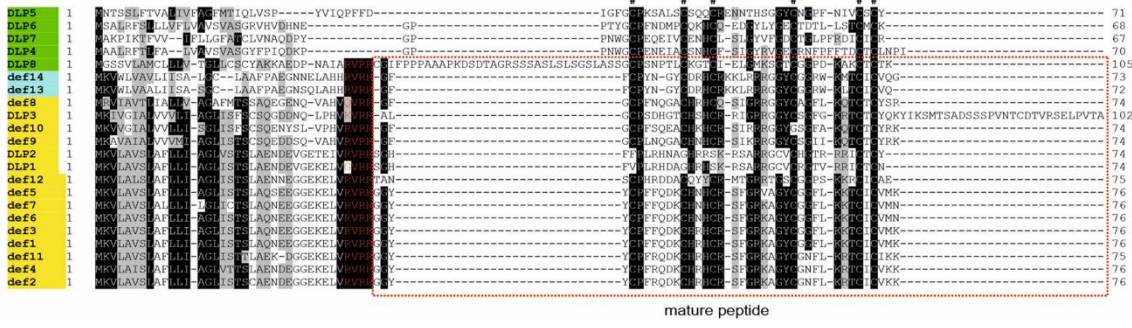


Figure 8: Evolution of tick chemosensory proteins. Trees have been midpoint rooted. Specific clades are represented by colored areas. **A** Maximum-likelihood phylogenetic tree of tick gustatory receptors (GRs). The tree was built using GR repertoires of the ticks *I. ricinus* (IricGRX, labels in blue) and *I. scapularis* (IscaGRX, labels in red), and of the mite *G. occidentalis* (GoccGRX, labels in black). Colored ranges indicate a tick-specific clade (red) and a mite-specific-clade (blue). Clades supported by an aLRT value over 0.9 are indicated by a black dot. Exterior circle: orange dots indicate mono-exonic genes. **B** Maximum-likelihood phylogenetic tree of tick ionotropic receptors (IRs). Color correspondence of labels: *I. ricinus* (IricIRX, in blue), *I. scapularis* (IscaIRX, in red), *G. occidentalis* (GoccIRX, in black) and *Drosophila melanogaster* (DmelX, in green). The ionotropic glutamate receptor clade was used as an outgroup. Black arrowheads show phylogenetic positions of the IR coreceptors found in *D. melanogaster* (IR25a, IR76b, IR8a and IR93a). The clades highlighted in red and green are respectively tick specific and acari specific. The clade highlighted in blue comprises *D. melanogaster* receptors involved in ammonia, amines and humidity detection. Clades supported by an aLRT value over 0.9 are indicated by a black dot.

A



B

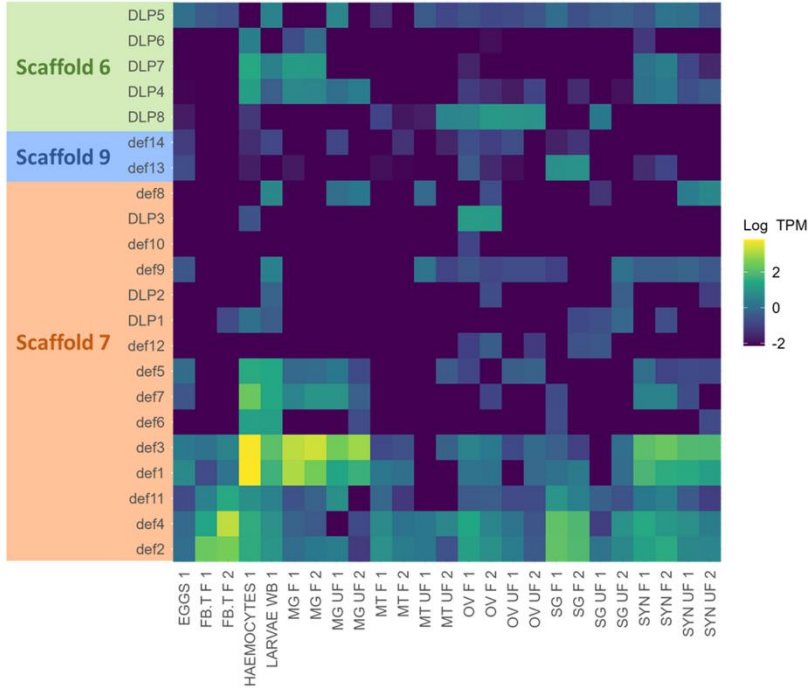


Figure 9: Multiple sequence alignment and tissue expression heatmap of identified *I. ricinus* prepro-defensins and defensin-like peptides. A Multiple amino-acid sequence alignment of identified prepro-defensins (def1-def14) and defensin-like peptides (DLP1-DLP8). Highlighted in yellow – genes located on scaffold 7; in blue – genes located on scaffold 9; in green – genes located on scaffold 6; red letters – furin cleavage motif; red dashed frame – predicted mature peptides; # – conserved cysteine residues. **B** Tissue expression heatmap based on TPM (transcripts per million) in respective transcriptomes using log transformation $\log_{10}(\text{TPM})$. SYN – synganglion; SG – salivary glands; OV – ovary; MT – Malpighian tubules; MG – midgut; FB.T – fat body/trachea; UF – unfed females; F – fully fed females; WB – whole body.

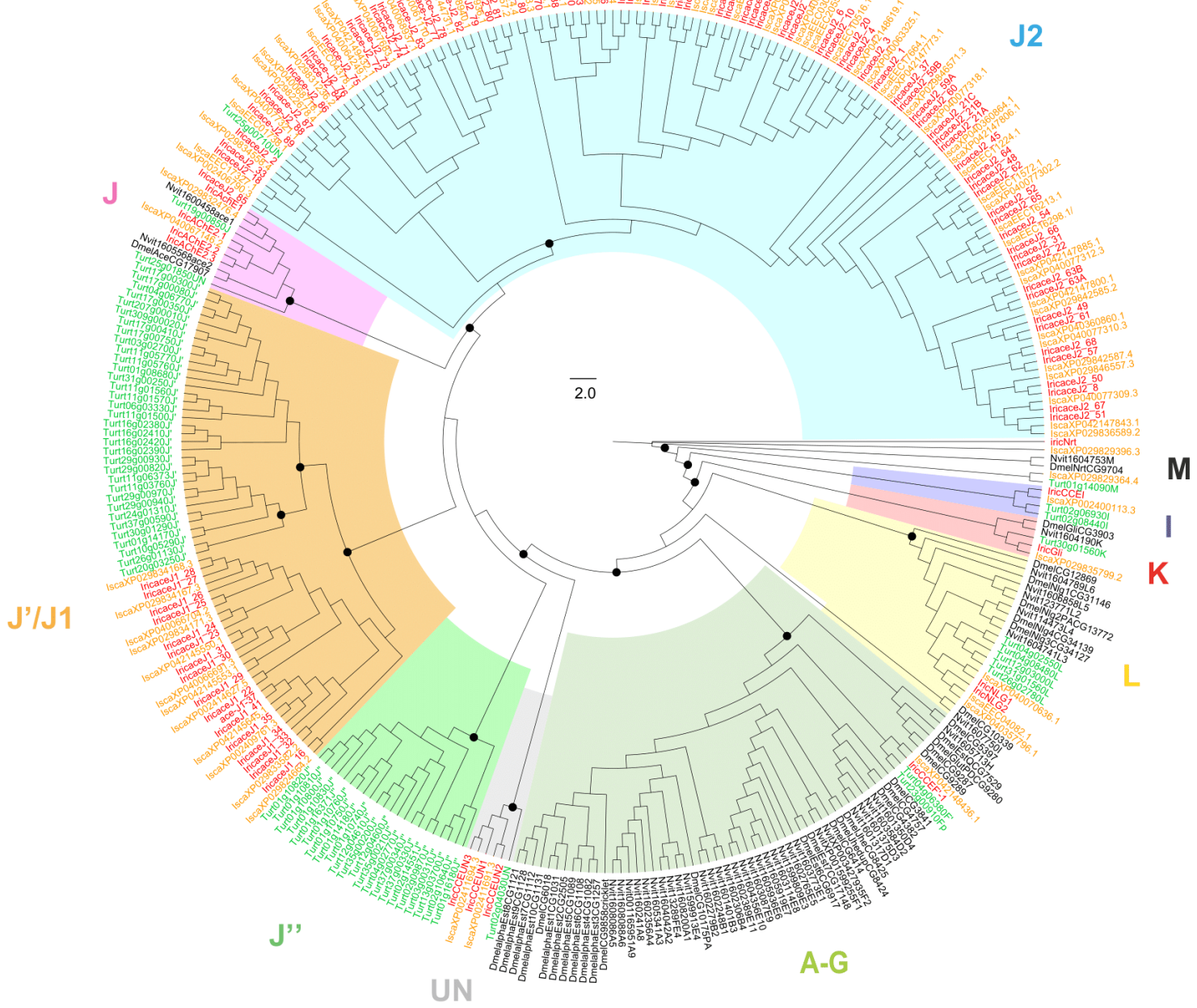
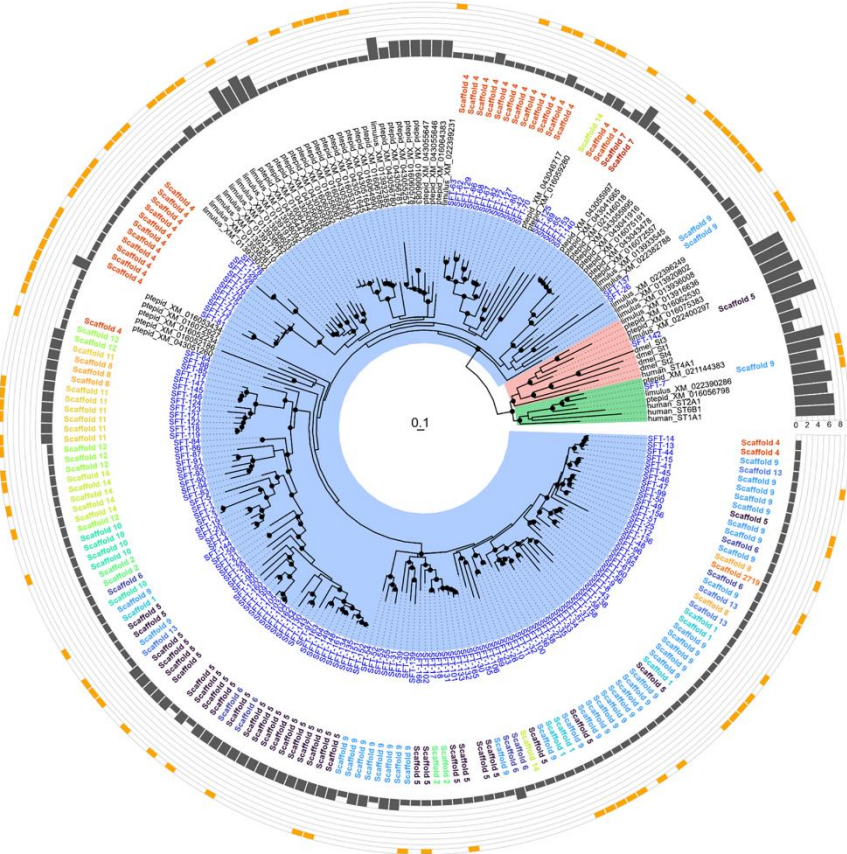


Figure 10: Phylogenetic tree of CCEs in ticks and other representative arthropod genomes. CCEs included are from *I. ricinus* (Iric in red), *I. scapularis* (Isca in orange), *Tetranychus urticae* (Turt in green), *Nasonia vitripennis* (Nvit in black) and *D. melanogaster* (Dmel in black). Dots on the tree correspond to bootstrap values above 0.87. Scale is given in the middle of the tree. Ticks show important expansion of the J2 clade.

A



B

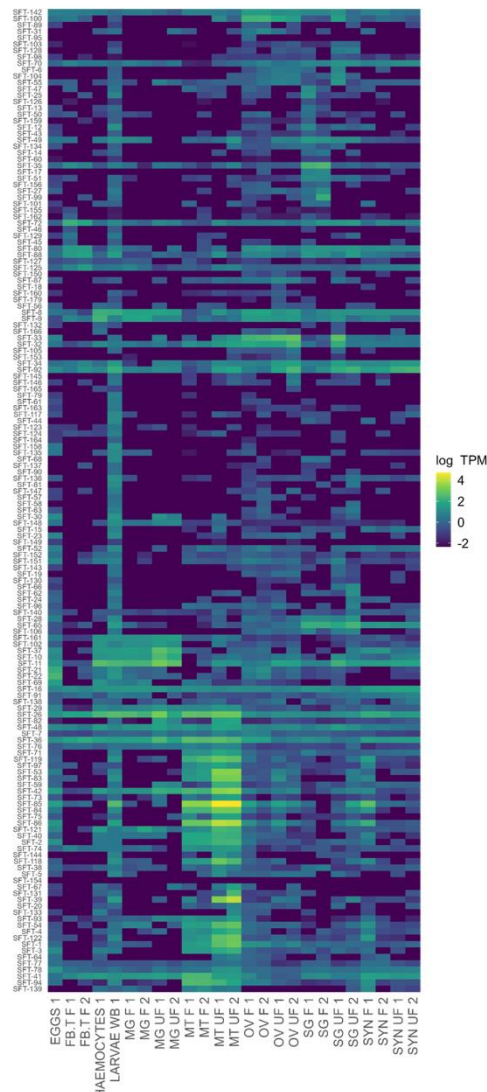
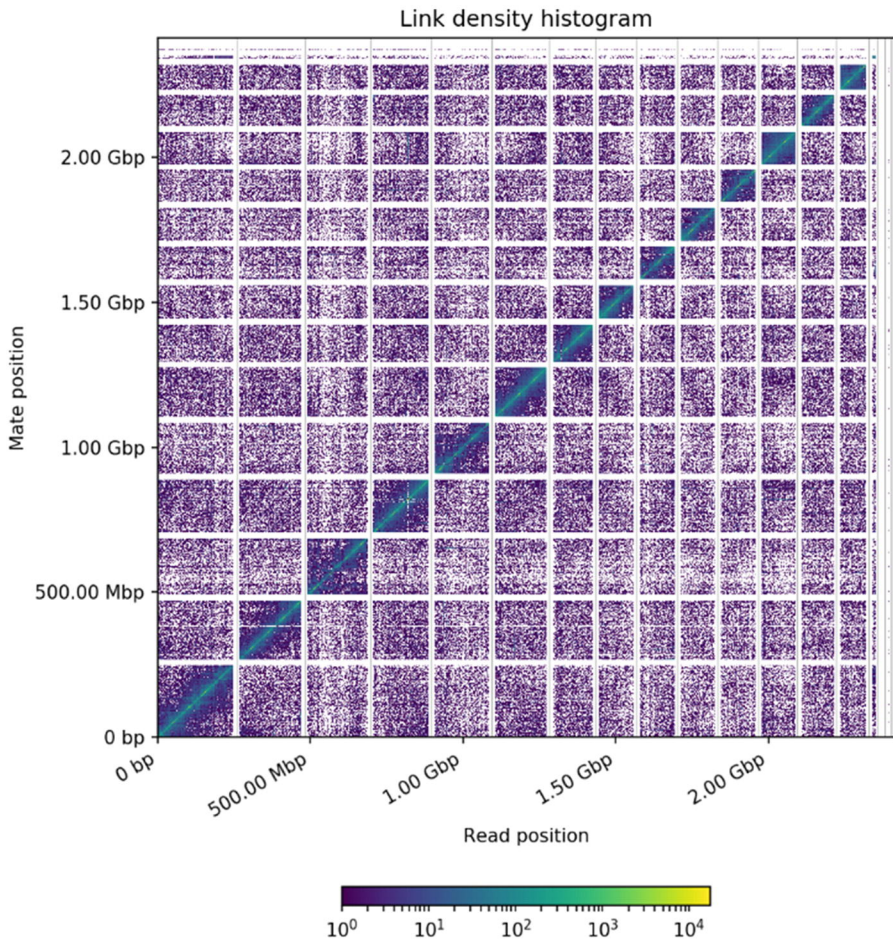
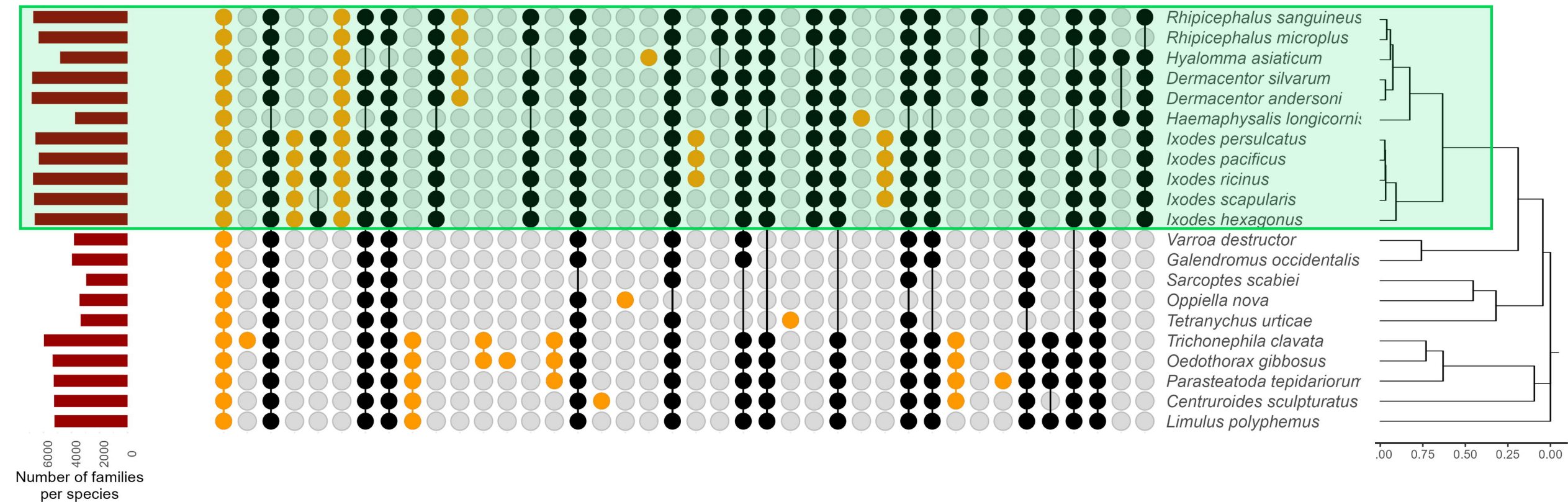
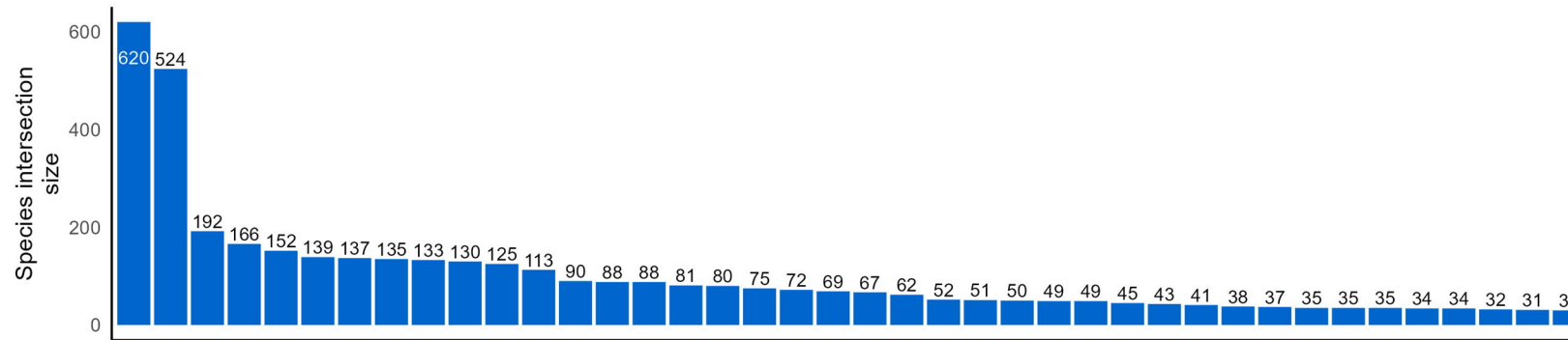
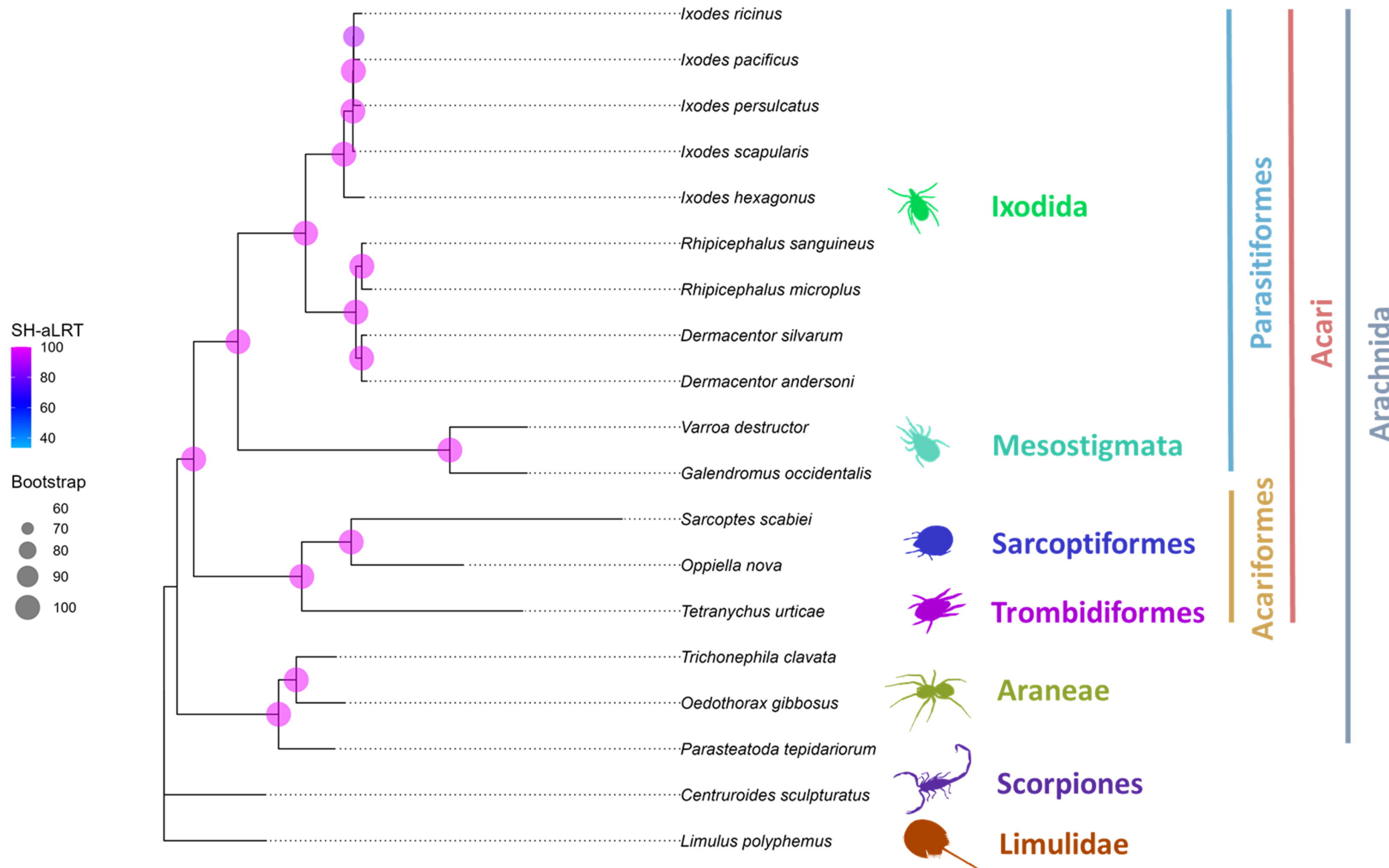
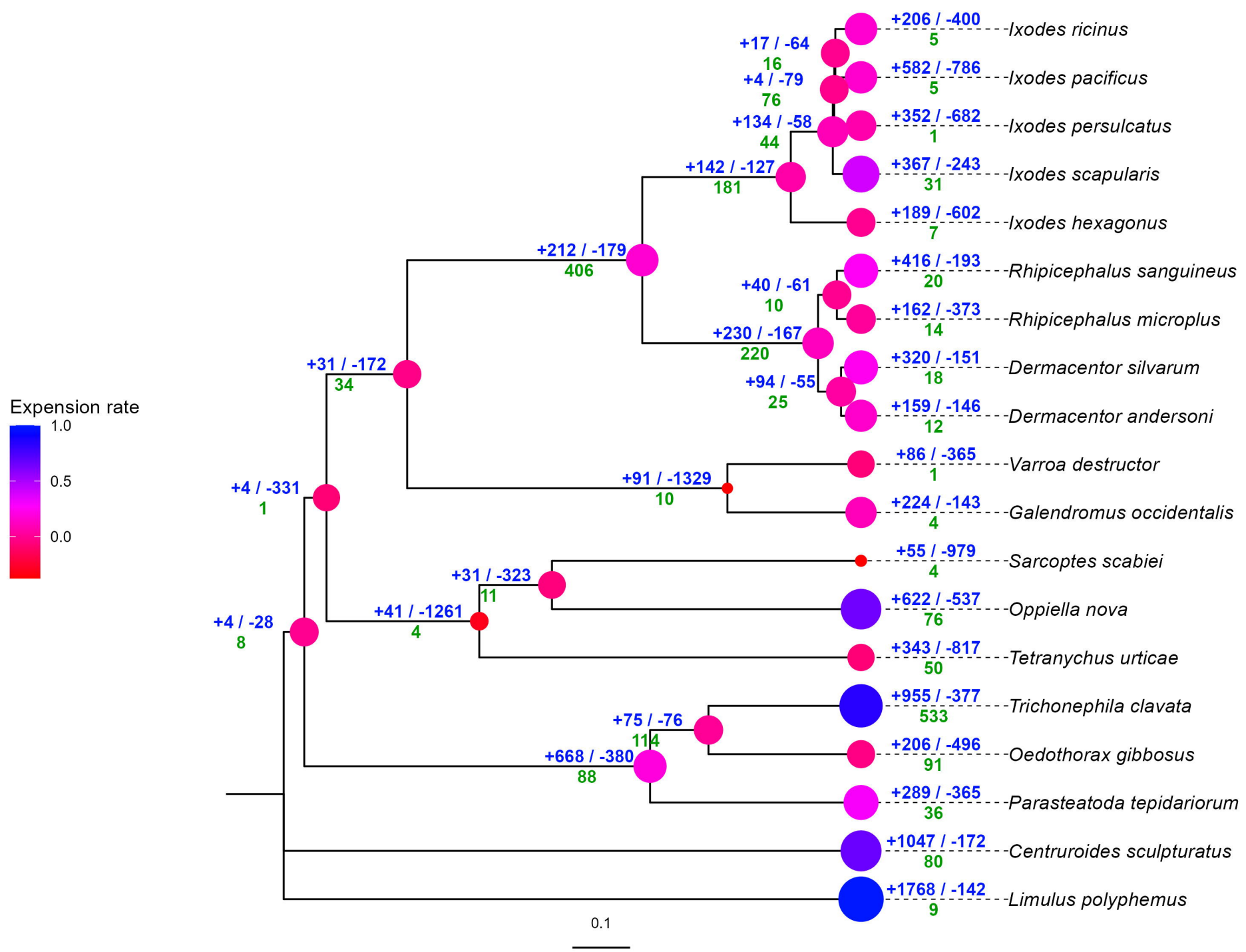


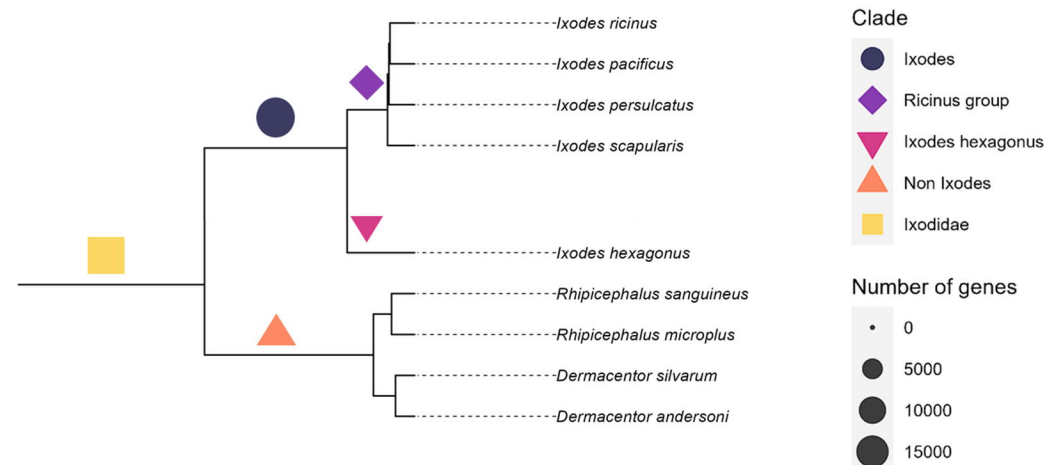
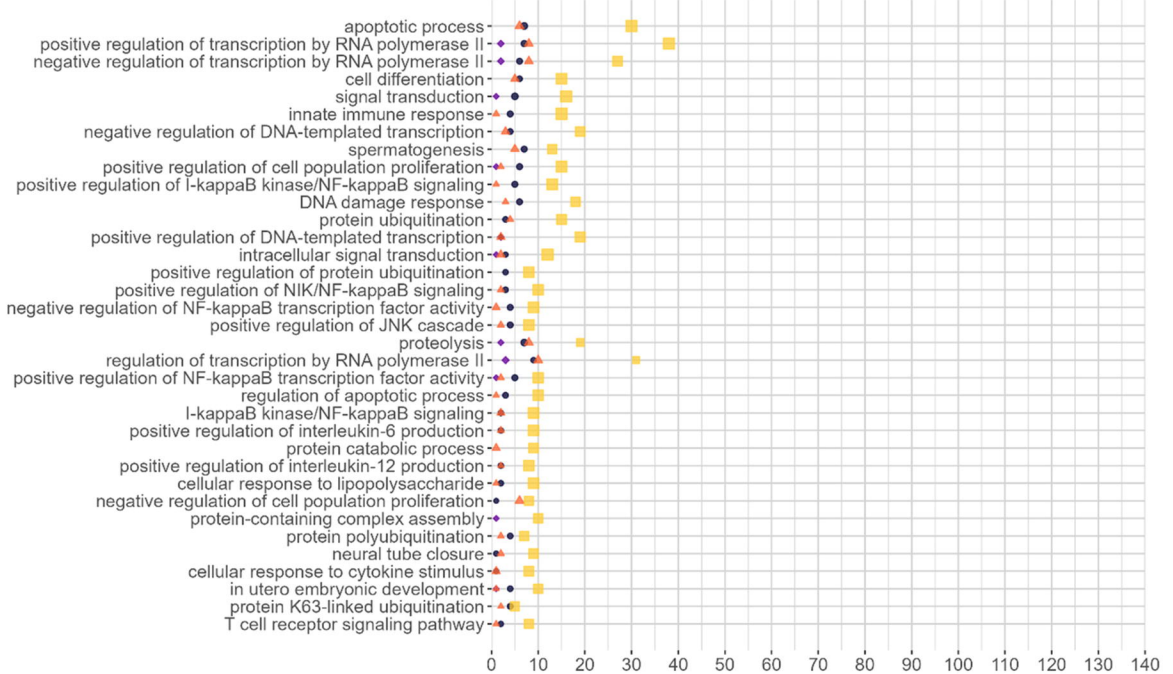
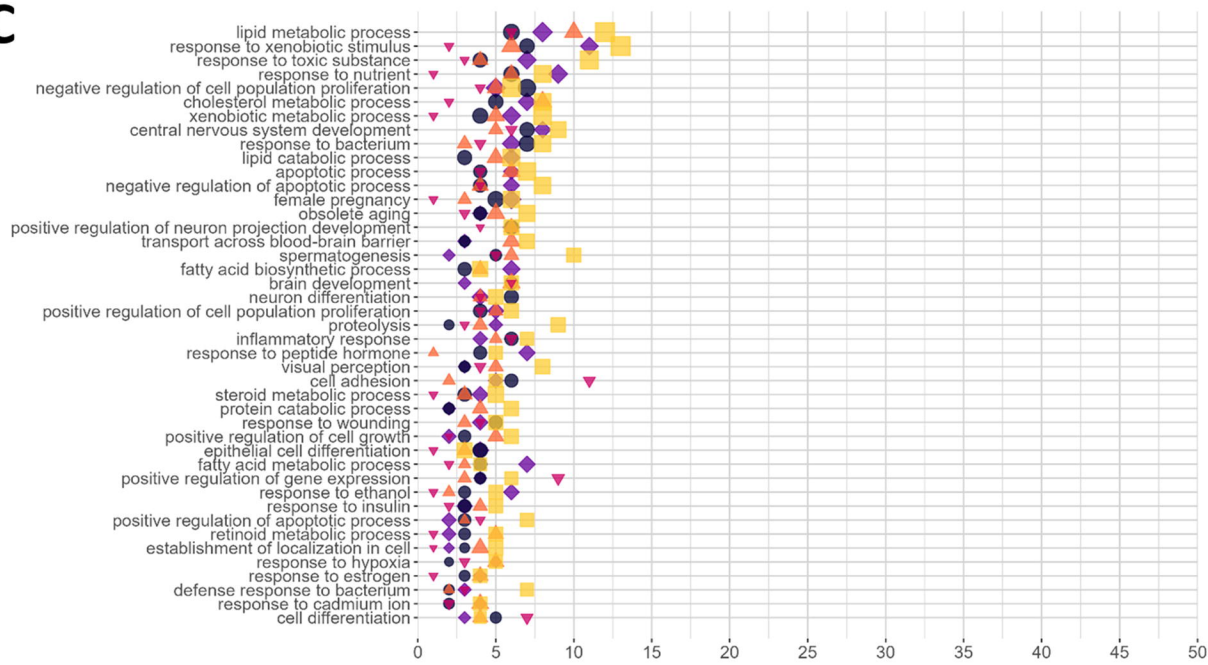
Figure 11: Expansion of the cytosolic sulfotransferases (SULTs) in the genome of ticks and other Chelicerata, with evidence for both retroposition events and re-exonization. **A** Phylogenetic tree of cytosolic sulfotransferases (SULTs). ML tree using the best-fit LG+I+G4 model of substitution. Sequences from ticks (*I. ricinus*, labels in blue), the spider *Parasteatoda tepidariorum*, the horse-shoe crab *Limulus polyphemus*, human and *D. melanogaster*. Well supported nodes are indicated by dark-filled circles (the width of circles varies with bootstrap values, ranging between 0.85 and 1). The chromosomal (scaffold number) localization is indicated in the first outer circle (each scaffold has its own color label). The next outer circle are bar-charts of the number of coding exons (dark filling) and 5'UTR-only exons (orange filling). The tree allows to define two « conserved » clades (A - green and B - red), with sequences shared between vertebrates and Chelicerata, and a clade (C - blue) with sequences exclusively in Chelicerata. **B** Heatmap of expression of SULTs in *I. ricinus*.

A**B**

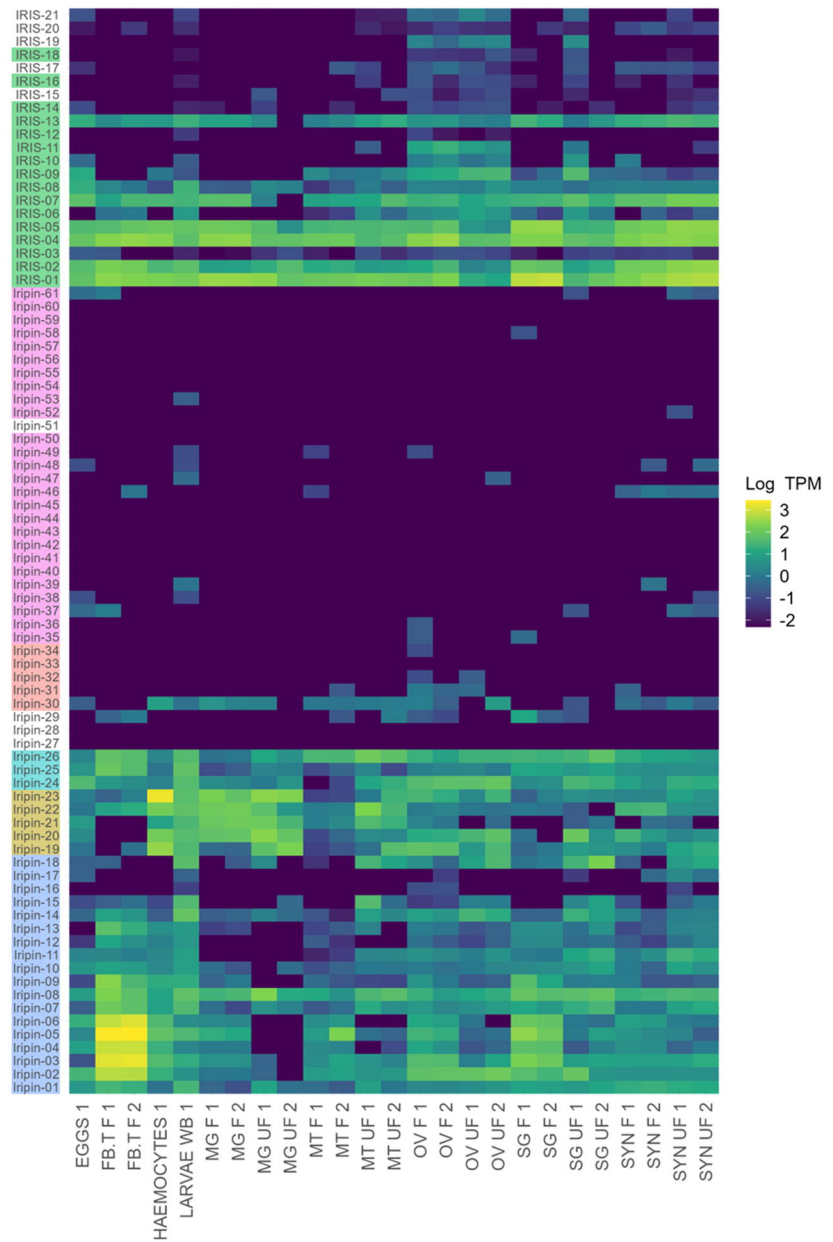




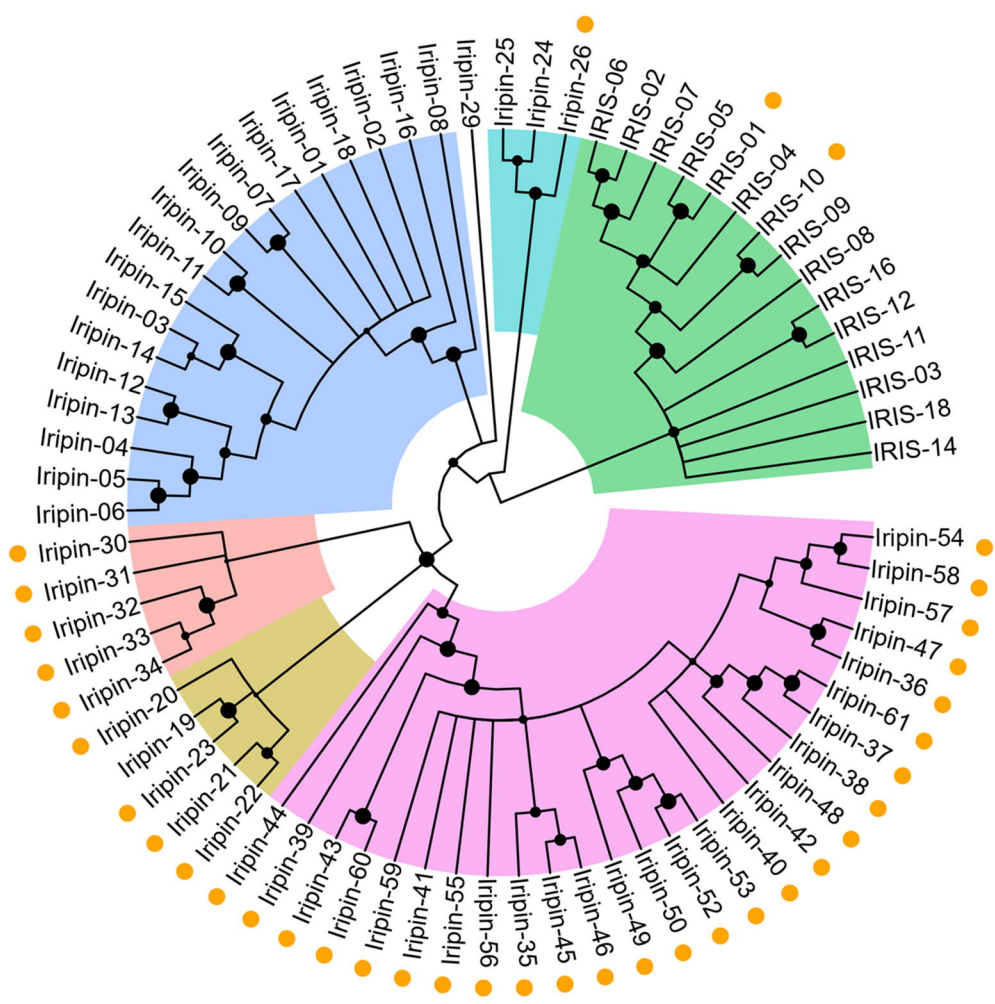


A**B****C**

A



B

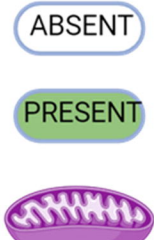


A

HAEM BIOSYNTHESIS

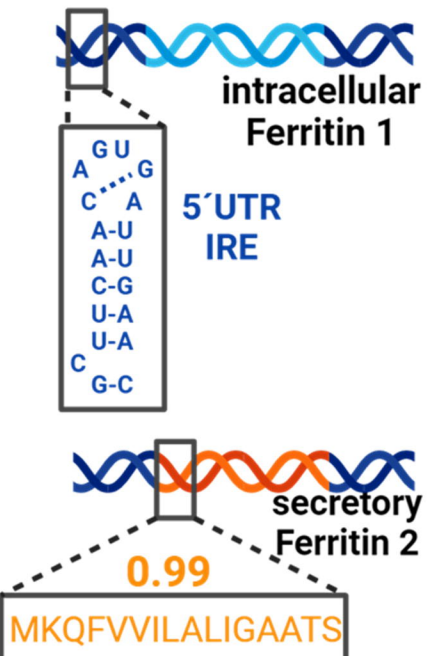


0.88 0.74 0.94

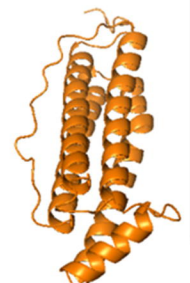
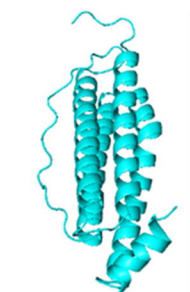


HAEM DEGRADATION

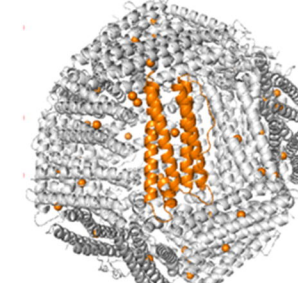
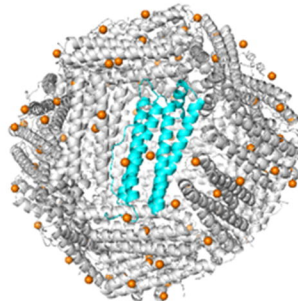
ho

B

Monomer

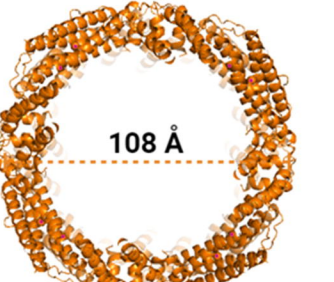


24-mer



124 Å

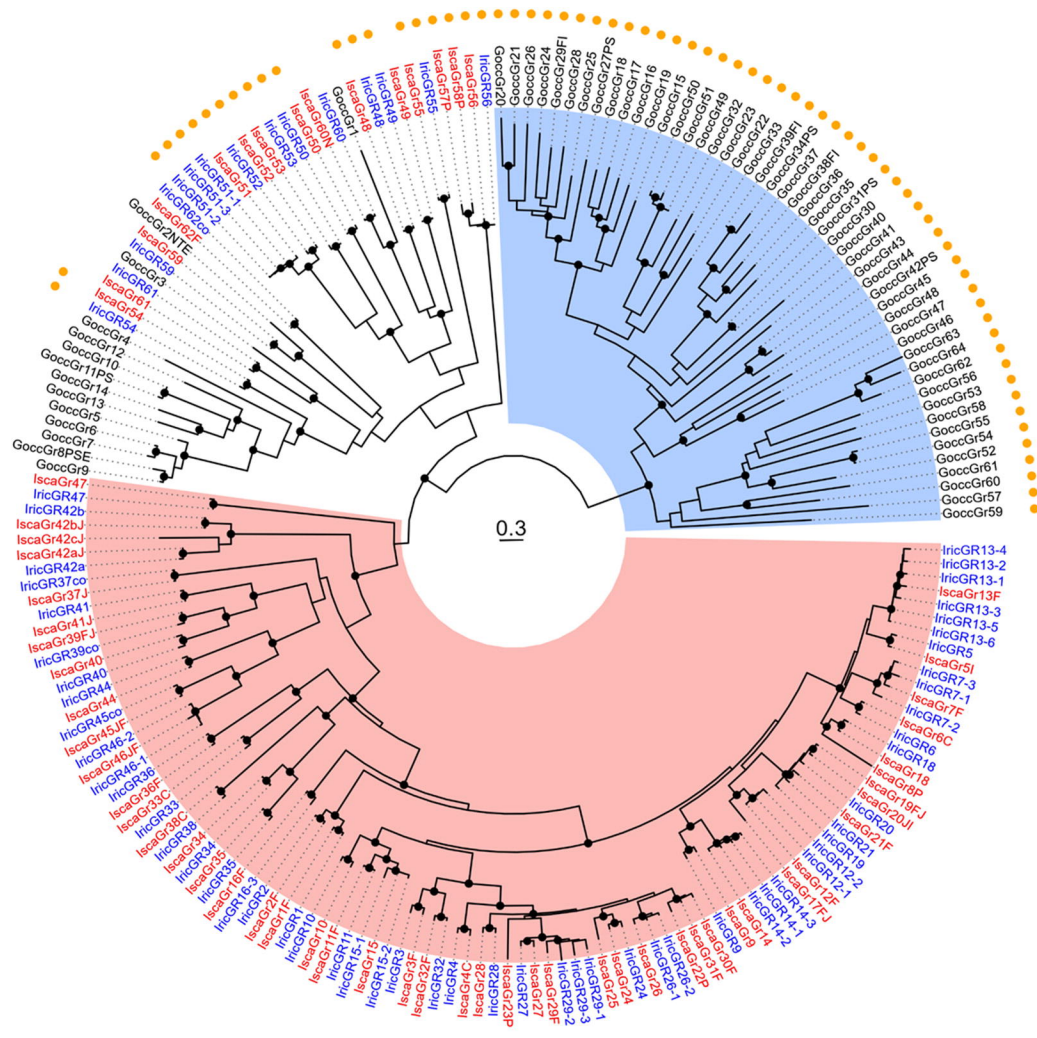
top view



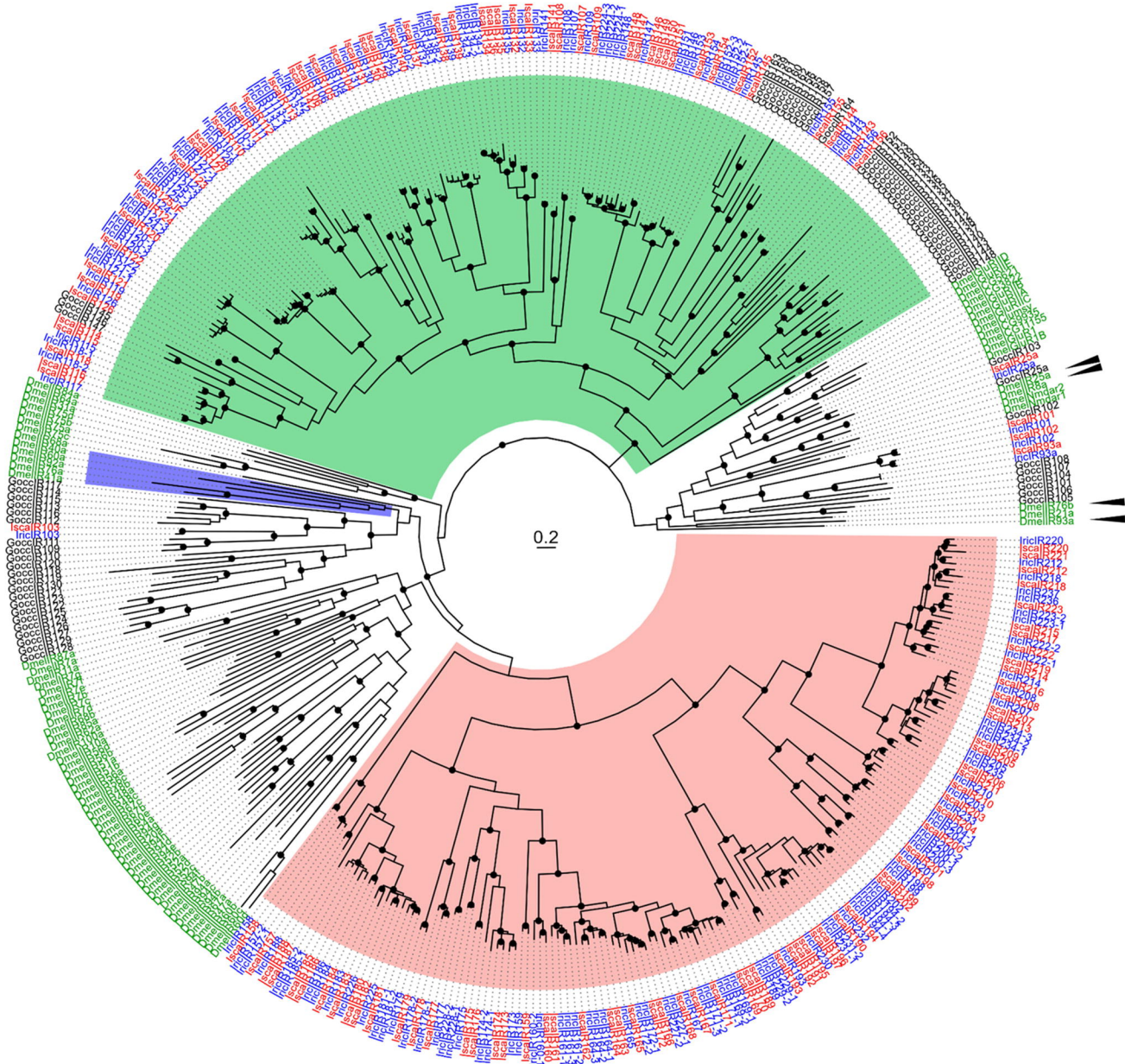
108 Å

central intersection

A

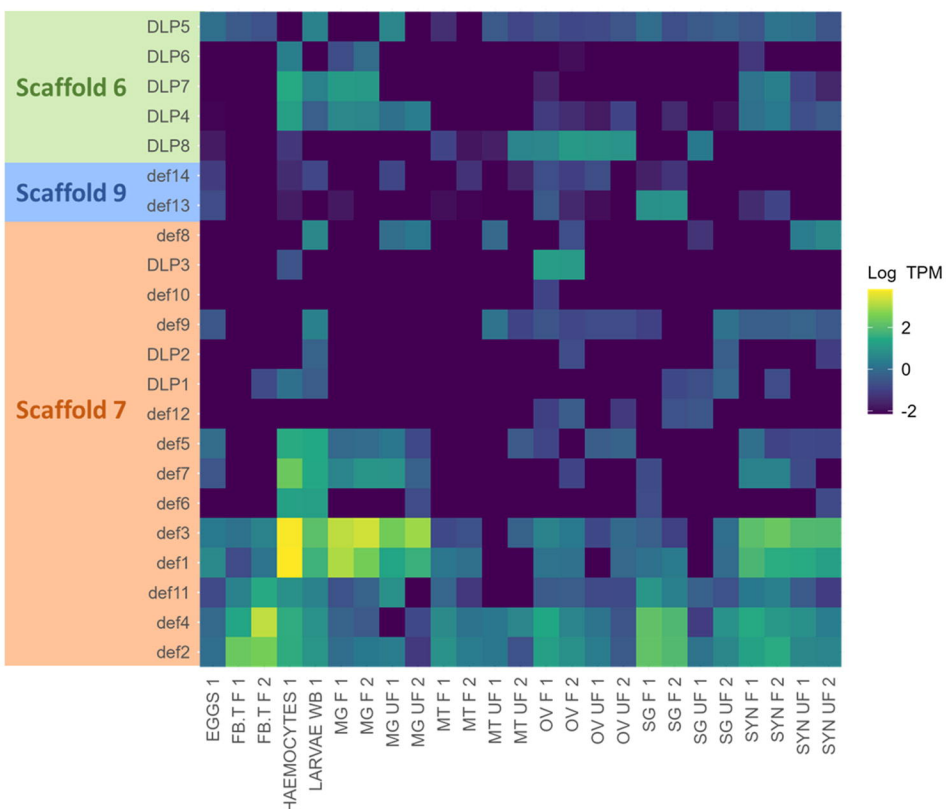


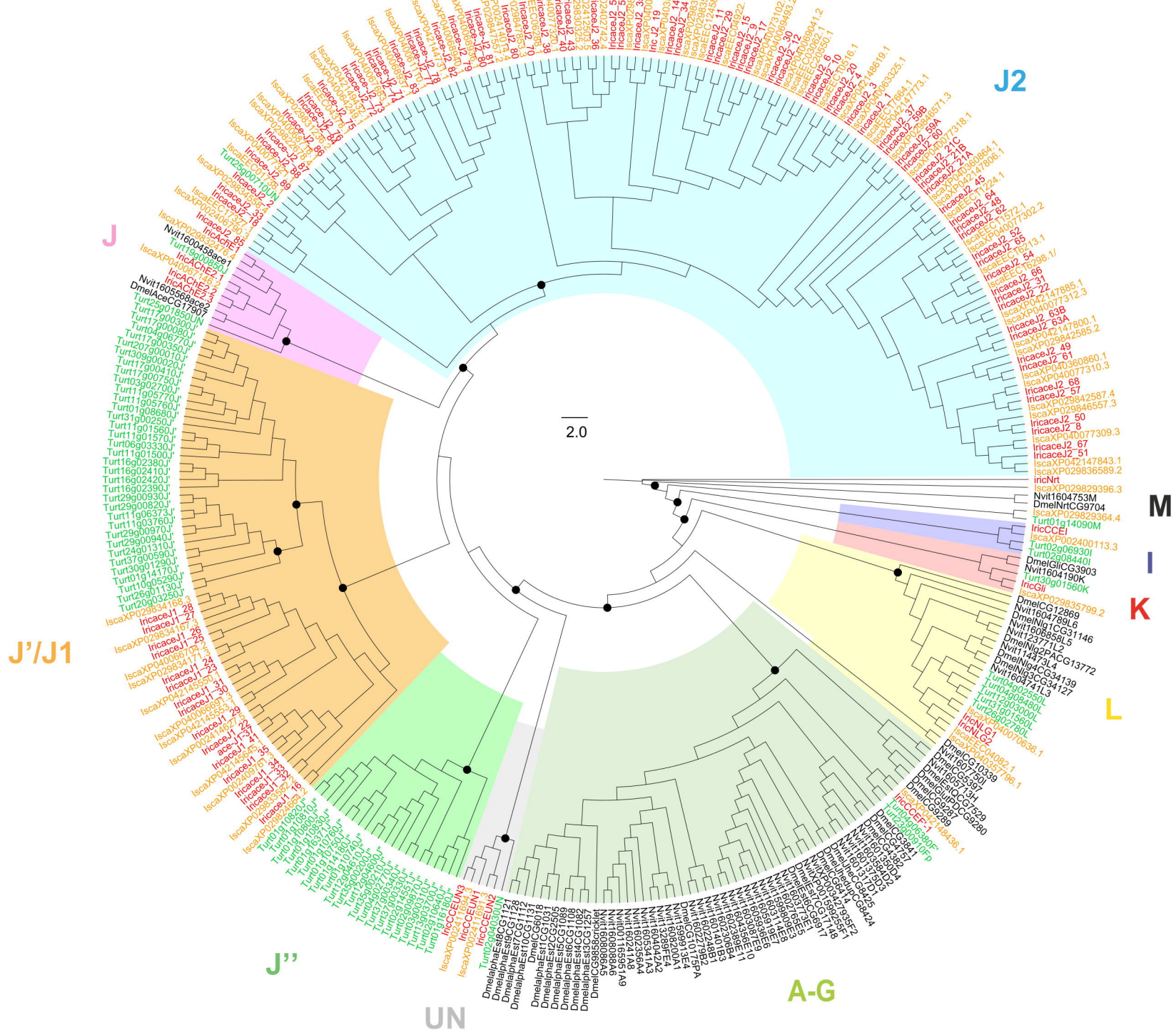
B



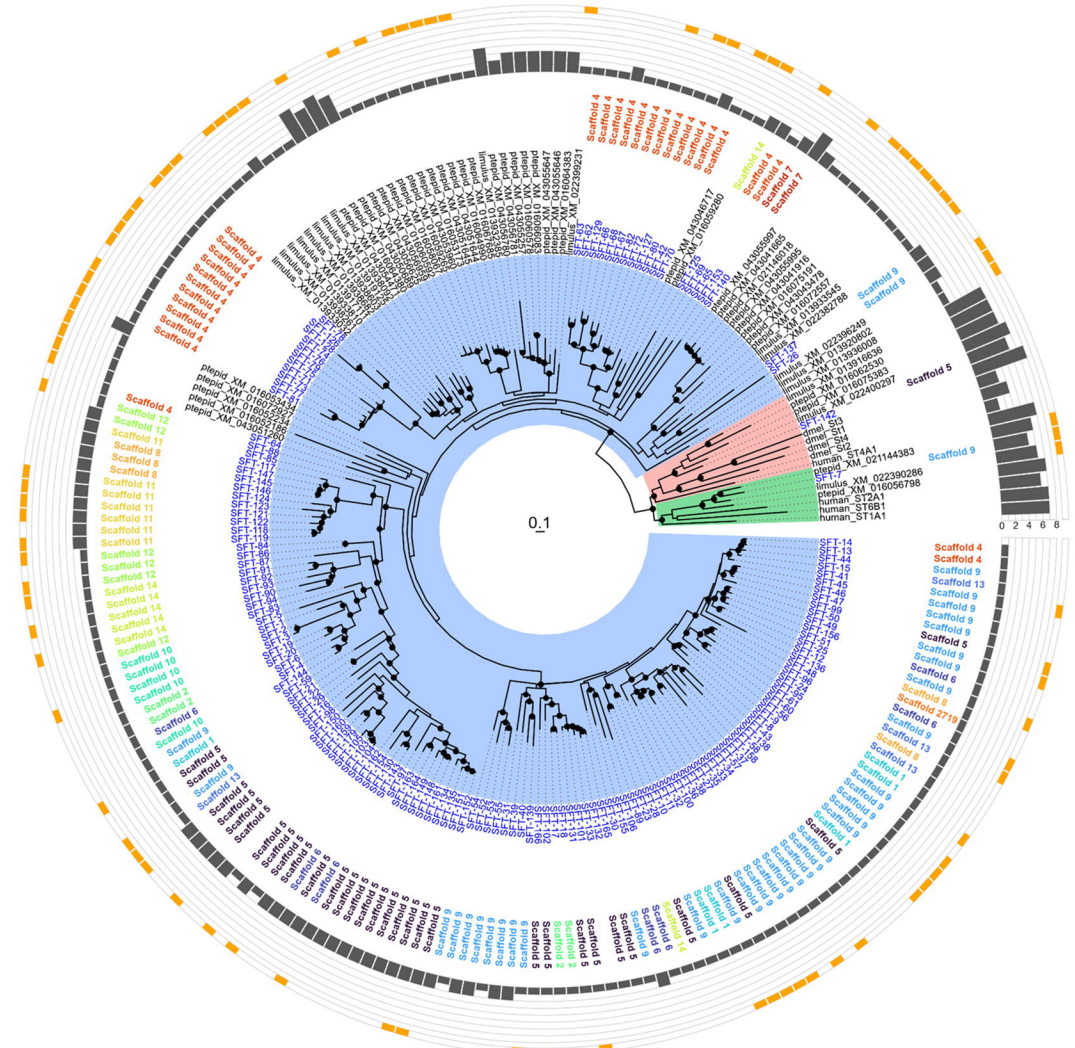
A

mature peptide





A



B

